PRION NUCLEATION AND PROPAGATION BY MAMMALIAN AMYLOIDOGENIC PROTEINS IN YEAST

A Dissertation
Presented to
The Academic Faculty

by

PAVITHRA CHANDRAMOWLISHWARAN

In Partial Fulfillment
of the Requirements for the Degree
Doctor of Philosophy in the
School of Biological Sciences

Georgia Institute of Technology
May 2018

PRION NUCLEATION AND PROPAGATION BY MAMMALIAN AMYLOIDOGENIC PROTEINS IN YEAST

Approved by:

Dr. Yury Chernoff, Adviser
School of Biological Sciences
Georgia Institute of Technology

Dr. Raquel Lieberman
School of Chemistry and Biochemistry
Georgia Institute of Technology

Dr. Kirill Lobachev
School of Biological Sciences
Georgia Institute of Technology

Dr. Vincent Conticello
Department of Chemistry
Emory University

Dr. Francesca Storici
School of Biological Sciences
Georgia Institute of Technology

DATE APPROVED: APRIL 5, 2018

ACKNOWLEDGEMENTS

गुरु ब्रम्हा गुरु विष्णू, गुरुः देवो महेश्वरा, गुरु शाक्षात परब्रम्हा, तस्मै श्री गुरुवे नमः

My experiences from 2010-18 has been very humbling and I never got to thank many lives who have impacted me which I think I can do in this section. I dedicate my life's work and write this section in loving memories and in honor of my deceased kids and family members, especially all my grandparents who are still with me in spirit and who desperately wanted to see me succeed. Thank you for being with me in good and bad times.

My journey from the beginning to the end of this PhD journey would undoubtedly not be possible without the saturnian dedication and kind yet focused mentoring of my PhD adviser, **Dr. Yury Chernoff** who has literally raised me up from when I was a student of unknown caliber who knew very little to a level at which I can independently function as a professional. I am humbled to have worked under his professorship and I take this opportunity to extend my sincere and heartfelt gratitude to him, who has withstood my frustrating ways and saw a flicker of hope in me and didn't let me give up until the end, for which I am grateful for a lifetime.

I am also very thankful to my committee members who have devoted their precious time on multiple occasions to provide feedback which has been very useful and helped me approach many aspects of my dissertation project in an angle that I was not used to seeing. Also, I am very thankful to Dr. Lieberman and Dr. Conticello for providing some material that were used in this dissertation and for choosing to work with me on collaborative projects. I am equally grateful to Dr. Lobachev and Dr. Storici for being kind and supportive in agreeing to be my recommenders for job applications.

My lab has always celebrated my successes and have always rooted for me in every endeavor and I am very grateful for their camaraderie, advices, and good spirits. Thank you for celebrating my birthday every year, it indeed made me feel appreciated. The list includes so many who are equally special in their own way – Zack Deckner, Rakhee Ganti, Aditi Sharma, Rebecca Howie, Lina Manuela Jay Garcia, Gary Newnam, Andrey Romanyuk, and Anastasiya Grizel. I also thank my mentors, He Gong and Meng Sun, who helped me during my first few semesters at Georgia Tech in understanding the research work and for mentoring me until a point where I could work independently. I am also thankful to many members of neighboring labs for their support and good memories - Sat Balachander, Chance Meers, Shilpa Choudhury, Havva Keskin, Zahra Nassri. I am especially thankful to my graduate coordinator Mrs. Lisa Redding for going out of her way to help me with academic paper work and saving me at the eleventh hour during deadlines.

I cannot forget to thank my TI:GER team members – Divakar BV, Alex Simon, Francisco Bravo, and Jon Lawler for working with me on commercializing certain aspects of this project, it was an amazing experience working with them, and I am very thankful to Margi Berbari from Scheller School of Business for giving me the opportunity to participate in such a program with very talented people from different disciplines.

Coming to the peptide backbone, I am extremely grateful in ways that cannot be explained in words to two people who are like the sun and moon in my earthy life, my parentablets, who have fiercely believed in me, accepted me, and injected their unwavering optimism and good vibes and humor into my life every day, despite my shabby schedules and rotten moods, and showered me with the unconditional love one can only hope in this lifetime. You have shown me the way by being the way. Thank you for being so kind when kindness was not fashionable and thank you for supporting education and charity in every way possible. Thank you for providing me a luxurious life despite you struggling financially

and physically through surgeries and working many jobs so that I could be comfortable, your pains and hard work will never be forgotten. Coming from a family of people who work in banks, I did not know of PhD programs until my sister, Aparna, a brilliant and ambitious lady, got admitted into the PhD program at Georgia Tech in CSE. She has always been my involuntary role model and I decided to follow in her footsteps. Thank you for being the light and shining a way in my life at many crucial junctures when my light was fading and thank you for always bolstering faith and humble support when didn't ask for it but really needed it. I am also thankful to my brother Eshwar for his timely humor and for choosing to spend his time and special days with me on many occasions and for small acts of kindness which has helped me a lot at various times. I thank every member in my family for their words of constant encouragement and positive vibes. I also thank my close friends who have been my biggest cheer leaders – LP and Anjana.

As a part of my own family, I cannot forget all the beautiful animals who have lived with me throughout this journey. It is my greatest privilege to have had the opportunity to rescue and rehabilitate many souls who in turn rescued me as well from the drudgery of life and showed me the unconditional love that was so hard to provide for myself during many days. They tolerated my shabby schedules and been very accommodating and adjusted to every twist and turn with enthusiasm and happy tails. It is very heart-wrenching that they had to leave this planet in such a short time and I regret every day that I couldn't help save them or devote the time they deserved but I only have the deepest gratitude for every second I spent with them. Thank you Shiva, Rocky, Choo Choo, and Suchi. I hope your souls rest in peace. Their loss was very hard to bear but I am very lucky that many more decided to live with me, thank you Boris, Minnie, Bobby, and Dooley for sharing your life with me. Your presence in my life gives a purpose to every day for me.

I cannot forget to mention these people in this section. I am very grateful to Georgia Tech Stingerette drivers – Mike and Cliff who have always ensured my safety during the wee hours of the morning despite their crazy schedules and for making my long nights feel less exhausting with stories of their colorful lives. I also thank our 5th floor janitor Ephram for keeping our lab and office spaces sparkly clean and safe, and for being kind enough to care about my work and me, despite his busy and tiring schedule.

I also thank some special people who helped me during tough times with their optimism and companionship on weekends when we shared good memories with beautiful animals– Ken Whitley and Anqi Zou from Fulton Country Animal Services, and Daniel Sweeney from Full Circle Farm Sanctuary.

I AM SORRY IF I LEFT ANYONE BUT EVERYONE WHO I HAVE MET DURING THIS PHD JOURNEY HAVE ONLY CONTRIBUTED TOWARDS MY LIFE'S JOURNEY VERY POSITIVELY, AND I AM THANKFUL FOR THE OPPORTUNITY WHATEVER IT WAS.

TABLE OF CONTENTS

LIST OF TABLES

LIST OF FIGURES

Chapter 1

Chapter 2

Chapter 3

Chapter 4

Chapter 5

Figure 5-11. Phenotypic detection of Ade^+ phenotype formed by tau WT-MC and tau mut-MC chimeric proteins.

LIST OF SYMBOLS AND ABBREVIATIONS

AD	Alzheimer's disease
TSEs	Transmissible spongiform encephalopathies
PD	Parkinson's disease
T2D	Type 2 diabetes
HD	Huntington's disease
Aβ	Amyloid beta
MAPT	Microtubule binding protein tau
Tau RD	Tau microtubule repeat region
α- syn	Alpha synuclein, also called NAC
IAPP	Islet amyloid polypeptide or amylin
Myocilin OLF	Myocilin olfactomedin domain
PrP	Prion protein
PolyQ	Polyglutamine
PrD	Prion domain
Prion	proteinaceous infectious particles
5-FOA	5-Fluoroorotic Acid
GuHCl	guanidine hydrochloride
CuSO4	copper sulphate
EDTA	ethylenediaminetetraacetic acid
SDS	sodium dodecyl sulphate
aa	amino acid
kDa	Kilo Dalton
SDD-AGE	semi-denaturing detergent agarose gel electrophoresis

SDS-PAGE	sodium dodecyl sulfate polyacrylamide gel electrophoresis
QN or Q/N	Glutamine and asparagine-rich stretch
ORs or NRs	region of oligopeptide repeats
ade1-14	allele containing a premature UGA stop codon
LB	Luria Bertani broth
Amp	Ampicillin

SUMMARY

Cross-β fibrous protein polymers, reproduced and spread via nucleated polymerization and termed amyloids, are associated with a variety of human and animal diseases, including Alzheimer's disease (AD), Parkinson's disease (PD), and Huntington's disease (HD). Various amyloids are suspected to possess transmissible (prion) properties, at least at a cellular level. Despite such a broad biological impact of amyloids and prions, the mechanism of their initial formation *in vivo* remains a mystery. One and the same amyloid protein can form various structural polymorphs ("strains") that may differ by biological and pathological properties. However, molecular bases of strain differences and strain propagation are still poorly understood. Simple eukaryotes like yeast also carry proteins that can generate and convert to distinct heritable prion strains that can be stably propagated and phenotypically detected. To understand the molecular mechanisms of initial prion nucleation, we employed a fusion of the prion domain (PrD) of yeast protein Sup35 to some non-Q/N-rich mammalian proteins (or peptides), associated with amyloid diseases. Transient overproduction of the chimeric proteins promoted nucleation of Sup35 prions in the absence of pre-existing aggregates. Biochemical detection of the chimeric proteins confirmed nucleation of protein aggregates in the yeast cell. Sequence alterations antagonizing or enhancing amyloidogenicity of mouse PrP (associated with prion diseases) or human Aβ (associated with Alzheimer disease) respectively antagonize or enhance nucleation of a yeast prion by these proteins. Different Sup35N-PrP or Sup35N-Aβ chimeric proteins induced different spectra of prion strains. In addition to mutational dissection of Aβ, the yeast-based prion nucleation assay, generated in our work, was also employed for identifying agents that could influence initial amyloid nucleation by Aβ. To specifically understand the formation and propagation of prion strains in yeast by Aβ and the aggregation prone repeat domain of another human protein, Tau, also associated with

AD, we employed a construct in which the Sup35 PrD or the Q/N-rich region encompassing first 42 amino acids of Sup35 PrD was replaced by Aβ or versions of tau repeat region, while the remaining portion of Sup35 remained intact. The chimeric proteins were able to switch from a soluble state to a non-functional prion state, that could be phenotypically detected. Detergent-insoluble aggregates of the chimeric proteins were detected biochemically, confirming the presence of the chimeric proteins in prion state. *In vitro* produced Aβ polymers converted the chimeric protein into a polymeric state upon transfection into yeast. Aβ-based chimeric construct formed distinct faithfully reproduced strains in the yeast cell. Our data show that prion properties of mammalian proteins detected in the yeast assays correspond with those found in mammals or *in vitro*, thus making yeast a powerful model for deciphering molecular foundations of amyloid/prion diseases.

CHAPTER 1. INTRODUCTION AND BACKGROUND: STUDYING MAMMALIAN AMYLOIDOGENIC PROTEINS USING YEAST PRIONS

This chapter includes data published in *PLoS Genetics*.

Gong, H., Romanova, N. V., Allen, K. D., **Chandramowlishwaran, P**., Gokhale, K., Newnam, G. P., Mieczkowski, P. Sherman., M.Y. Chernoff, Y. O. (2012). Polyglutamine Toxicity Is Controlled by Prion Composition and Gene Dosage in Yeast. PLoS Genetics, 8(4). doi:10.1371/journal.pgen.1002634

1.1 Summary

Amyloid formation is implicated in more than forty animal and human diseases including Alzheimer's disease (AD), Transmissible spongiform encephalopathies (TSEs), Parkinson's disease (PD), Type 2 diabetes (T2D), and glaucoma. Various amyloids are suspected to possess transmissible (prion) properties, at least at a cellular level. Many of the amyloid disease-causing proteins contain intrinsically unstructured regions in a non-amyloid form. Information about the structure of amyloid forms for some of these proteins have been derived from solid state NMR, cryo-EM, and molecular dynamics simulations, but these data mostly apply to amyloids formed *in vitro.* This is further complicated by the manifestation of amyloids as distinct structure polymorphs (strains) that may correspond to their different pathologies in mammalian models. Since the discovery of endogenous yeast prions, *S. cerevisiae* has become a convenient experimental model for studying the factors that regulate the misfolding and aggregation of mammalian amyloids. For modeling human amyloid diseases in yeast, the yeast homolog of the gene implicated in the disease is directly studied for its function. For human genes that have no yeast homologs, they are heterologously expressed in yeast and phenotypically characterized. These two approaches have been used successfully to perform a functionally or phenotypically analyze human disease genes in yeast. Several yeast assays for studying disease-associated proteins such as Aβ and tau (associated with AD), PrP (associated with TSE), α-synuclein (associated with PD), and polyQ stretches (associated with HD) were

proposed previously. Yeast models for Aβ employed either a fusion of Aβ to green fluorescent protein (GFP) or to the functional domain of Sup35, causing a defect in terminating translation followed by protein oligomerization, or were directed to the secretory pathway, causing cytotoxicity in yeast cells. Similar models have been developed for studying α-synuclein (α-syn) expressing multiple copies of α-syn that t demonstrated a gene dosage-dependent α-syn aggregation, interfering with a broad range of cellular processes to exert its toxicity. These models have been useful to identify compounds of therapeutic potential that also showed promise in animal and/or clinical trials, thus confirming the translational relevance of the yeast-based assays. However, none of these studies have addressed if the aggregation or toxicity witnessed in all these diseases is exclusively driven by amyloid polymerization of the mammalian protein. They all address the consequence of the aggregation pathway rather than a cause of the disease, i.e. initial nucleation of an amyloid/prion. Previous studies have also shown interactions between different mammalian proteins in yeast (e.g. Aβ and PrP, α-synuclein and tau) in yeast that parallel the interactions between these proteins in animals and human brains, and *in vitro*. Yeast models expressing different isoforms or mutated versions of human tau have also provided important insights into their aggregation patterns. The phosphorylation and aggregation of tau using the yeast orthologues of important tau kinases highlighted opportunities for the use of yeast models in studying mammalian amyloids. However, this has not been shown that tau aggregates formed in yeast are of amyloid nature. Our group has previously shown that fusions of Sup35 prion domain to extended polyQ tracts promoted nucleation of the Sup35 protein in the absence of other Q/N rich proteins. This was an important first step in addressing the cause of protein aggregation, i.e. initial nucleation. However, it has not been performed systemically for non-Q/N rich proteins primarily formed by a sporadic protein misfolding event. Moreover, there are no models for studying a prion formed and propagated exclusively by

a mammalian protein in yeast. Overall, a yeast system allowing for controlled monitoring and detection of switches between amyloid and non-amyloid forms, that is necessary for studying initial amyloid nucleation and strain formation/propagation by mammalian proteins is currently lacking.

1.2 Mammalian amyloidosis and disease-related proteins

Protein misfolding in humans and animals have been linked to more than 40 diseases, some of which are fatal and incurable. They include neurodegenerative disorders Alzheimer's disease (AD), Parkinson's disease (PD), transmissible spongiform encephalopathies (TSEs), Huntington's diseases (HD), as well as systemic disorders such as type II diabetes (T2D) and glaucoma[1,2,3]. These diseases are typically associated with atleast one protein or peptide that misfold to acquire an amyloid state, in which they form elongated cross-β fibrous polymers, that are found in tissues or organs where the disease-specific damage occurs[1].

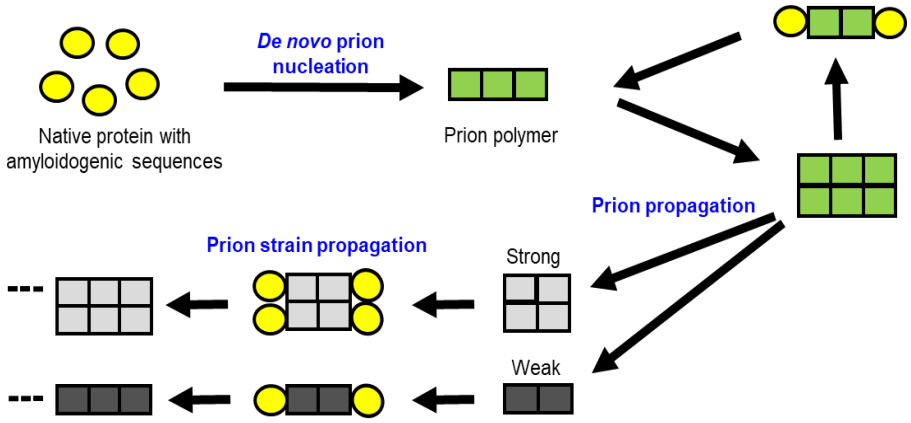

Figure 1-1. Pathway of amyloid/prion replication by nucleated polymerization. A soluble native or unfolded protein with amyloidogenic sequences undergoes a conformational conversion via nucleation and self-assembles to form a prion polymer with monomer addition to the nuclei. The prion polymer is propagated into a range of different aggregated forms or strains exhibiting different replication and propagation properties (based on ref. 4).

Most of these diseases are associated with the sporadic formation of amyloids, with a small exception of familial cases. The relationship between protein misfolding and amyloid formation followed by disease in the pathogenesis of protein misfolding diseases was first demonstrated by postmortem histopathological studies showing a hallmark feature *of* each disease is the accumulation *of* amyloid deposits composed of a different protein[5]. This was confirmed by genetic studies showing mutations in the genes that encode the proteins forming the aggregates to be transmitted by inheritance[6]. These inherited mutations which resulted in an early onset and a more severe disease than in sporadic cases, were also found to be associated with a higher burden of amyloid aggregates[6]. Among protein misfolding diseases, TSEs are a rare group of invariably fatal neurodegenerative disorders that are caused by the abnormal accumulation of infectious amyloids called prions. It is the transmissibility of prion disorders which distinguishes TSEs from other protein misfolding diseases[2]. Some examples of amyloid and prion diseases along with their associated proteins are shown (Table 1-1) and discussed below.

Table 1-1. Amyloid/prion diseases and their associated proteins

AMYLOID DISEASES	**DISEASE-ASSOCIATED PROTEIN**
Alzheimer's disease (AD)	Amyloid beta (Aβ) and/tau
Parkinson's disease (PD)	α-synuclein
Type 2 diabetes	Amylin
Glaucoma	Myocilin
Huntington's disease (Polyglutamine diseases)	Huntingtin
Transmissible Spongiform Encephalopathies (TSEs) – prion disease	Prion protein (PrP)

1.2.1 Alzheimer's disease (AD) and amyloid-β

AD is typically reported as the 6th most frequent cause of death in the United States[7]; however, this is certainly an underestimate, as AD was routinely underdiagnosed in the past, and a significant portion of Americans over the age of 65 are dying from complications caused by AD. Therefore, estimates evaluating AD as the 3rd most frequent cause of death in the United States, and possibly in other developed countries with a long life-expectancy are likely to be more realistic. Moreover, the healthcare costs related to dementias (i.e. mostly to AD) are estimated at the level of $259 billion in the year 2016[8], and AD is one of the major factors affecting the quality of life at an advanced age[9]. The most common form of AD is late onset AD (patient age greater than 65 years), while early-onset AD, typically familial cases, accounts for approximately 1% to 6% of all cases (patient age between 30 to 65 years). More than 90% of AD cases appear to be sporadic and usually with a late onset age[10]. The brains of Alzheimer's disease (AD) patients are characterized by the presence of amyloid plaques and neurofibrillary tangles (NFTs) as diagnostic hallmarks.

Amyloid beta (Aβ) - Amyloid plaques are caused by the aggregation of Amyloid beta (Aβ), a peptide that is generated through the cleavage of amyloid protein precursor (APP) by β-secretase and γ-secretase[11](Figure 1-2). The cleavage products are extremely hydrophobic peptides that include Aβ1-40, Aβ1-42, and Aβ1-43, with the last two being more prone to aggregation and more neurotoxic while the former is found in greater concentrations in familial AD when compared to the latter. Although the classical view is that Aβ is deposited extracellularly, emerging evidence from transgenic mice and human patients indicate that intracellular accumulation of Aβ in the neurons precedes the formation of extracellular Aβ[12]. Moreover, the extracellular form can re-enter the neuronal cells and damage them.

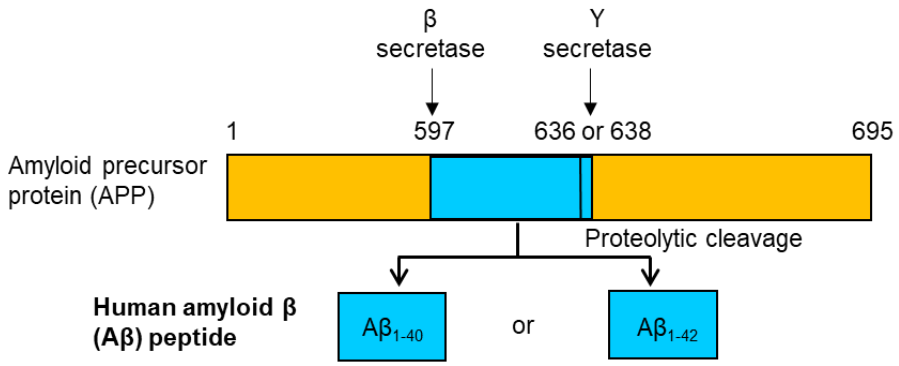

Figure 1-2. Structural organization of human Amyloid beta (Aβ) peptide. Aβ peptide is a product of an abnormal proteolytic cleavage of Amyloid precursor protein (APP) by β and γ secretases to produce two isoforms – Aβ1-40 and/ Aβ1-42.

Mutations in Aβ - APP mutations falling within the Amyloid beta (Aβ) sequence lead to a wide range of disease phenotypes, associated with familial AD (FAD). These amino acid substitutions have been reported to increase the amount of Aß produced, increase the ratio of Aß42 to Aß40, increase the aggregation potential of the mutant Aß variant, or promote the formation of particularly toxic conformations of aggregates, such as oligomers. E.g. FAD Aβ mutations, such as the Italian (E22K) and Arctic (E22G) mutations[13], are believed to exert their pathogenic effects by inducing the formation of stable oligomers and protofibrils. FAD mutations, like E22G and Iowa (D23N[14]), that cluster at residues 21-23 lead to familial cerebral amyloid angiopathy (CAA), a disease distinct from AD characterized by microhemorrhages and often, premature death. The A21G mutation is another CAA-causing FAD mutations that increases total Aβ production in addition to causing biochemical and structural alterations in Aβ. One of the most interesting features of the FAD mutations within the Aβ sequence is that they lead to remarkable phenotypic diversity reminiscent of prion strain polymorphisms. There is increasing evidence that distinct amyloid structures distinguished by amyloid conformation dependent monoclonal antibodies have similarly distinct roles in pathology. It is possible that this phenotypic diversity of FAD associated with mutations within the Aβ sequence is

due to differences in the conformations adopted by mutant Aβ peptides[13], but the effects of FAD mutations on aggregation kinetics and conformational and morphological changes of the Aβ peptide are poorly defined.

Tau is another protein associated with AD. Tau is a major microtubule-associated protein present in mature neurons. Microtubules are involved in the intracellular transport of proteins and organelles. Additionally, they interact with proteins such as actin and signaling molecules. Therefore tau, through its interaction with microtubules, actin, and other molecules, can potentially have a significant effect on various cellular processes[15]. The phosphorylation of tau modulates its microtubule binding affinity and in doing so regulates the morphology of neurons and intracellular transport. However, the hyperphosphorylation of tau depresses this biological activity of tau. In Alzheimer disease (AD) and a family of related neurodegenerative diseases, called tauopathies, tau protein is abnormally hyperphosphorylated and aggregated into bundles of filaments that is polymerized into paired helical filaments (PHF), forming neurofibrillary tangle which are intracellular tau aggregates in AD brains[15].

Mutations in tau - The neuronal inclusions of AD are the defining neuropathological characteristic of frontotemporal dementias as well. The discovery of mutations in the tau gene in familial frontotemporal dementia and parkinsonism linked to chromosome 17 (FTDP-17) has provided a direct link between tau dysfunction and dementing disease[15]. Known mutations produce either a reduced ability of tau to interact with microtubules, or an overproduction of tau isoforms with four microtubule-binding repeats. This leads in turn to the assembly of tau into filaments similar or identical to those found in AD brains. Several missense mutations also have a stimulatory effect on heparin-induced tau filament formation. Assembly of tau into filaments may be the gain of toxic function that is believed to underlie the demise of affected brain cells. Tau mutations in FTDP-17 are missense

mutations that are located in the microtubule-binding repeat region or close to it[16]. Mutations in exon 9 (G272V), exon 12 (V337M), and exon 13 (R406W) affect all six tau isoforms. By contrast, mutations in exon 10 (N279K, ΔK280, P301L, P301S and S305N) only affect tau isoforms with four microtubule-binding repeats or their expression[16]. Most missense mutations reduce the ability of tau to interact with microtubules, as reflected by a marked reduction in the ability of mutant tau to promote microtubule assembly

The amyloid cascade hypothesis - The amyloid cascade hypothesis (Aβ hypothesis) suggests a causal role of amyloid peptides in AD etiology that has been the mainstream explanation for the pathogenesis of AD for over 25 years[17]. Accumulating experimental evidence in *in vitro* models, *in vivo* models, and from biomarkers analysis in patients supports the amyloid cascade and particularly Aβ-induced tau-pathology. While the hallmark pathology of AD is extracellular Aβ deposits and intracellular tau tangles (Figure 1-3), several studies suggest that intracellular Aβ[12] precedes extracellular Aβ, since intraneuronal Aβ accumulation commonly precedes its extracellular deposition in AD brains and transgenic mice models of AD[17].

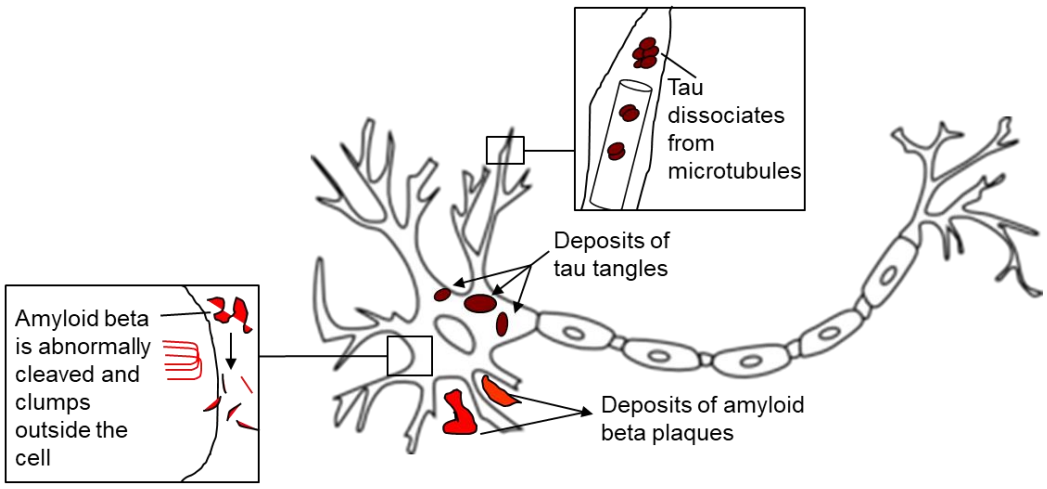

Figure 1-3. A diagrammatic representation of a neuron in an AD brain. Extracellular and intracellular formation of Amyloid beta plaques and intracellular formation of neurofibrillary tau tangles (refer [17]).

Also, an accumulating body of evidence has indicated that soluble forms of Aβ and tau work together, independently of their accumulation into plaques and tangles[12], to drive healthy neurons into the diseased state and that the hallmark toxic properties of Aβ require tau. Therefore, the most likely scenario is that, Aβ is upstream of tau in AD pathogenesis and triggers the conversion of tau from a normal to a toxic state, but there is also evidence that toxic tau enhances Aβ toxicity via a feedback loop. Most importantly, the soluble toxic aggregates of Aβ and tau can self-propagate and spread throughout the brain by prion-like mechanisms[17]. Thus, successful therapeutic intervention for AD would benefit from an initial detection of Aβ before the formation of plaques, tangles, and cognitive impairment become evident. Also, the neurofibrillary degeneration of the Alzheimer type is primarily seen in human neurodegenerative disorders, but it is sparsely seen in aged and in cognitively impaired animals, thus highlighting an urgent need for cell-based or *in vitro* models to study tau aggregation.

1.2.2 Transmissible spongiform encephalopathies (TSEs) and PrP

Transmissible spongiform encephalopathies (TSEs), also called as prion diseases, are a group of neurodegenerative disorders which have in common the formation of amyloid plaques. Different variants of TSE exist in many mammalian species. In humans, five different prion diseases have been reported to date: Kuru, Gerstmann-Straüssler-Scheinker Syndrome (GSS), Fatal Familial Insomnia (FFI), Creutzfeldt-Jakob Disease (CJD), and Variably Protease-sensitive Prionopathy (VPSPr)[18]. Each variant presents with distinct clinical signs and a different prion accumulation pattern in the brain. Besides human prion diseases, the best-known examples due to the number of affected animals are: Scrapie in sheep and goat, Transmissible Mink Encephalopathy (TME), Bovine Spongiform Encephalopathy (BSE), and Chronic Wasting Disease (CWD) in cervids. In the case of TSEs, the epidemics of “mad cow” disease led to huge losses in the European

cattle industry[20]. Similar to other neurodegenerative diseases, prion diseases include three forms: sporadic, familial and acquired by infection.

Prion protein, PrP - The amyloid plaques in TSEs are caused by the accumulation of an infectious prion protein (PrP). PrP is a cell surface protein consisting of a flexibly disordered N-terminal segment (residues 23-120) and a structured C-terminal domain (121-231) (Figure 1-4)[18]. The cellular form of PrP (PrP^C) is converted to the disease-associated form, known as PrP scrapie (PrP^{Sc}) in the central nervous system (CNS). The misfolding of PrP^C to PrP^{Sc}, leads to neuronal damage and is invariably fatal. Unlike PrP^C, PrP^{Sc} is an insoluble protein, mainly composed by β-sheet structures, partially resistant to proteolysis, with a high propensity to form amorphous and amyloid aggregates. In humans, the residues 90 to 230 of PrP^{Sc} form a structured, protease-resistant core. Depending on the infection portal of entry, the origin of the exogenous infectious prion agent, or the presence of a mutation, the form of prion diseases caused by PrP infection, may display distinct phenotypes called prion strains linked to the conformational diversity of PrP^{Sc} and they correspond to different pathological features[18].

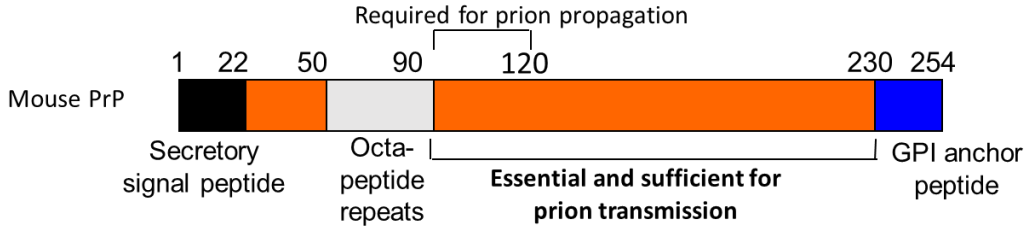

Figure 1-4. Structural organization of mouse mammalian prion protein (PrP). The signal peptide (1-22) is cleaved after translocation of PrP, N-terminus (23-120) is disordered, C-terminus of PrP (121-231) is structured, GPI (glycophosphatidyl-inositol) is a membrane anchor.

Mutations in PrP – Mutations in PrP are predominantly clustered within the C-terminal globular domain. Two stop mutations have been observed in patients that result in a

truncated version of PrP- Y145stop and Q160stop[20] of the human prion protein (huPrP23–144), that lacks almost the whole structure C-terms regions and are associated with a hereditary amyloid disease known as PrP cerebral amyloid angiopathy. The largely missing C-terminal globular domain is required to import the complete PrP into the ER, thus retaining the truncated PrP in the cytosol, leading to an increased aggregation[21]. Mutations within the globular domain are believed either to destabilize PrP^C and increase its propensity to misfold or to promote the formation of a toxic intermediate conformer during misfolding[21]. Alterations in the octapeptide repeat region within the unstructured N-terminal domain are believed to alter copper and glycosaminoglycan binding affinities[23]. However, the process by which mutations outside these regions of PrP lead to pathogenesis is unclear, and it has been shown that one common pathogenic mutation outside the globular region, P102L, has no effect on the stability of PrP. The difficulties and costs associated with the maintenance, long incubation periods related to interspecies transmission barriers and an inability to adapt and study certain prion strains has significantly hindered progress in TSE research despite the advances achieved using naturally susceptible animal models. Moreover, the sequence elements or regions that control the aggregation patterns of wild type and mutant PrP initiating the conversion of PrP to a scrapie form are unknown. This indicates an opportunity for cell-based PrP models to be employed for further elucidation. Also, a system for the identification of PrP mutations associated with pathogenic isoforms may have therapeutic potential.

1.2.3 Parkinson's disease (PD) and α-Synuclein

Parkinson's disease (PD) is the second most common neurodegenerative disorder, prevalent in 1% of the population over the age of 60 and is defined as one of the synucleinopathies. PD is characterized by the relatively selective loss of dopaminergic neuronal cells and by the presence of intraneuronal inclusions, known as Lewy bodies or

Lewy neurites in surviving neurons, which are considered the hallmark of PD pathology[11]. The main component of these abnormal aggregates was found to be a presynaptic protein called α-synuclein (α-syn), encoded by the gene *SNCA*, suggested to regulate neurotransmission[11].

α-synuclein - α-Syn is a 140-amino acid protein of predominantly presynaptic localization in neurons, although it is ubiquitously expressed. It is comprised of 3 domains, (1) an N-terminal lipid binding α-helix, (2) a non-amyloid ß component (NAC) domain and (3) an unstructured C-terminus. All three regions are important for the misfolding of α-syn, a process critical for the induction of synucleinopathies[11]. α-Syn is primarily a natively unfolded cytosolic protein and binds to membranes via its N-terminal α-helix, upon which it adopts an α-helical structure. It is also on the membrane that α-syn can misfold and begin to form aggregates. When misfolding occurs, the random coil of the NAC region forms β-sheets, leading to protofibril and fibril formation. The C-terminus plays a role in inhibiting this fibril formation, but also contains phosphorylation sites, of which hyperphosphorylation at S129 (pS129) is associated with α-syn pathology.

Mutations in α-syn - Both mutations and duplication or triplication in *SNCA* cause autosomal dominant forms of PD and are the basis of the risk of developing sporadic PD, strongly implicating α-syn in PD pathogenesis[23]. The α-syn present in Lewy pathology exhibits a conformational change from the native soluble protein to an insoluble, fibrillar form, rich in β-pleated sheets. Recent studies suggested that the misfolding of *α*-synuclein causes it to aggregate and spread in certain sites, where the inflammation induced by it is intimately involved in the pathogenetic dysfunction underlying PD[24]. All of this indicates that *α*-synuclein plays a central role in the pathogenesis of PD.

Prion-like behavior of α-syn - Most importantly, α-syn aggregates arise first in the brainstem and then spread to telencephalic structures, a dynamic that is indicative of prion-like spread of protein aggregation. Numerous studies have shown cell-to-cell transmission of soluble or aggregated α-syn, both in cultured cells and in mouse brains, resulting in α-syn aggregation and neuronal dysfunction in the recipient cells. Importantly, injections of synthetic (human or mouse) α-syn fibrils also induce the recruitment of endogenous soluble α-syn protein to form LB-like pathology and neuronal degeneration in primary cell culture and in non-transgenic (wild type) host mice[24]. Moreover, it has also been shown that two different α-syn polymorphs (fibrils and ribbons) exhibit marked differences in their propensity to penetrate the cells, as well as in their toxicity and seeding aggregation in cells, suggesting the existence of different α-syn strains, thus demonstrating a prion-like propagation of pathological α-syn in brain, similar to prion diseases. Though, α-syn has been shown to propagate, the observation of subsequent seeding has proved to be challenging, owing to difficulties in modeling seeding experiments in cell culture or animal models.

1.2.4 Type 2 diabetes (T2D) and amylin (IAPP)

T2D is a complex metabolic disease characterized by chronic insulin resistance, progressive loss of β-cell function and β-cell mass, which leads to impaired insulin release and hyperglycemia. Genetic and environmental factors are believed to predispose some individuals (~20% of the population) to β-cell failure under conditions of chronic insulin resistance. Accumulating evidence suggests that toxic aggregates of IAPP may contribute to β-cell dysfunction and disease[25, 26].

Amylin – T2D, associated with Islet amyloid polypeptide (IAPP) is a 37-residue peptide hormone, also known as amylin, co-secreted with insulin by the endocrine β-cells of the

pancreas. More recently, it has been established that islet amyloid deposits are present in over 90% of T2D patients25. Similar to AD and PD, IAPP aggregates can also be observed in non-diabetic individuals, indicating that aged individuals free of T2D disease symptoms might be in process of developing the disease. Several studies have linked IAPP aggregation with β-cell loss and progression of T2D. A mutation in the IAPP gene that elevates its aggregation propensity is associated with early induction of T2D[25].

In addition to the recognized amyloidogenic region, human IAPP (hIAPP) 20–29, the peptides human or rat IAPP 30–37 and 8–20, assume β-conformation and form fibrils. These three amyloidogenic regions of hIAPP can be modelled as a folding intermediate with an intramolecular β-sheet. Although intracellular fibrils have been identified in experimental systems, extracellular deposition predominates in animal models and man. Extensive fibril accumulations replace islet cells[26]. The cause and origin of IAPP aggregation is yet to be explored in detail.

1.2.5 Glaucoma and myocilin

Glaucoma is a term used to refer to a heterogeneous group of optic neuropathies that cause a progressive loss of vision. It is a prevalent disease (occurring in 1–2% of the world population over the age of 40 years) and a leading cause of blindness in the world. Many glaucoma cases are hereditary, and this fact has resulted in the application of genetic methods to investigate the pathogenic mechanisms of the disease at the molecular level[3].

Myocilin - Mutations in the glaucoma gene, *MYOC*, are responsible for the development of juvenile open-angle glaucoma and a subset of adult-onset primary open angle glaucoma[27]. The *MYOC* gene encodes a 57-kDa protein known as myocilin. Myocilin is a secreted 55-57 kDa glycoprotein that forms dimers and multimers. Characteristic

structural motifs include a myosin-like domain, a leucine zipper region and an olfactomedin domain. Most of the mutations that have been identified in patients with POAG are localized in the olfactomedin domain, which is highly conserved among species. Myocilin is found as discrete intracellular particles surrounding the trabecular meshwork cell nucleus. It is secreted into tissue culture media and is also associated with the extracellular matrix. Although no alternative splice variants of myocilin have been reported, there are several posttranslational modifications of myocilin that give rise to four or more isoforms of the myocilin protein. Increased myocilin expression has been detected in the TM of patients with several different types of glaucoma[28].

Mutations in myocilin - Emerging evidence supports the hypothesis that the autosomal-dominant early-onset form of glaucoma is caused by genetic defects in myocilin. Wild-type (WT) myocilin has been associated with steroid-induced glaucoma, and myocilin isoforms/variants have been linked to early-onset, inherited glaucoma. Elevated levels and aggregation of myocilin hasten increased intraocular pressure and glaucoma-characteristic vision loss due to irreversible damage to the optic nerve. Full-length mutant myocilin expressed in mammalian cells forms intracellular amyloid-containing aggregates, like WT and mutant myocilin (P370L)[29]. The WT and mutant amyloid fibrils, grown under a variety of conditions in a nucleation-dependent and self-propagating manner, localized to the C-terminal olfactomedin (OLF) domain. Full-length mutant myocilin expressed in mammalian cells forms intracellular amyloid-containing aggregates as well. The molecular properties of the highly conserved OLF domain suggests a novel protein-based hypothesis for glaucoma pathogenesis. A systematic study of the molecular properties of the highly conserved OLF will lead to new insights in amyloid formation by myocilin, in the context of protein-based inheritance.

1.2.6 ***Polyglutamine (polyQ) diseases and Huntingtin***

Polyglutamine (polyQ) diseases are neurodegenerative disorders, encompassing at least nine heritable disorders, including Huntington disease (HD) and the spinocerebellar ataxias SCA1, SCA2, SCA3, SCA6, SCA7 and SCA17. Each of these disorders results from the expansion of a CAG repeat, coding for a glutamine tract (polyQ) that is present in the wild-type protein[30].

Huntingtin - In healthy individuals the polyQ tract varies between 35–50 repeats, depending on the disease. In patients or carriers, the polyQ tract reaches above 40 and often over 100 glutamines. These repeat expansion mutations are unstable, resulting in changes in repeat length between generations as well as between different cells and tissues of the same person. PolyQ expansion causes huntingtin, associated with HD, to acquire an unusual conformation, which facilitates their aggregation into intracellular inclusion bodies and causes cell toxicity. Recombinant proteins with an expanded polyQ stretch (51–122 glutamines) were found to form insoluble high molecular weight protein aggregates *in vitro*[31]. Electron micrographs of these aggregates revealed fibrillar structures with a morphology closely resembling that of scrapie prion rods and β-amyloid fibrils in AD[30]. These observations have shown that huntingtin could be the result of toxic amyloid fibrillogenesis, as has been proposed for AD.

1.3 Yeast amyloids and prions

Amyloids also manifest in yeast and other fungi as endogenous infectious proteins called “prions”, that are heritable via the cytoplasm (non-Mendelian inheritance). To simplify the process of monitoring amyloid formation and propagation, the high-resolution power of yeast genetics tools significantly aids in amyloid characterization, and connection of yeast to detectable phenotypic traits simplifies amyloid monitoring[32]. Yeast prion proteins

contain so-called prion domains (PrDs) that are entirely responsible for the intermolecular interaction leading to the formation of an amyloid axis, and are, at least in some cases, distinct from domains responsible for the major cellular functions of the same proteins[32]. Yeast PrDs are generally unrelated to the major cellular function of a protein and typically contain a QN-rich sequence (Figure 1-5). Some yeast prions control easily detectable phenotypic traits, typically resulting from a partial loss of the cellular function of a protein because of its incorporation into prion polymers[32].

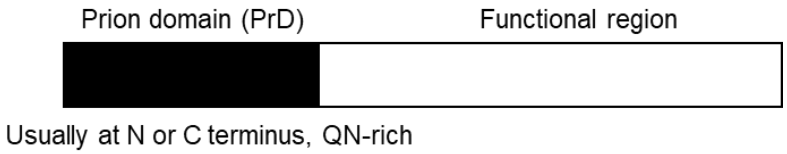

Figure 1-5. An example of a typical yeast prion protein. The prion domain (PrD) denotes the glutamine/asparagine-rich regions (shaded in figure) that is located at the terminal ends of proteins, followed by a functional region that is responsible for the cellular function of the protein (based on ref. 32).

Many phylogenetically unrelated prions, some of them with the potential to impact a wide range of cellular processes, have now been described in *S. cerevisiae* (Table 1-2)

Table 1-2. Examples of yeast prion proteins and their functions

Protein	Prion	Protein function
Sup35	[*PSI*$^+$]	Translation termination
Rnq1	[*PIN*$^+$]	Not known
Mod5	[*MOD*$^+$]	tRNA modification enzyme
Swi1	[*SWI*$^+$]	Subunit of chromatin remodeling complex
Lsb2	[*LSB*$^+$]	Endocytosis/ actin cytoskeleton polymerization

1.3.1 Sup35 protein and [PSI$^+$]

The most well-characterized yeast prion forming protein is the translation termination factor, Sup35 (eukaryotic release factor eRF3), denoted phenotypically as [*PSI*$^+$] in its prion form. Sup35 consists of three domains – a Q/N-rich and oligopeptide repeat containing prion domain in the N terminus, a middle domain rich in charged residues, and a C terminus domain that is essential for Sup35 protein function (Figure 1-6)[32]. When Sup35 exists in its prion conformation, it forms insoluble aggregates, rendering it non-functional, resulting in an increased readthrough of nonsense codon in a specifically designed yeast strain with a premature stop codon (Figure 1-6)[32]. [*PSI*$^+$] can be phenotypically monitored using specially designed yeast strains and appropriate media[32]. It also forms amyloid fibers *in vitro* when seeded with amyloid aggregates mimicking the conformational conversion of prion proteins[32] *in vivo*, thus providing us a model to study a wide range of amyloidogenic proteins and their prion behavior in a controlled manner.

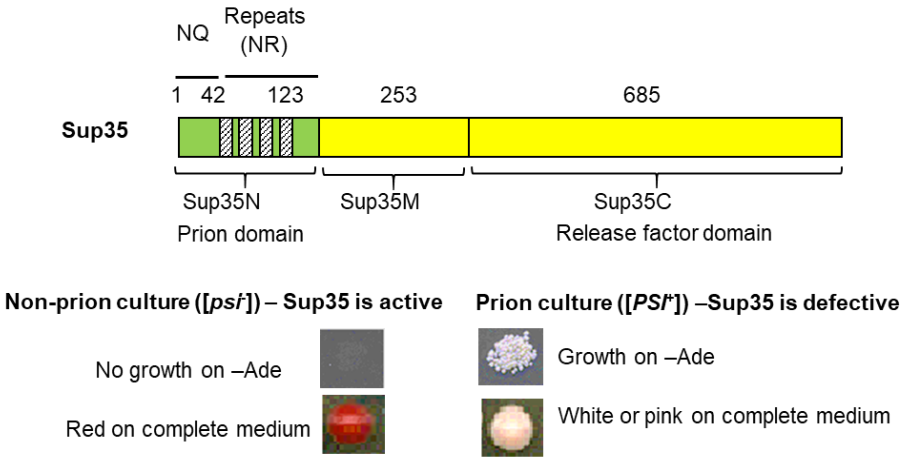

Figure 1-6. Structural and functional organization of the yeast prion protein, Sup35. N, M and C refer to Sup35N, Sup35M and Sup35C regions respectively. Numbers correspond to amino acid positions (not to scale). NQ and NR in Sup35N region refers to asparagine, glutamine rich region and oligopeptide repeat region respectively. In yeast strains containing *ade1-14* (UGA) reporter, defect of translational termination caused by [*PSI*$^+$] is detectable by growth on –Ade medium or color on YPD medium, due to accumulation of a red pigment, an intermediate in adenine biosynthesis (based on ref. 32).

1.3.2 De novo formation of [PSI$^+$]

Using yeast models, it was demonstrated that *de novo* prion nucleation is quite rare but *de novo* prion formation by transiently overproduced prion protein can be facilitated by other non-homologous aggregated QN-rich protein(s)[33,34,35,36]. However, an efficient prion induction by overproduced Sup35 protein or its PrD requires the presence of another prion, usually [*PIN*$^+$] (or [*RNQ*$^+$]), a prion form of Rnq1 protein[37,38]. It was proposed that Rnq1 prion polymers nucleate the initial assembly of the Sup35 polymers (Figure 1-7). A transient direct association between Rnq1 polymers and Sup35 appears likely as the prion domains of both these proteins are rich in Q, N residues. This is true for a majority of other yeast prion proteins, and the presence of the other (in most cases, QN-rich) protein in an aggregated form was shown to reproduce the effect of Rnq1 prion on [*PSI*$^+$] induction.

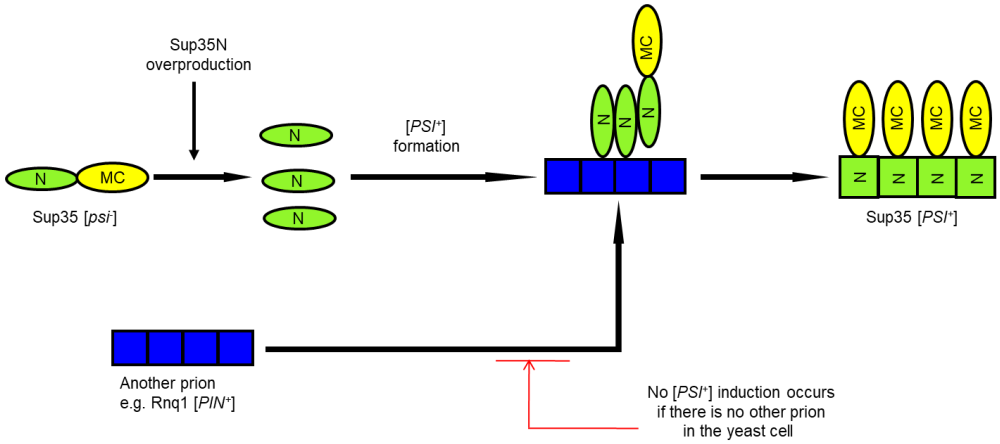

Figure 1-7. *De novo* [*PSI*$^+$] nucleation by overproduction of Sup35 (or N or NM). The spontaneous nucleation of [*PSI*$^+$] is rare but the overproduction of Sup35 or Sup35N can induce *de novo* [*PSI*$^+$] formation, facilitated by the presence of another prion, e. g. [*PIN*$^+$], the prion isoform of Rnq1 (based on ref. 32).

De novo prion formation by transiently overproduced prion protein is also enhanced by actin cytoskeletal structures that are physically associated with aggregates of some overproduced prion-forming proteins. The simultaneous overproduction of Lsb2, a yeast

short-lived yeast cytoskeletal protein that is triggered by stress, and Sup35, could nucleate [*PSI*$^{+}$] *de novo*, in the absence of pre-existing [*PIN*$^{+}$][40].

*1.3.3 [*PSI^{+}*] propagation by Hsp104*

Misfolded proteins are recognized by molecular chaperones that facilitate their folding into native states, as specified by their primary sequence. The chaperone, Hsp104, is a homohexameric AAA ATPase, that is required for induced thermotolerance. In the context of prions, Hsp104 is required for the propagation of [*PSI*$^{+}$][41]. The levels of Hsp104 expression is crucial for [*PSI*$^{+}$] propagation; either an overproduction or a deletion of Hsp104 eliminates [*PSI*$^{+}$], and only a transient overproduction of Hsp104 is sufficient to eliminate [*PSI*$^{+}$], and when the normal levels of Hsp104 level is established, the prion state does not reappear[41]. The proposed mechanism of [*PSI*$^{+}$] elimination by Hsp104, called curing, is by breaking [*PSI*$^{+}$] fibers into smaller prion seeds that can efficiently promote the prion conversion of monomeric or newly synthesized Sup35. When Hsp104 levels are depleted, the larger prion fibers are not fragmented into prion seeds, and thus inefficiently transmitted to daughter cells. On the other land, an excess of Hsp104 can disaggregate amyloid fibers rapidly to a degree that most of the Sup35 proteins are monomerized and easily refolded into their native conformations or degraded by the ubiquitin/proteasome pathway[41]. The efficiency of polymer fragmentation by chaperones relative to polymer growth explains phenotypic differences between prion variants[32]. The polymers of strong [*PSI*$^{+}$] variants are readily fragmented and therefore produce a larger number of prion units per cell. As the functional ends of prion polymers are active in attracting new protein molecules to the polymers, a larger number of polymers results in the more efficient immobilization of newly synthesized Sup35 protein into polymers. In contrast, polymers of weak [*PSI*$^{+}$] variants are less efficiently fragmented, resulting in fewer polymer ends and less efficient capture of new Sup35 molecules[32]. Thus, weaker [*PSI*$^{+}$] variants are

characterized by a larger average polymer size and a higher proportion of non-aggregated Sup35, causing lesser nonsense suppression in [*PSI*$^{+}$] phenotypic assays, compared to stronger [*PSI*$^{+}$] variants (Figure 1-8).

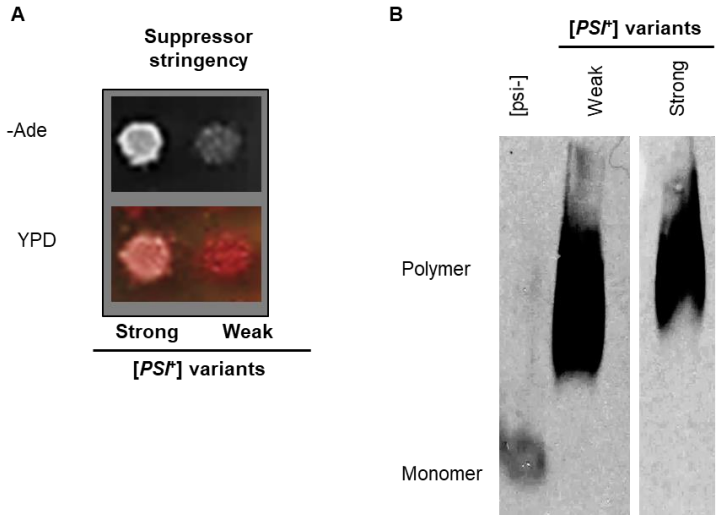

Figure 1-8. Phenotypic and biochemical differences in [*PSI*$^{+}$] variants. (A) Prion variant strength can be measured by color on YPD or by suppression on media lacking adenine. (B) A smaller average size of SDS-resistant prion polymers, uncovered by semi-denaturing detergent agarose gel electrophoresis, generally correlated with a stronger prion phenotype than a weaker or intermediate prion phenotype (images belong to the same gel and were cropped for a better demonstration).

*1.3.4 [*PSI^{+}*] propagation by infection with prion aggregates*

The proof for protein-only hypothesis for prion propagation was first demonstrated in fungal proteins, Sup35, apart from another prion protein HET-s in the fungus *Podospora anserine.* Purified prion aggregates were added to yeast cells to cause infection with the prion[32]. Since [*PSI*$^{+}$] could also be induced *de novo* by the overexpression of Sup35 or its domains, specific prion variants were used to generate amyloid fibers at different temperatures, indicative of distinct conformations. After the amyloid aggregates were transfected into [*psi*$^{-}$] yeast, they produced the corresponding variants of [*PSI*$^{+}$] used for

transfection[32]. Thus, taking all of this into account, it can be conclusively said that yeast models employing Sup35 have been successful in delineating the molecular mechanisms leading to [*PSI*$^{+}$] nucleation and propagation in yeast using different phenotypic and biochemical methods.

1.4 Yeast models for amyloid nucleation and propagation

Yeast is a powerful model eukaryotic cell for studying the fundamental cellular processes and protein functions that are also associated with complex multicellular eukaryotes such as humans. The basic mechanisms and pathways underlying neurodegenerative diseases such as transcriptional dysfunction, defect in trafficking, defect in clearance pathways such as proteasome or autophagy, mitochondrial dysfunction, transcriptional dysregulation etc., are highly conserved between yeast and human species and have been studied for many years. The universal problem of protein misfolding and its consequences also affect yeast and by its genome and shared attributes to human cells, yeast can be easily manipulated to investigate the role of prions and heritable amyloids associated with mammals and humans. As described above, yeast is specifically pliable for studying protein-based inheritance because endogenous yeast prions follow a pattern of non-mendelian inheritance, like mammalian prion protein, PrP, associated with TSEs[32]. Thus, the basic molecular events involved in these processes can be studied in simple organisms such as yeast[42]. For modeling human amyloid diseases in yeast, the yeast homolog of the gene implicated in the disease is directly studied for its function. For human genes that have no yeast homologs, they are heterologously expressed in yeast and phenotypically characterized. These two approaches have been used successfully to perform a functionally or phenotypically analyze human disease genes in yeast[43]. Some of the yeast models that have helped in a better understanding of amyloid/prion formation and propagation in various amyloid diseases are discussed briefly as follows:

Table 1-3. Summary of some yeast models for studying amyloid aggregation by mammalian proteins

MECHANISM	YEAST MODEL	ADVANTAGES	SHORTCOMINGS
Aβ aggregation, toxicity, and interactions with other proteins	Aβ40 or Aβ42 fused to GFP[44] or Sup35MC[45], MBP fused to Aβ42[46,] deletions of genes encoding AD susceptibility gene[48,] FRET analysis between Aβ,PrP[49]	Identified 2 drugs and reproduced data in animal models. Identified clathrin-mediated endocytosis as a target for Aβ toxicity	Fusions to GFP are toxic by itself, and produced a non-functional aggregated protein complex that cannot be used for studying amyloid formation. They do not address Aβ polymerization
Tau phosphorylation, toxicity, aggregation	Deletion of kinases (Δ*mds1* and Δ*pho85*)[50], co-expression of tau and α-synuclein[51], expression of FTDP-17 mutants[52]	Reproduced tau pathology in yeast. Demonstrated common mechanisms of aggregation and toxicity between tau and α-syn	It was not checked if the process if associated with a loss of a cellular function of tau or tau polymerization
Structural determinants of mouse PrP residues, propagation by PrP	Altered Sup35 with PrP insertions between N and M domains[55] PrP fused to Sup35MC (*I*C)[53,54]	Identified phenotypes, independent of Hsp104. Confirmed that oligopeptide repeat region of Sup35 is essential for [*PSI*$^+$] propagation	It had low rates of switching from non-amyloid state to a heritable amyloid state, thus not pliable for studying propagation
α-synuclein (α-syn) toxicity and clearance	α- syn fused to GFP/ eGFP [56,60] in yeast mutants[59], screening protein mediators of α-syn cytotoxicity[57]	Demonstrated that α-syn interferes with a broad range of cellular processes to exert its toxicity. Identified suppressors and enhancers of α-syn toxicity	It was not checked if the processes associated with α-syn toxicity is associated with α-syn polymerization
Polyglutamine (PolyQ) aggregation and modulation/ clearance	Fusions of Sup35 to polyQ of different lengths or Rnq1[61,62], polyQ expressed in the presence of [*PIN*$^+$][63] or attached to proline region[64]	Promoted nucleation of the Sup35 protein in absence of other Q/N rich proteins. Proved that polyQ toxicity is controlled by prion composition and gene dosage in yeast	This has not been done so far for non-Q/N-rich proteins in yeast

While proteins are the cause of these amyloid diseases and the mechanisms leading to the initial formation (nucleation) of these amyloids and their continuous spread (propagation) of the infection remains unclear. The long asymptomatic period in disease development has made it difficult for traditional experimental assays to identify pharmaceuticals that can target the initial nucleation of an amyloid or identify environmental factors associated with the increased/decreased incidence of these diseases. Therefore, prophylactic strategies to prevent nucleation or propagation of amyloids are essentially non-existent.

1.5 Objectives

The overall objective of this work is to establish yeast-based models for both 1) initial prion nucleation by mammalian proteins (or domains) and 2) mammalian protein-based prion propagation.

Before this work was started, our lab had established a yeast-based assay for studying the prion properties of mammalian prion protein, PrP. Our objective was to further characterize the sequence elements of PrP that influenced prion nucleation by PrP in yeast. Most importantly, we wanted to use the prion nucleation assay to demonstrate that several non-Q/N rich, human amyloidogenic proteins, could nucleate a prion in yeast in the absence of pre-existing prions. Specifically, we sought to examine the prion properties of Amyloid beta (Aβ) associated with Alzheimer's disease (AD) by performing mutational analyses based on *in vivo, in vitro,* and computational studies for Aβ, to identify the sequence elements of Aβ that controlled prion nucleation by Aβ in yeast. Furthermore, we wanted to demonstrate an application of the assay in the identification of agents that can influence Aβ nucleation in yeast. In the light of many recent studies that indicate the propagation of misfolded mammalian proteins e.g., Aβ and another protein, microtubule

associated binding protein tau in AD, by a prion-like mechanism, we aimed to establish a yeast model for prion propagation by Aβ and tau by checking if they can propagate a prion state on their own or after transfection with *in vitro* generated amyloid seeds. This would confirm the translational relevance of yeast-based assays.

CHAPTER 2. GENERAL MATERIALS AND METHODS

2.1 Materials

2.1.1 Strains

The genotype of *Saccharomyces cerevisiae* strains used in this study are listed in Appendix Table A. Haploid [*PSI*$^{+}$ *PIN*$^{+}$] strains GT81-1C and GT81-1D are meiotic spore clones of the homozygous (except mating type) autodiploid GT81. The [*psi*$^{-}$ *pin*-] strains GT409 and GT197 were obtained respectively from GT81-1C and GT81-1D via curing them of [*PSI*$^{+}$] by guanidinium hydrochloride (GuHCl), while the [*psi*$^{-}$ *PIN*$^{+}$] strain GT159 was obtained via curing GT81-1C of [*PSI*$^{+}$] using excess Hsp104. The *rnq1*Δ strain GT564 was obtained by K. Gokhale in Chernoff lab via replacing the *RNQ1* gene with *the Schizosaccharomyces pombe* ortholog of the *HIS3* gene in the strain GT159. Strain 33G-D373, described previously and containing a double point mutation in the *ADE2* gene, was used for determining the functionality of the Ade2-based chimeric proteins. To make sure that our results are not strain-specific, we also checked [*PSI*$^{+}$] induction by some chimeric constructs in the [*psi*$^{-}$ *pin*$^{-}$] strain GT17 of the 74-D694 genotype (data not shown in thesis). Prototype “strong” (ψ^{+}1-74-D694, or OT56) and “weak” (ψ^{+}7-74-D694, or OT56) strains, obtained as described earlier, were employed for the phenotypic comparisons to [*PSI*$^{+}$] strains, induced by chimeric constructs. GT81-1C and GT409 were employed for the comparisons to [*PSI*$^{+}$] strains induced by chimeric constructs in SDD-AGE experiments. The [*psi*$^{-}$ *pin*-] strain, GT671, was used as the source for all the plasmid shuffle experiments in Chapter 5 and is a haploid derivative of GT81. GT671 contained the *sup35Δ::HIS3* transplacement on the chromosome and was maintained alive by a Sup35-expressing plasmid, pASB2, with the *LEU2* marker.

2.1.2 Plasmids

Appendix Table B provides a list of all plasmids constructed or used for this work together with their descriptions.

2.1.3 Primers

Appendix Table C provides a list of all primers used for this work with their sequences and descriptions.

2.1.4 Enzymes and antibodies

Enzymes used for molecular cloning, PCR, ligation, and site-directed mutagenesis, including restriction endonucleases BamHI, EcoRI, XbaI, NotI, SacI, ClaI, XhoI, PstI, Mung Bean nuclease, Taq and Pfu DNA polymerases, and T4 DNA ligase, were purchased from New England Biolabs. The antibodies to Sup35N and Hsp104 were a gift of S. Lindquist (Whitehead Institute for Biomedical Sciences). Sup35M (4A5) and PrP (4H11) have been described previously. Antibody to HA was purchased from Covance. Antibody to Aβ (6E10, Covance, catalog number SIG 39320) was a gift of L. Walker (Emory University School of Medicine). Antibody to Sup35C was a gift of Dr. D. Bedwell (University of Alabama, Birmingham).

2.2 Genetic and microbiological techniques

2.2.1 Standard yeast media and growth conditions

Yeast cultures were grown at 30°C. Standard yeast media and standard procedures for yeast cultivation, phenotypic, and biochemical analysis were used[68]. Cell counts were performed using a hemacytometer (Brightline). Optical densities of yeast cultures were measured at 600 nm using Shimadzu UV-2450 spectrophotometer. Standard synthetic

medium contains 3 μM copper sulfate ($CuSO_4$); it was supplemented with 10, 50, 100, or 150 μM $CuSO_4$ as indicated to induce higher expression of P_{CUP1} promoter. Synthetic media lacking adenine, leucine, or uracil are designated as –Ade, -Leu, and -Ura, respectively. In all cases when the carbon source is not specifically indicated, 2% glucose (Glu) was used. The synthetic medium containing 2% galactose (Gal) or 2% galactose and 2% raffinose (Gal+Raf) instead of glucose was used to induce the *GAL* promoter. Organic complete YPD medium containing yeast extract (1%), peptone (2%) and glucose (2%) was used for color detection. Organic YPG medium containing glycerol (3%) instead of glucose was used to identify respiratory incompetent (Pet^-) transformants that arose due to loss of mitochondrial DNA during transformation and were eliminated from further analysis. Detection assay for [*PSI*$^+$], based on the readthrough of the *ade1-14* (UGA) allele, that results in growth on –Ade medium and lighter color on YPD medium is described previously[32]. Liquid cultures were grown with at least a 1/5 liquid/flask volumetric ratio in a shaking incubator (200-250 rpm). Yeast transformations were performed according to the standard Li^+ protocol. Curing of [*PSI*$^+$] by guanidine hydrochloride (GuHCl) was performed by incubating cultures for three consecutive passages (approximately 20-40 generations) on YPD plates with 5 mM GuHCl, followed by streaking out on YPD and checking individual colonies by both color and growth on -Ade medium.

2.2.2 Bacterial transformation procedure

Chemicals competent DH5α *E. coli* were transformed using standard laboratory protocols[68].

2.2.3 Yeast transformation procedure

A single yeast colony was inoculated into 5mls YPD and cultured at 30°C with shaking to OD600 = 1.0-5.0. The culture was diluted with 5 ml of YPD and allowed to grow for 2-4 hours as described. Cells were collected using centrifugation at 4000 x g for 5 minutes and were resuspended in 10 mls of Lithium Acetate-TE solution (LiAc-TE) (100 mM lithium acetate, 10 mM Tris-HCl, 1 mM EDTA, pH 8.0) and were grown for 1 hour at 30° C with shaking. Cells were collected and resuspended in 0.5-1 ml LiAc-TE. 100 µl of cells was added to a microcentrifuge tube together with 20 µg carrier DNA and 1-10 µg of plasmid DNA. Tubes were placed on a rotator at room temperature for 30 minutes. 700 µl PEG-LiAc-TE (40% PEG 4000, 100 mM lithium acetate, 10 mM TrisHCl, pH 7.5, 1 mM EDTA) was added, and cells were rotated at room temperature for 1 hour. The sample was heat-shocked for 5 minutes in a 42° C waterbath and was centrifuged at 3000 x g for 5 minutes to pellet the cells. Cells were resuspended in 150 µl water and plated on media selective for the plasmid.

2.2.4 Plate assay for [PSI$^+$] nucleation

To check for [*PSI*$^+$] nucleation in Chapters 3 and 4, plasmids bearing chimeric and control genes under the P_{CUP1} *or* P_{GAL} promoter were transformed into the yeast [*psi*$^-$] strain. For plate assays, transformants were grown on the media. selective for the plasmid (*e. g.* –Ura) containing 2% glucose as a carbon source and a background concentration (3 µM) of Cu^{++}, and then velveteen replica plated onto the same medium with addition of 0, 10, 50, 100 or 150 µM $CuSO_4$ as specified in Figure legends (for P_{CUP1} constructs), or onto the same medium with 2% galactose instead of glucose (for P_{GAL} constructs), to induce expression of the chimeric genes. After induction (usually for 2 days), plates were replica plated to –Ade medium with glucose and without additional $CuSO_4$, where overexpression

was turned over (Figure 2-1). [*PSI*$^{+}$] formation was scored by growth on –Ade medium, typically after about 10 days of incubation. At least 8 (and usually more) independent transformants were checked per each strain/plasmid combination to assure reproducibility. Transformants carrying the control and experimental plasmids were always compared on one and the same plate. One or two representative transformants for each strain/plasmid combination are shown on Figures. In all cases, there were no differences in growth detected on the completed medium or medium selected for the plasmid (for the simplicity, respective images are not shown on most Figures).

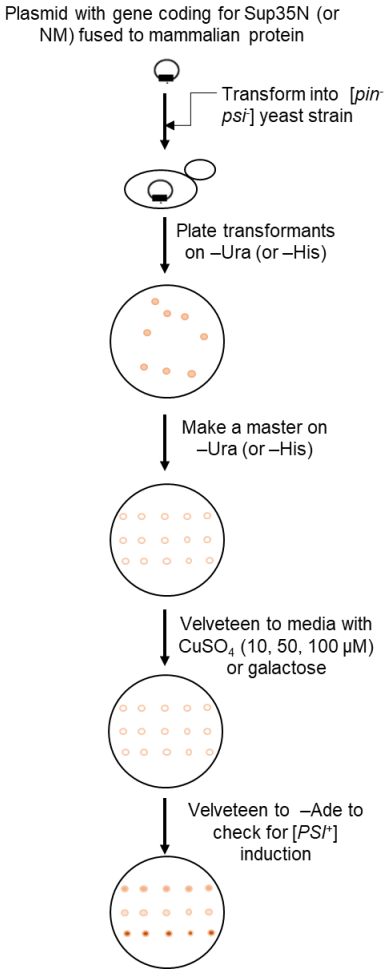

Figure 2-1. Scheme of plate assay for checking prion nucleation by chimeric proteins.

2.2.5 Semi-quantitative measurement of prion nucleation

A pre-culture obtained from a fresh transformant colony was grown in the liquid synthetic medium selective for the plasmid up to OD_{600}=2.5, and then inoculated into the liquid plasmid-selective media with additional $CuSO_4$ (usually 100 µM) at starting concentration of 10^6 cells/ml. Cultures were incubated at 30°C with shaking, with aliquots taken at desired time points, washed with water, diluted appropriately and either spotted (as serial decimal dilutions) or plated onto both plasmid-selective medium containing adenine (to count numbers of viable plasmid-containing cells) and plasmid-selective medium lacking adenine (*e. g.*, –Ura-Ade), to detect [*PSI*$^+$]. Frequency of *[PSI*$^+$] induction was calculated as a ratio of the number of Ade$^+$ colonies to the total number of viable plasmid containing cells plated. To ensure accuracy, only dilutions that produced plates with fewer than 500 colonies were counted. For each construct, quantitative assay was repeated with at least three cultures, each originated from an independent transformant to assure reproducibility, and standard deviations were calculated[68]. Cultures with prion-inducing and control plasmids were always run in parallel in the same experiment.

2.3 DNA analysis and constructions

2.3.1 E. coli *small-scale DNA isolation protocols*

Alkaline lysis method was used for quick isolation of small amounts of plasmid DNA from *E. coli* for obtaining cleaner DNA than that that obtained from the traditional boiling prep method. *E. coli* was patched onto LB plates containing antibiotics selective for a target plasmid. Wooden toothpicks were used to collect cells that were then resuspended in 100 µl of Solution I (25 mM Tris-HCl, 10 mM EDTA, 50 mM glucose, pH 8.0). 200 ul of Solution II (0.2 M NaOH, 1% sodium dodecyl sulfate (SDS)) was added and mixed by inversion, and the samples were kept on ice. 150 µl of Alkaline Lysis Solution III (5 M potassium

acetate, pH 5.0) was added and mixed by inversion. The sample was then incubated on ice for 3-5 minutes and centrifuged at 16,000 x g for 5 minutes at 4°C to pellet the cell debris. The supernatant was collected in a new tube, and 2 volumes of 95% ethanol was added, followed by vortexing to mix, and incubated at room temperature for 5 minutes. The sample was centrifuged at 16000 x g (4°C) for 5 min, and the supernatant was discarded. The pellet was washed with 70% ethanol and vortexed briefly. The sample was centrifuged again at 16000 x g (4°C) for 5 minutes, and the supernatant was discarded. The DNA pellet was dried thoroughly and resuspended in 50ul of TE (or water) containing 10ug/ml RNase A. The sample was incubated at 37° for 30 minutes for RNA removal.

2.3.2 DNA extraction from agarose gels

DNA fragments generated from restriction digestion or PCR reaction were separated by running the fragments on a 1% TBE agarose gel stained with ethidium bromide (100V). Bands were visualized using a UV transilluminator (UVP Gel Doc-it 300 Imaging system.) DNA bands corresponding to desired products were visualized using a UV transilluminator (Fischer Biotech 312nm Variable Intensity Transilluminator) and excised with a scalpel and were purified using an IsoPure DNA Purification Prep Kit (Denville).

2.3.3 Site-directed mutagenesis of DNA

Mutations in the region coding for PrP or Aβ were generated using site-directed mutagenesis. Oligonucleotide primers that already incorporate the desired nucleotide substitution (point mutation) were designed using Primer X program. Unlike ordinary PCR primers, mutagenic primers do not anneal perfectly to the template DNA and thus, special considerations including GC content, primer length, and melting temperature of the oligonucleotide were made regarding their design. The site-directed mutagenesis

procedure was carried out using the protocol (Figure 2-2) in QuikChange SiteDirected Mutagenesis protocol (Agilent Technologies, Santa Clara, CA, USA).

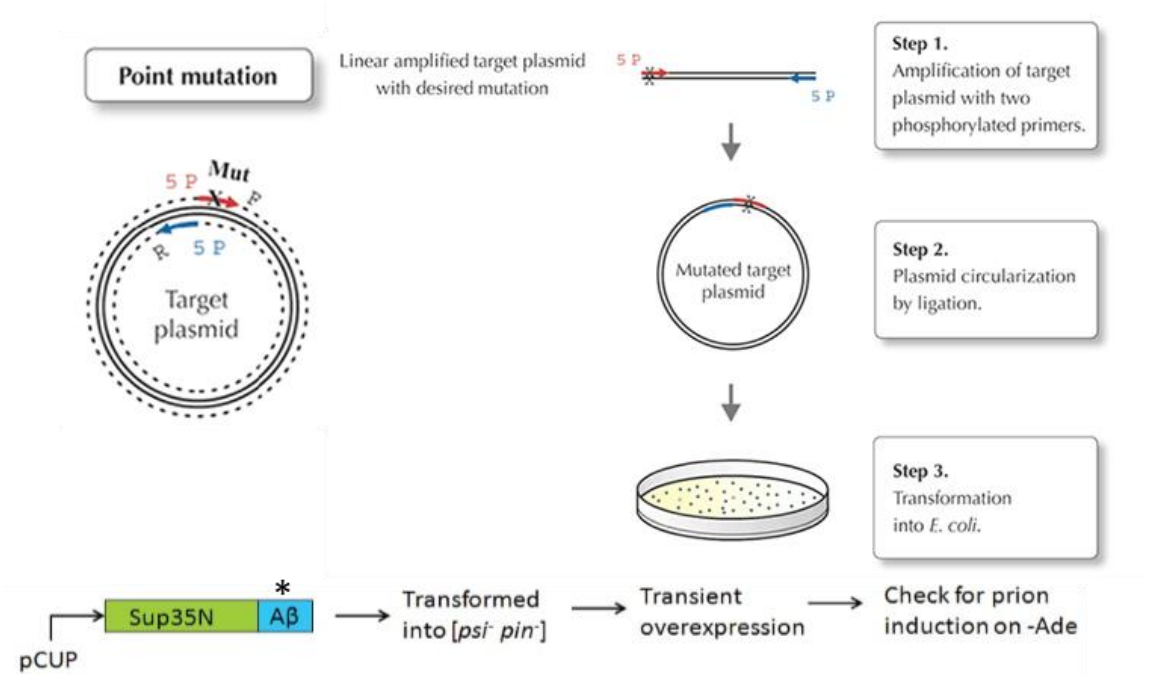

Figure 2-2. Scheme of site-directed mutagenesis to introduce point mutations in PrP (Chapter 3) or Aβ-based chimeric proteins (Chapter 4).

2.3.4 DNA sequencing

DNA was purified for sequencing using an IsoPure DNA Purification Prep Kit (Denville) and was eluted in water. DNA sequencing was performed by Eurofins MWG Operon Sequencing (Huntsville, AL).

2.4 Protein Analysis

2.4.1 Yeast total protein isolation

For isolation of the total yeast protein, cells grown in the liquid medium were collected by centrifugation at 2,000 g for 5 min at 4ºC, washed with 300 µl of ice-cold lysis buffer (25 mM Tris pH 7.5, 0.1M NaCl, 10mM EDTA, 100 µg/ml cycloheximide, 2 mM benzamidine,

20 µg/ml leupeptin, 4 µg/ml pepstatin A, 1 mM N-ethylmaleimide, 1X protease inhibitor cocktail form Roche Diagnostics GmbH, 2 mM PMSF), resuspended in 2 volumes of icecold lysis buffer, and mixed to ~300 µl of acid washed glass beads. Cells were lysed by vortexing 6 times for 30 sec, with at least 1 min on ice inbetween each time. Cell debris were removed by centrifugation at 2,000 g for 5 min. The amount of protein in the samples were determined by Bradford reagent (BioRad) and normalized using lysis buffer.

2.4.2 SDS-PAGE and western blotting

Proteins were isolated from yeast as described and boiled for 10 minutes prior to loading onto SDS-polyacrylamide (SDSPAGE) gel. After electrophoresis, proteins were transferred onto Immobilon-P 0.45 µm polyvinylidene difluoride blotting membrane (EMD Millipore) or Amersham Protran Premium 0.45 µm Nitrocellulose Blotting membrane (GE Healthcare) and reacted to appropriate antibodies. Reaction was detected by using the chemiluminescent detection reagents as described in the GE Healthcare protocols.

2.4.3 SDD-AGE

Semi-denaturing detergent-agarose gel electrophoresis (SDD-AGE) followed by transfer to the nitrocellulose membrane was performed[69], with the modification (addition of 0.1% SDS to the transfer buffer). Protein concentrations were normalized by Bradford assay.

CHAPTER 3. PROMOTION OF PRION NUCLEATION BY MAMMALIAN PROTEINS IN YEAST

This chapter includes data published in Journal of Biological Chemistry.

Chandramowlishwaran, P., Sun, M., Casey, K. L., Romanyuk, A. V., Grizel, A. V., Sopova, J. V., Rubel, A. A., Nussbaum-Krammer, C., Vorberg, I. M., and Chernoff, Y. O. (2018) Mammalian amyloidogenic proteins promote prion nucleation in yeast. *Journal of Biological Chemistry*. 293:3436-3450

3.1 Summary

The formation of the amyloid fibril is postulated to occur through a two-step process. First, the normal soluble protein is converted into small aggregates or nuclei of the prion isoform of that protein by a process called nucleation. Second, these nuclei seed the conversion of protein molecules containing the same or similar amino acid sequence thereby sequestering them into long fibrils. A similar molecular mechanism is employed by yeast prions, which are not homologous to known mammalian amyloid and prion proteins by sequence, and control heritable traits. We have developed a yeast-based assay that allows us to study the initial nucleation mechanism of any mammalian amyloidogenic protein. Here, we show that chimeric proteins composed of Sup35 fragments, including prion-forming domain and fused to aggregation-prone regions of mammalian prion protein (PrP), human Amyloid beta (associated with Alzheimer's disease), human α-synuclein (associated with Parkinson's disease), human amylin (associated with Type 2 diabetes), or a peptide stretch within the olfactomedin domain of myocilin (associated with glaucoma), nucleate new Sup35 prions even in the absence of the Rnq1 prion or any other pre-existing nuclei. Sup35N-PrP chimera produced detergent-resistant polymers in the yeast cells and promoted the immobilization of endogenous Sup35 into an aggregated

fraction. Moreover, our data indicate that the prion/amyloid properties of PrP that are detected in yeast and mammalian systems are controlled by the same sequence elements. Different Sup35N-PrP chimeras also induced different spectra of prion strains in yeast. Overall, our yeast-based nucleation assay enables us to perform genetic dissection of molecular processes leading to the initiation of prion and amyloid diseases.

3.2 Specific materials and methods

3.2.1 Materials

Strains, plasmids, and oligonucleotide primers used in this study are described in Appendix tables A, B, and C respectively. The antibodies to Sup35N, Hsp104, Sup35M, PrP, and HA used in this study are described in Chapter 2.

The overall scheme for construction of the chimeric genes that code for Sup35N (or NM) fused to mammalian amyloidogenic proteins of interest (Figure 3-1) is described in detail as follows. The DNA regions coding for Sup35NM (with HA tag) and PrP90-230, were initially inserted in the pcDNA3.1/Zeo (+) backbone; the chimeric genes coding for Sup35N-PrP90-230, Sup35NM-PrP90-230, and Sup35NM-PrP120-230 were initially generated in pcDNA3.1/Zeo (+) as well[70]. Then, respective constructs were excised by using restriction endonucleases *Bam*HI and *Xba*I or *Sac*I, and inserted under the copper-inducible promoter (P_{CUP1}) into a respective centromeric shuttle vector with the *URA3* marker. The plasmid pmCUP1-Sup35N-PrP120-230 was constructed via replacing the *Eco*RI fragment that contains the P_{CUP1}-*SUP35NM* fragment from the plasmid pmCUP1-Sup35NM-PrP120-230 with the *Eco*RI fragment that contains P_{CUP1}-*SUP35N* fragment from the plasmid pmCUP1-Sup35N-PrP90-230. The pmCUP1-Sup35N plasmid was constructed by inserting the PCR-amplified *Bam*HI-*Sac*I fragment that contains the *SUP35N* region from the plasmid Sup35N-PrP90-230, into the pmCUP1 vector at the

position following the P_{CUP1} promoter. The genes coding for Sup35N-PrP90-119, Sup35N-PrP90-144, Sup35N-PrP90-159, and Sup35N-PrP90-171 were constructed by inserting the PCR amplified *Bam*HI-*Xba*I fragments, that code for the respective PrP domains, from the plasmid pmCUP1-Sup35N-PrP90-230 into the pmCUP1 vector at the position following the P_{CUP1} promoter. Constructs coding for the HA-tagged derivatives of the Sup35N and Sup35N-PrP90-230 proteins were produced by PCR-amplifying the *Bam*HI-*Sac*I fragments, coding for respective proteins, from pmCUP1-Sup35N-PrP90-230 with primers adding an HA tag coding sequence to a C-terminal end of each fragment, and inserting resulting constructs into the pmCUP1 vector at the position following the P_{CUP1} promoter. Both HA-tagged and non-tagged constructs produced the same results in the [*PSI*$^{+}$] induction assays. The chimeric gene coding for Sup35NM-PrP90-159 was constructed by replacing the *Eco*RI fragment that contains the P_{CUP1}-*SUP35N* cassette from the plasmid pmCUP1-Sup35N-PrP90-159, with the *Eco*RI fragment that contains the P_{CUP1}-*SUP35NM* cassette from the plasmid pmCUP1-Sup35NM-PrP90-230. The chimeric gene coding for Sup35N-PrP23-230 was constructed by inserting the PCR amplified *Bam*HI-*Xba*I fragment that codes for the region 23-230 of PrP from plasmid mPrPcyto[49] into the pmCUP1-Sup35NM-PrP90-230 vector at the position following the Sup35NM-coding sequence, replacing the PrP90-230 coding fragment. The gene coding for Sup35NM-Aβ1-42 was constructed by inserting the PCR amplified *EcoR*I-*Not*I fragment that contains Aβ1-42 from the plasmid pcDNA3.1(+)-Aβ42 (kindly provided by Dr. K. Ugen, University of South Florida) containing the human Aβ1-42-coding sequence[72], into the pmCUP1-Sup35NM-PrP90-230 vector at the position following the Sup35NM-coding sequence, replacing the PrP90-230 coding fragment. The DNA sequence coding for Aβ1-42 was placed under the P_{CUP1} promoter by inserting the PCR amplified *Bam*HI-*Xba*I fragment that codes for Aβ1-42, from the plasmid pmCUP1-Sup35NM-Aβ1-42, into the pmCUP1 vector at the position following the P_{CUP1} promoter. The genes coding for

Sup35N-Aβ1-42 and Sup35N-Aβ3-42 were constructed by replacing the *Eco*RI fragment that contains the P_{CUP1}-*SUP35NM* cassette from the plasmid pmCUP1-Sup35NM-Aβ1-42, with the *Eco*RI fragment that contains P_{CUP1}-*SUP35N* from the plasmid pmCUP1-Sup35N-PrP90-230. The digestion of an additional *Eco*RI site at the 3rd codon of Aβ1-42 resulted in the generation of pmCUP1-Sup35N-Aβ3-42, while pmCUP1-Sup35N-Aβ1-42 was generated by incomplete digestion. To construct the series of plasmids that are more convenient for construction procedures using the *Eco*RI digestion, the pmCUP1 vector was digested with *Eco*RI, the resulting 5' overhang was blunted using Mung Bean nuclease and religated with the same vector to disrupt the *Eco*RI site upstream the sequence coding for P_{CUP1}. This plasmid, named pmCUP1-nERI, was used to construct pmCUP1-nERI-Sup35N-Aβ3-42 by inserting the PCR amplified *Bam*HI-*Xba*I fragment that contains the Sup35N-Aβ3-42-coding sequence from the plasmid pmCUP1-Sup35N-Aβ3-42, into the pmCUP1-nERI vector at the position following the P_{CUP1} promoter. To disrupt an additional *Eco*RI recognition site spanning the nucleotide positions 7-12 of Aβ1-42-coding sequence without changing the amino acid sequence, the 3rd codon of Aβ1-42 (GAA) that codes for glutamic acid was mutated to the synonymic codon GAG, and the PCR amplified *Eco*RI-*Xba*I fragment containing the Aβ1-42-coding sequence with respective change (Aβm1-42), was inserted into the plasmid pmCUP1-nERI-Sup35N at the position following the sequence coding for Sup35N. In the [*PSI*$^+$] induction assays, the Sup35N-Aβm1-42 construct produced results similar to the unmodified Sup35N-Aβ1-42 construct. The gene coding for Sup35N-Aβ1-40 was constructed by inserting the PCR amplified *Bam*HI-*Xba*I fragment, that contains Aβ1-40-coding sequence from the plasmid pmCUP1-nERI-Sup35N-Aβm1-42, into the plasmid pmCUP1-nERI-Sup35N-Aβm1-42 at the position following the sequence coding for Sup35N. The gene coding for Sup35NM-Aβ1-40 was constructed by replacing the *Eco*RI fragment, that contains P_{CUP1}-*SUP35N* cassette, in the plasmid pmCUP1-Sup35N-Aβ1-40 with the *Eco*RI fragment that contains

the P_{CUP1}-*SUP35NM* cassette from the plasmid pmCUP1-Sup35NM-PrP90-230. Individual base substitutions in the pmCUP1-Sup35N-PrP90-230 was generated in the Aβ1-42-coding sequence using the QuikChange Site-Directed Mutagenesis protocol (Agilent Technologies, Santa Clara, CA, USA) and as described in Chapter 2 under methods. The genes coding for Sup35N-NAC or Sup35N-IAPP or Sup35N-Myocilin were constructed by inserting the PCR amplified *EcoR*I-*Not*I fragment that contains NAC-HA and IAPP and myocilin regions from the plasmid p106.NAC, containing the human NAC-coding sequence that corresponds to codons 61-95 of α-synuclein gene; from the plasmid pJ201:66979-IAPP2_optSc containing the codons 41-70 of human Islet amyloid polypeptide (IAPP)- coding sequence that corresponds to residues 8-37 in mature amylin; and from the plasmid pMAL-p4X Myocilin WT that corresponds to codons 426-441 of MYOC gene respectively, into the plasmid pmCUP1-nERI-Sup35N-Aβ1-42 at the position following the sequence coding for Sup35N, replacing the Aβ1-42 coding fragment. Original plasmids p106.NAC and pJ201:66979 - IAPP2_optSc were kindly provided by Dr. V. Conticello from Emory University. Original plasmids pMAL-p4X Myocilin WT was kindly provided by Dr. R. Lieberman from Georgia Tech. The plasmids pmCUP1-Sup35NM-NAC and pmCUP1-Sup35NM-IAPP were constructed by inserting the PCR amplified *Eco*RI-*Not*I fragments that contain NAC-HA and IAPP regions from pmCUP1-Sup35N-NAC and pmCUP1-Sup35N-IAPP, and inserted into the plasmid pcDNA3.1(Zeo)-Sup35NM-PrP90-230 at the position following the Sup35NM-coding sequence, replacing the PrP90-230 coding fragment. Then, respective chimeric genes were cut from plasmids pcDNA3.1(Zeo)-Sup35NM-NAC and pcDNA3.1(Zeo)-Sup35NM-IAPP with *Bam*HI and *Xba*I and inserted into the pmCUP1 vector at the position following the P_{CUP1} promoter. The plasmid coding for the C-terminal fusion of Lsb2 with GFP, expressed under the P_{CUP1} promoter in the pRS316 backbone was constructed earlier[71]. The chimeric gene coding for Sup35N-LacZ was constructed by inserting the PCR amplified *Eco*RI-*Xba*I fragment

that contains the *lacZ*-coding sequence from the plasmid pSVA1 (kindly provided by Dr. M.D. Ter-Avanesyan, Moscow) into the plasmid pmCUP1-nERI-Sup35N-Aβm1-42 at the position following the Sup35N- coding sequence, replacing the Aβ1-42 coding fragment. The gene coding for Sup35NM-LacZ was constructed by replacing the *Eco*RI fragment of the plasmid pmCUP1-Sup35N-LacZ that contains the PCUP1-SUP35N cassette with the *Eco*RI fragment that contains the P_{CUP1}-*SUP35NM* cassette from the plasmid pmCUP1-Sup35NM-PrP90-230. The gene coding for Sup35N-GFP was constructed by inserting the PCR amplified *Eco*RI-*Sac*II fragment that contains GFP-coding sequence from the plasmid pmCUP1-NM-GFP[71] into pmCUP1-nERI-Sup35N-Aβm1-42 at the position following the Sup35N-coding sequence, replacing the Aβ1-42-coding sequence. The gene coding for Sup35NM-Ade2 was constructed by inserting the Ade2 coding fragment from the plasmid pRS316GAL-Sup35NM-Ade2, into the plasmid pmCUP1-Sup35NM-Aβ1-42 at the position following the sequence coding for Sup35NM, replacing the Aβ1-42-coding sequence. The gene coding for Sup35N-Ade2 was constructed by replacing the *Eco*RI fragment that contains the P_{CUP1}-*SUP35NM* cassette from the plasmid pmCUP1-Sup35NM-Ade2, with the *Eco*RI fragment that contains the P_{CUP1}-*SUP35NM* cassette from the plasmid pmCUP1-Sup35N- PrP90-230. Plasmids with constructs under P_{GAL} promoter were constructed by inserting the *Bam*HI-*Xba*I fragments with respective chimeric genes from constructs with P_{CUP1} promoter into the centromeric *HIS3* vector pLA1 [82] under the galactose-inducible promoter, P_{GAL}. Plasmid pLH105, containing the HSP104 gene under the strong constitutive P_{GPD} promoter, was a gift from S. Lindquist quoted earlier[71]. Plasmids pLA1-Sup35N and pLA1-Sup35, containing respectively P_{GAL}-*SUP35N* and P_{GAL}-*SUP35N* expression cassettes, were described earlier. The plasmid pmCUP1-PrP-GFP(URA3), kindly provided by A.P. Galkin and coding for the PrP90-231-GFP chimeric protein, was described earlier [88]. The plasmid pmCUP1-Aβ1-42-GFP(URA3) was constructed via inserting the DNA fragment, encoding Aβ1–42 and obtained from the

human brain mRNA by RT-PCR, with the addition of *Bam*HI and *Sac*II sites, into the plasmid pmCUP1-GFP [85, digested with *Bam*HI and *Sac*II. All regions that underwent PCR amplification as well as immediate flanking regions were verified by sequencing, performed at Eurofins MWG Operon (Huntsville, AL). Isolation of plasmid DNA from bacteria was performed according to standard procedures.

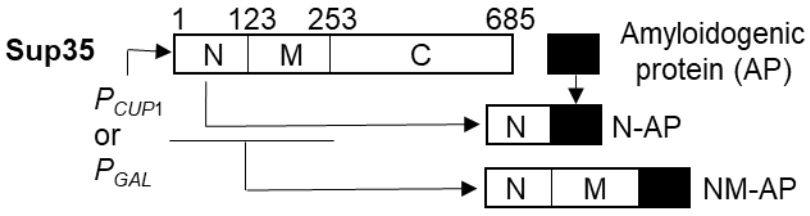

Figure 3-1. Scheme of construction of Sup35N (or NM) fused to amyloidogenic protein of interest (AP). The chimeric genes contain regions coding for mammalian amyloidogenic proteins (AP) attached to the C-terminus of the region coding for Sup35N or Sup35NM. Numbers indicate amino acid position in the Sup35 sequence.

3.2.2 Methods

Standard protocols were used for DNA isolation, gel electrophoresis, restriction digestion, gel extraction, ligation, and bacterial transformation[67] and are described in Chapter 2. Standard yeast media and standard procedures for yeast cultivation, phenotypic analysis, and transformation were used and are described in Chapter 2. The plate assay for [*PSI*$^+$] nucleation and semi-quantitative/quantitative [*PSI*$^+$] measurements are described in Chapter 2. The protein analysis including SDS-PAGE for measuring protein levels and SDD-AGE[69] for characterizing the amyloid aggregates are described in Chapter 2. The scheme for mutations in the region coding for PrP were generated using site-directed mutagenesis and are described in Chapter 2.

3.3 Results

*3.3.1 Phenotypic detection of [*PSI$^+$*] nucleation by PrP or Aβ* in trans

It has previously been shown that co-overproduction of some yeast prionogenic proteins can promote prion formation by another yeast prion protein in the strain lacking pre-existing prions[38,39]. To determine if mammalian amyloidogenic proteins exhibit such an effect on prion formation by the yeast protein Sup35, we have overproduced the mouse prion protein (PrP), associated with TSEs, and the human amyloid β peptide (Aβ), associated with AD, in a yeast strain lacking pre-existing prions ([*pin*$^-$ *psi*$^-$]) either individually or simultaneously with separately expressed Sup35 PrD, Sup35N (Figure 3-2). In the case of PrP, we have employed the region between positions 90 and 230 which is sufficient to generate and maintain a prion state in mammals[71]. In the case of Aβ, the most amyloidogenic and pathogenic 42-residue[72] variant (Aβ1-42) has been employed. We have confirmed that the PrP90-230 protein is produced in yeast (Figure. 3-3A). However, the levels of Aβ1-42 were below detection limits (data not shown), possibly due to a low proteolytic stability of this short peptide in yeast cells. Therefore, we have also used the PrP90-231-GFP and Aβ1-42-GFP fusion proteins that are both produced at high levels in yeast cells (Figure 3-3A). The PrP- and Aβ-based constructs produced amyloid-like detergent-resistant aggregates, in yeast[49], and confirmed by us (Figure 3-3B) using the semi-denaturing agarose gel electrophoresis, SDD-AGE[69]).

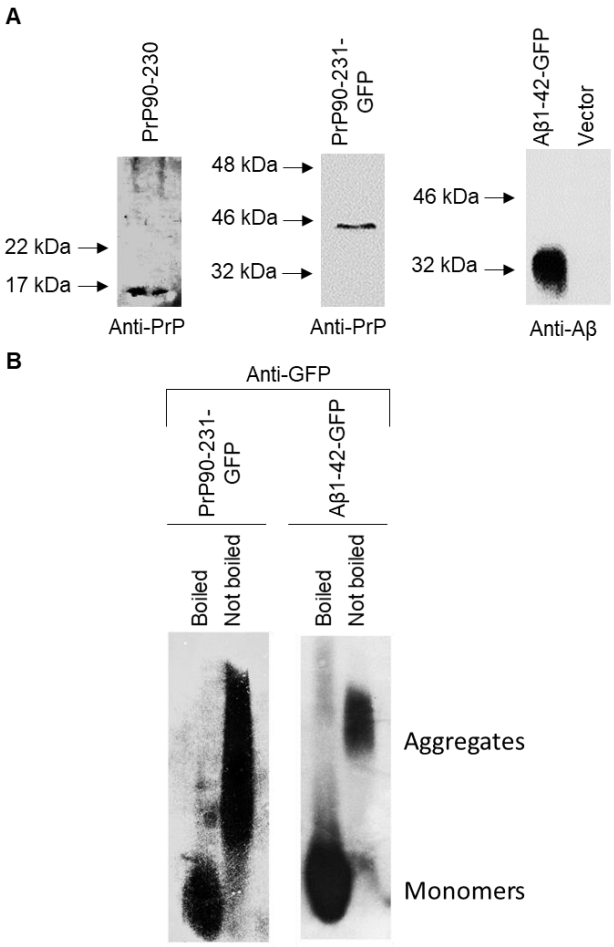

Figure 3-2. Detection of PrP- and Aβ-based constructs in yeast. (A) Expression of PrP90-230, PrP90-231-GFP and Aβ1-42-GFP proteins in yeast after induction with 100 μM $CuSO_4$, as detected by SDS-PAGE and Western blot, with anti-PrP antibody 4H11 or anti-Aβ antibody 6E10. Positions of molecular weight markers are indicated. (B) Aggregation of chimeric proteins PrP90-231-GFP and Aβ1-42-GFP in yeast, as detected by semi-denaturing detergent agarose gel electrophoresis (SDD-AGE), followed by Western blotting and reaction to anti-GFP antibody. Cell lysates were treated with 3% sodium lauroyl sarcosinate and run on the agarose gel. Boiling of the samples before electrophoresis converts aggregates to monomers.

To detect [*PSI*$^+$] formation, we employed the *ade1-14* (UGA) reporter[32]. The [*psi*$^-$] strains bearing this reporter are Ade$^-$ (i.e., do not grow on medium lacking adenine) and only rarely produce spontaneous Ade$^+$ colonies, in part due to reversions or suppressor mutations. The conversion of endogenous Sup35 into a prion form leads to a termination defect and readthrough of *ade1-14*, resulting in an Ade$^+$ phenotype. Therefore, [*PSI*$^+$] induction can be detected as an increase in the frequency of Ade$^+$ colonies over a low

background. None of the mammalian proteins (PrP90-230, PrP90-231-GFP, Aβ1-42, or Aβ1-42-GFP) was able to induce [*PSI*$^{+}$] formation, both at normal levels of Sup35 and in the presence of excess Sup35N (Figure 3-2A, B). This contrasted with the yeast prionogenic QN-rich protein Lsb2 (fused to GFP), that promoted [*PSI*$^{+}$] formation in the presence of excess Sup35N (Figure 3-2A, B) and as shown previously[34,40,73].

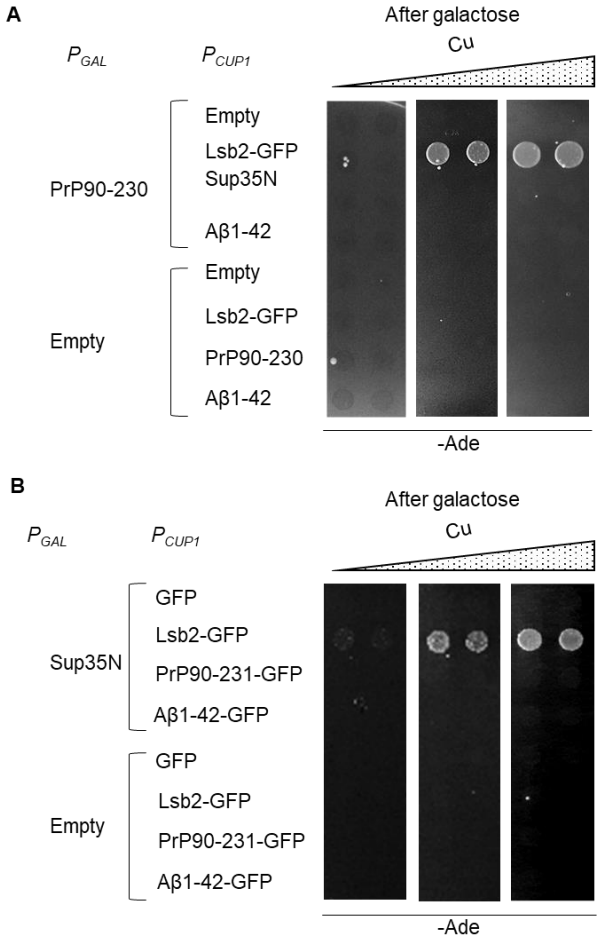

Figure 3-3. A lack of [*PSI*$^{+}$] nucleation by PrP or Aβ *in trans.* *(*A) Overexpression of PrP90-230 or Aβ1-42, or B- of their respective fusions to GFP from the copper-inducible promoter, P_{CUP1} induces [*PSI*$^{+}$] formation in the [*psi*$^{-}$ *pin*$^{-}$] strain neither on its own nor in the presence of excess Sup35N (produced under the control of the galactose inducible promoter, P_{GAL}). (B) - The QN-rich prion-inducing protein Lsb2, fused to GFP is shown as a positive control. Cultures were pre-incubated on the medium containing additional $CuSO_4$ at a concentration of 0, 50, and 150μM from left to right.

3.3.2 Phenotypic detection of [PSI$^+$] nucleation by mammalian proteins fused to Sup35N

Next, we checked what happens if a mammalian amyloidogenic protein is physically attached to the fragment of Sup35 containing the PrD. We prepared a series of such constructs as shown in Figure 3-1. Some of them also contained an HA tag (see materials and methods) which does not influence the ability of the protein to induce a prion, according to our data (not shown). The Sup35N fragment (roughly equivalent to Sup35 PrD), produced from a copper-inducible (P_{CUP1}) promoter can slightly induce the formation of Ade$^+$ ([*PSI*$^+$]) colonies in a [*pin*$^-$] strain at high concentrations of $CuSO_4$ (*e. g.* see Table 1), but this effect is weak and is not clearly detectable in plate assays (*e. g.* see Figure 3-3) unless very high concentrations of $CuSO_4$ and/or very long incubation periods are used. No [*PSI*$^+$] induction occurs when Sup35N alone is expressed from the galactose-inducible P_{GAL} promoter (*e. g.* see Figure 3-4C). The Sup35NM fragment, bearing both PrD and the middle region (Sup35M), which contains a high concentration of charged residues and is responsible for keeping Sup35 in a soluble state, does not induce the formation of Ade$^+$ colonies in the [*pin*$^-$] strain (*e. g.*, see Fig 3-4B, C and Table 3-1). Notably, an attachment of the region coding for either mouse PrP90-230 or human Aβ1-42 to the C-terminus of Sup35N (Figure 3-1) enabled such a chimeric construct to induce Ade$^+$ colonies after incubation in the presence of $CuSO_4$ even in conditions when induction by Sup35N alone was not detectable (Fig 3-4A and Table 3-1). [*PSI*$^+$] induction by Sup35N-Aβ1-42 was stronger than that by Sup35N-PrP90-230, and could be detected even at background levels of $CuSO_4$ as seen in the quantitative assay (Table 3-1). More importantly, the ability of these chimeric constructs to induce Ade$^+$ colonies was not promoter-specific and did not depend on the presence of $CuSO_4$ per se, as it was reproduced by using the chimeric constructs expressed from the P_{GAL} promoter (Figure 3-4C). Aβ1-42 also promoted Ade$^+$ formation when fused to the Sup35NM fragment and expressed from either a P_{GAL} (Figure

3-4C) or P_{CUP1} (Figure 3-4B) promoter, albeit at a lower frequency (Table 3-1) and in the latter case, at higher concentrations of $CuSO_4$ when compared to Sup35N-Aβ1-42. However, we have not detected Ade^+ induction by the Sup35NM-PrP90-230 construct (Figure 3-4B, C).

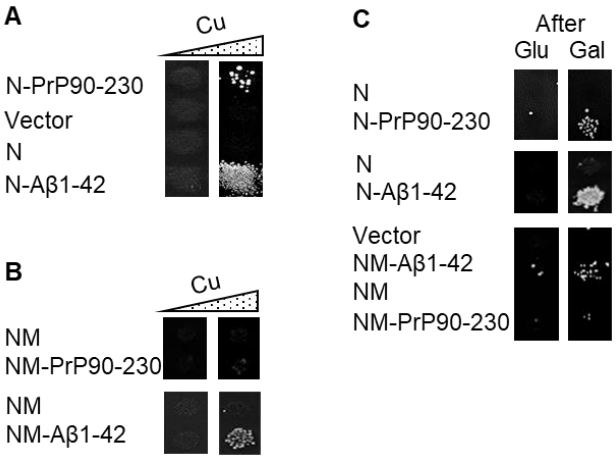

Figure 3-4. Phenotypic detection of prion nucleation by chimeric constructs containing mammalian amyloidogenic proteins, PrP or Aβ in yeast. (A), (B) and (C) Transient copper-induced (A and B) or galactose-induced (C) overproduction of the chimeric proteins containing Sup35N (A and C) or Sup35NM (B and C), fused each to PrP90-230 or Aβ1-42, promotes the *de novo* formation of [PSI^+] in a [psi^- pin^-] strain. On panel C, the images from -Ade plates obtained after pre-incubation on the glucose medium (left column) or on the medium with 2% galactose instead of glucose (right column) are shown. For frequencies of [PSI^+] induction, see Table 3-1.

Table 3-1. Frequencies of [PSI^+] induction by chimeric and control plasmids

Inducer	**Frequency (+/- standard deviation) of Ade^+ colonies per 10,000 cells after 100 μM $CuSO_4$**	
	0 hrs.	**24 hrs.**
Vector	0.08+/-0.02	0.07+/-0.04
Sup35N	0.07+/-0.05	0.31+/-0.11
Sup35N-PrP90-230	0.07+/-0.02	8.4+/-0.7
Sup35N-PrP120-230	0.01+/-0.02	0.25+/-0.23
Sup35N-PrP90-144	0.11+/-0.05	54+/-17
Sup35N-PrP90-159	0.06+/-0.05	736+/-44
Sup35N-PrP90-171	0.07+/-0.07	35+/-6

We have shown that the vast majority of Ade$^+$ colonies induced by the PrP- or Aβ-based chimeric constructs in the [*pin*$^-$] strain retain suppression after the loss of the inducing plasmid and are curable by serial passages on medium containing an antiprion agent guanidine hydrochloride, GuHCl (Table 3-2). These data confirm that the majority of these colonies arise from the conversion of the endogenous Sup35 protein into [*PSI*$^+$].

Table 3-2. Guanidine curability of Ade$^+$ colonies induced by chimeric constructs

Inducer	Colonies curable by GuHCl	Total number of colonies tested
Sup35N-PrP90-230	35	43
Sup35N-PrP90-144	39	40
Sup35N-PrP90-159	30	33
Sup35N-PrP90-171	27	29
Sup35N-Aβ1-42	28	29

The ability to promote [*PSI*$^+$] nucleation in the absence of [*PIN*$^+$] upon fusion to Sup35N or NM is not restricted only to Aβ1-42 or PrP90-230, as three other human amyloidogenic peptides, namely the aggregation-prone region (“non-amyloid component”, or NAC) of α-synuclein, associated with PD[51] and amylin (or IAPP) peptide, associated with type II diabetes[25], and a short peptide sequence of the olfactomedin domain of myocilin, associated with glaucoma[27], exhibited such an effect (Figure 3-5).

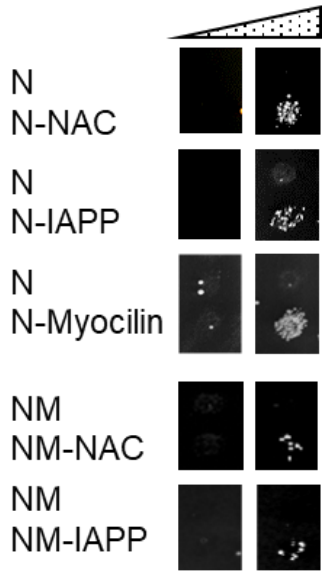

Figure 3-5. Phenotypic detection of prion nucleation by chimeric constructs containing mammalian amyloidogenic peptides in yeast. Transient overproduction of Sup35N (or NM) fused each to NAC61-93 or IAPP41-69 or to myocilin (426-441) promotes the *de novo* formation of [*PSI*$^+$] in a [*psi*$^-$ *pin*$^-$] strain. The images from –Ade plates are shown, obtained without (left column) or with (right column) pre-incubation in the presence of additional (100 μM) $CuSO_4$.

*3.3.3 Phenotypic detection of [*PSI$^+$*] nucleation by multimerization prone non-amyloidogenic proteins fused to Sup35N*

In contrast, several proteins without known amyloidogenic properties, specifically yeast AIR-carboxylase (Ade2), bacterial β-galactosidase (LacZ), and jellyfish green fluorescent protein (GFP) did not induce [*PSI*$^+$] formation at any noticeable level when fused to Sup35N (Figure 3-6A) or NM (Figure 3-6B). Notably, some of these proteins are known to form multimers, and in a separate experiment employing the *ade2* mutant strain, we have specifically shown that the Sup35N-Ade2 and Sup35NM-Ade2 constructs produce functional AIR carboxylase in yeast (Figure 3-6C). This confirms that these chimeric proteins form multimeric complexes in yeast, because the functionality of AIR carboxylase depends on its multimerization[74]. Therefore, our data show that the ability of a protein to

promote prion nucleation in a fusion to a fragment bearing the PrD of Sup35 depends on the amyloidogenic properties of such a protein, rather than with its ability to form multimeric complexes per se.

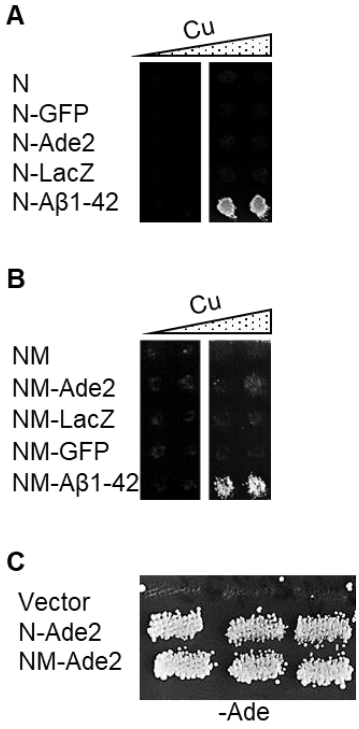

Figure 3-6. Phenotypic detection and functional analysis of prion nucleation by chimeric constructs containing multimerization prone, non-amyloidogenic proteins in yeast. (A) and (B) Transient overproduction of Sup35N fused to Ade2, LacZ, or GFP fails to promote *de novo* [*PSI*$^{+}$] formation in a [*psi*$^{-}$ *pin*$^{-}$] strain. The Sup35N-Aβ1-42 (A) or Sup35NM-Aβ1-42 (B) construct was used as a positive control. On panels A and B, the images from –Ade plates are shown, obtained without (left column) or with (right column) pre-incubation in the presence of additional (100 μM) $CuSO_4$. (C) Functionality of the Ade2-based chimeric constructs. Plasmids expressing the Sup35N-Ade2 and Sup35NM-Ade2 constructs compensate for the growth of a yeast strain, bearing the *ade2* mutant allele, on the medium lacking adenine.

As expected, both PrP- or Aβ- based chimeric constructs, as well as control Sup35N protein efficiently induced [*PSI*$^{+}$] formation in a [*PIN*$^{+}$] strain (Figure 3-7A, B).

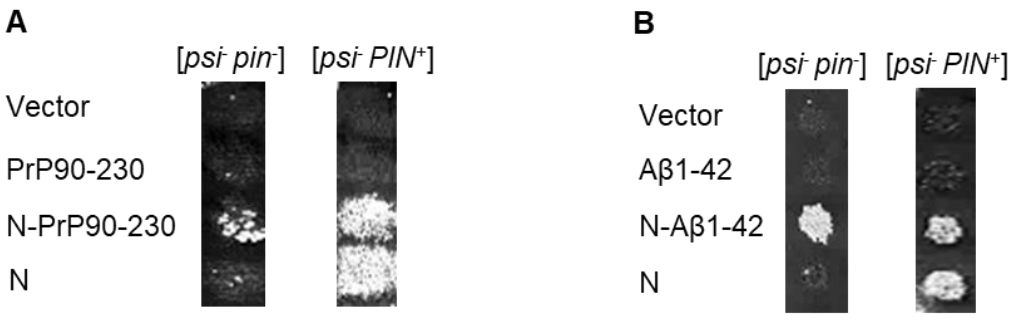

Figure 3-7. Comparison of [*PSI*$^+$] induction by the PrP or Aβ-based chimeric constructs in the [*pin*$^-$] and [*PIN*$^+$] background. Chimeric constructs bearing PrP90-230 (A) or Aβ1-42 (B), in various prion backgrounds. [*PSI*$^+$] formation is detected on –Ade medium after transient overproduction of respective constructs from the P_{CUP1} promoter, induced by addition of 100 µM $CuSO_4$.

*3.3.4 Analysis of proteotoxic stress induced by [*PSI$^+$*] nucleated by PrP or Aβ*

Notably, a high expression of the PrP- or Aβ-based constructs (fused to either GFP or Sup35 PrD) did not inhibit the growth of the [*pin*$^-$] yeast strain (data not shown) and did not increase the levels of the stress-inducible chaperone Hsp104 (Figure 3-8). These results show that prion induction by the PrP- or Aβ constructs is not a consequence of proteotoxic stress.

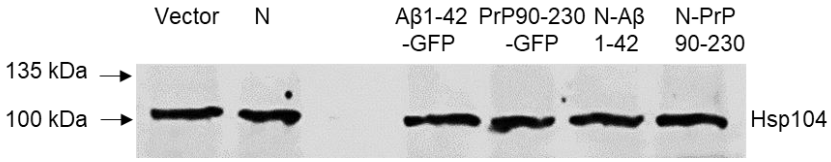

Figure 3-8. Additional characterization of chimeric constructs in yeast. Lack of Hsp104 induction by chimeric constructs. Cultures were grown in the synthetic medium selective for the plasmids. Expression of a respective chimeric construct (as indicated) was induced with the addition of 100 µM $CuSO_4$. Proteins were isolated and run on SDS-PAGE, followed by Western blotting and reaction to the anti-Hsp104 antibody. Protein levels were normalized using Bradford assay (BioRad).

3.3.5 Phenotypic detection of [PIN$^+$] appearance in [PSI$^+$] nucleated by PrP or Aβ

Both Sup35N-PrP90-230 and Sup35N-Aβ1-42 constructs were capable of nucleating the [*PSI*$^+$] prion in an *rnq1*Δ strain, lacking the Rnq1 protein (Figure 3-9A). This shows that a chimeric protein does not promote formation of [*PSI*$^+$] indirectly, via inducing [*PIN*$^+$], a prion form of Rnq1, which would in turn induce [*PSI*$^+$]. However, it is known that other endogenous yeast QN-rich proteins in an aggregated form can substitute for the [*PIN*$^+$] in [*PSI*$^+$] induction[34]. To make sure that chimeric PrP- or Aβ-based constructs do not induce [*PSI*$^+$] by generating other prions that confer a [*PIN*$^+$]-like effect, we mated a sample of independently obtained Sup35 derivatives, induced by Sup35N-PrP90-230 or Sup35N-Aβ1-42 in the [*psi*$^-$ *pin*$^-$] strain, to the [*psi*$^-$ *pin*$^-$] strain of opposite mating type, bearing a plasmid with *HSP104* gene under a strong constitutive P_{GPD} promoter and a plasmid with *SUP35* gene under a galactose-inducible P_{GAL} promoter (Figure 3-9B). Excess Hsp104 is known to cure [*PSI*$^+$][76] but not [*PIN*$^+$][34] or a majority of other known yeast prions[77]. Therefore, if [*PSI*$^+$] formation was due to the formation of [*PIN*$^+$] or another prion with similar [*PSI*$^+$]-inducing capability, we would expect that the [*psi*$^-$] derivative of such a [*PSI*$^+$] isolate, cured of both the inducing plasmid and induced [*PSI*$^+$], would stay [*PIN*$^+$] and therefore be reinduced into a [*PSI*$^+$] state after the overproduction of Sup35. However, the vast majority of [*psi*$^-$] derivatives, being cured of [*PSI*$^+$] as well as of the original inducer plasmid and *HSP104* plasmid, were unable to turn into a [*PSI*$^+$] state (Ade$^+$ phenotype) after Sup35 was overproduced on galactose, indicating that they stay [*pin*$^-$] (Figure 3-9C). These data show that [*PSI*$^+$] nucleation in the presence of chimeric constructs bearing mammalian amyloidogenic proteins is not due to the induction of [*PIN*$^+$] prion or other yeast non-Sup35 prions with a similar effect.

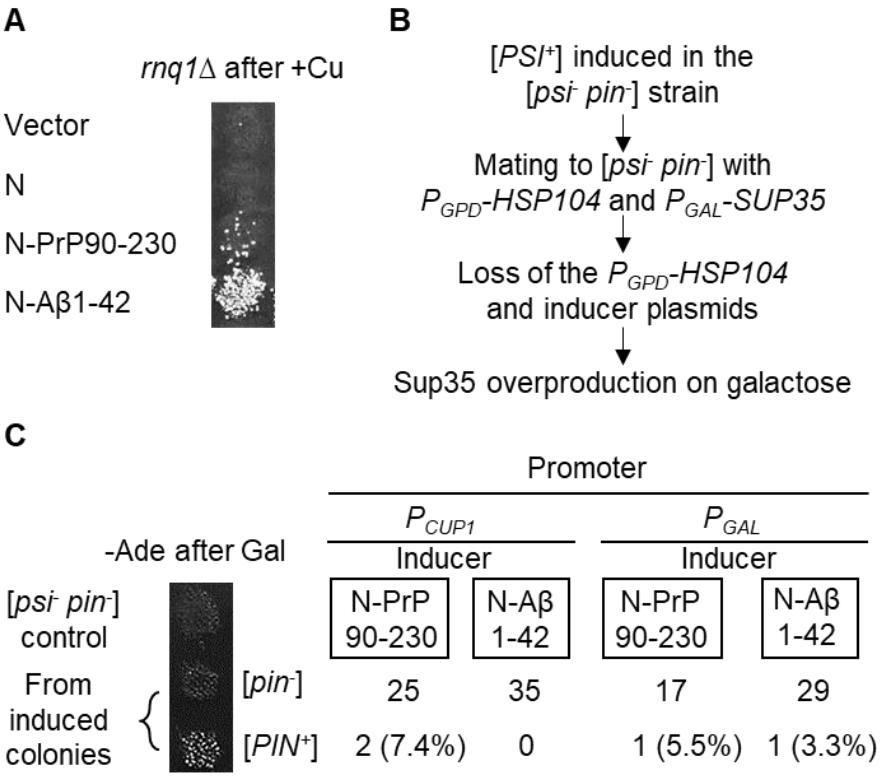

Figure 3-9. Phenotypic detection of [*PIN*$^+$] formation in [*PSI*$^+$] nucleated by PrP- or Aβ-based chimeric constructs. (A) Induction of [*PSI*$^+$] by chimeric constructs, expressed in the *rnq1*Δ strain with the addition of 100 μM $CuSO_4$. (B) Scheme of the experiment for the detection of the formation [*PIN*$^+$] or other prions with [*PIN*$^+$]-like effect in the [*PSI*$^+$] cells, induced by chimeric constructs. The [*PSI*$^+$] colonies, induced in the [*psi*$^-$ *pin*$^-$] strain by plasmids carrying Sup35N-PrP90-230 or Sup35N-Aβ1-42 (each colony originated from an independent transformant), were mated to the isogenic [*psi*$^-$ *pin*$^-$] strain of the opposite mating type, carrying the plasmid with the *HSP104* gene under a strong constitutive P_{GPD} promoter and the plasmid with the *SUP35* gene under galactose-inducible P_{GAL} promoter. Resulting diploids (cured of [*PSI*$^+$] by the constitutive overproduction of Hsp104) were then cured of the inducer and P_{GPD}-*HSP104* plasmids and placed onto a galactose medium to overexpress Sup35. Following transient induction of Sup35 on galactose, colonies were velveteen replica plated to the -Ade medium with glucose to check for [*PSI*$^+$] reinduction. (C) Results of the experiment described in panel B. Only [*PIN*$^+$] isolates can generate Ade$^+$ (*i.e.*, [*PSI*$^+$]) colonies in these conditions. Most of the colonies derived from the [*PSI*$^+$] isolates, that were induced by PrP- or Aβ-containing chimeric constructs, stayed [*pin*$^-$].

*3.3.6 Effects of alterations in PrP on [*PSI$^+$*] nucleation by Sup35N-PrP*

Next, we checked if correspondence between known effects of sequence alterations on the amyloid formation in other systems and on prion nucleation in yeast also holds true for

PrP. Amino acid substitution P101L in mouse PrP (see Figure 3-10A) corresponds to the human mutation P102L, associated with a heritable prion disease, and is shown to cause disease accompanied by a production of the infectious PrP protein in mice[14]. In contrast, the substitution Q167R is shown to inhibit prion replication in mice[78]. In agreement with these data, substitutions P101L and Q167R in Sup35N-PrP90-230 construct respectively increased or decreased [*PSI*$^+$] nucleation in the yeast assay (Figure 3-10B).

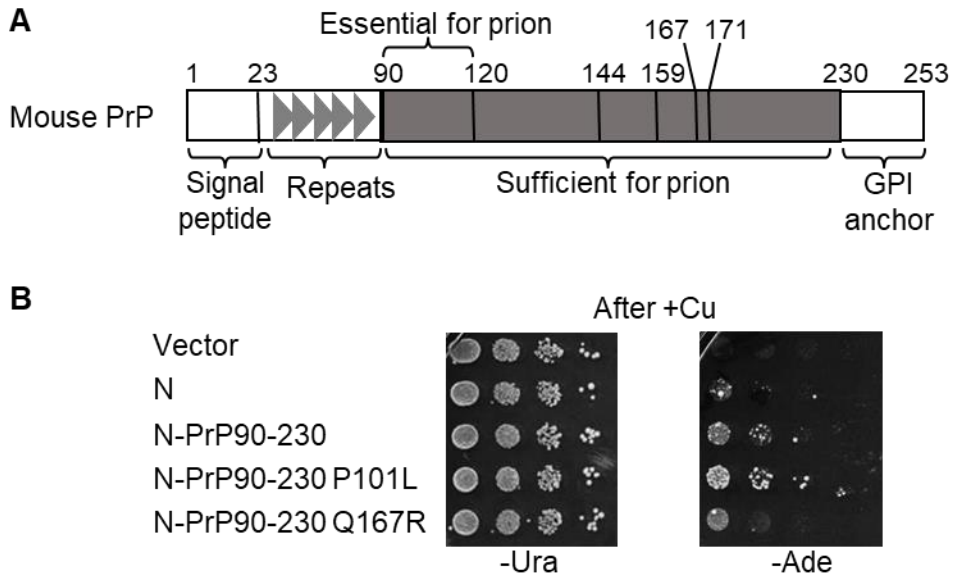

Figure 3-10. Effect of mutations in PrP on [*PSI*$^+$] nucleation by PrP-based chimeric constructs in yeast. (A) Scheme of construction of the chimeric Sup35N-PrP90-230 derivatives. Numbers indicate amino acid positions, corresponding to mutations or truncations made in our work. (B) Phenotypic detection of [*PSI*$^+$] nucleation by wild type and mutant PrP-based chimeric constructs in yeast. Transient overproduction of the Sup35N-PrP constructs was induced on the medium with additional 100 μM $CuSO_4$, and serial decimal dilutions were spotted onto the –Ura medium selective for the plasmid (left image) and onto the –Ade medium selective for [*PSI*$^+$] (right image).

The region between amino acid residues 90 and 119 is required for the susceptibility to prion disease in mammals[79-81]. We have shown that a deletion of this region knocks out [*PSI*$^+$] nucleation by the chimeric Sup35N-PrP protein in yeast (Figure 3-11A and Table 1). Truncation of human PrP after positions 144 or 159, eliminating the C-terminal region, leads to a heritable disease with symptoms similar to prion disease [],

and truncated PrP forms amyloids *in vitro*[80,81]. We have shown that C-terminal truncations of mouse PrP (at positions 144, 159 or 171) in the Sup35N-PrP chimeras significantly increased both [*PSI*$^+$] nucleation (Figure 3-11A and Table 1), and truncation at position 159 of PrP also enabled [*PSI*$^+$] nucleation in a fusion to Sup35NM (Figure 3-11A). These data agree with the notion that C-terminal PrP truncations trigger the formation of disease via nucleating prion-like aggregates, even though transmissibility of such aggregates has not been proven. Notably, the PrP fragment including only residues from 90 through 119 did not promote [*PSI*$^+$] nucleation when fused to Sup35 (Figure 3-11A), indicating that while this region is essential for prion formation (see above), it is not sufficient for this process. The presence of the N-terminal region of PrP (23-89) increased [*PSI*$^+$] nucleation in yeast, as demonstrated by the ability of the chimeric Sup35NM-PrP23-230 protein to nucleate [*PSI*$^+$], (Figure 3-11C), in contrast to the Sup35NM-PrP90-159 construct (see above, Figure 3-11B). While the 23-89 region of PrP is not necessary for prion formation or propagation in mammals, it contains oligopeptide repeats, whose expansions are known to cause a heritable disease with symptoms similar to a prion disease[81,82], Overall, our data show that PrP alterations influence its ability to nucleate prions in yeast in the same direction as they influence (or are suggested to influence) prion diseases in mammals and humans.

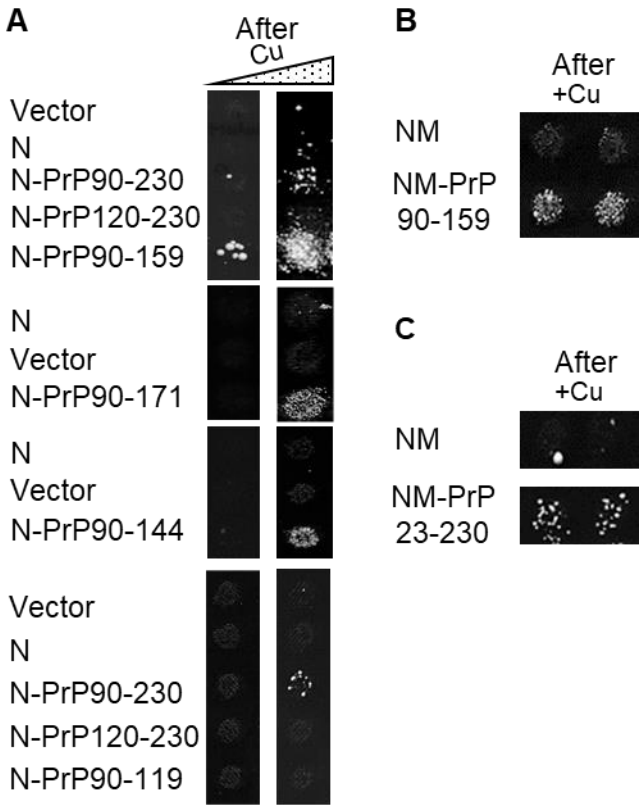

Figure 3-11. Effect of truncations in PrP on [*PSI*$^+$] nucleation by PrP-based chimeric constructs in yeast. (A) Comparison of [*PSI*$^+$] nucleation by the Sup35N-PrP derivatives with various truncations after growth on the medium with additional 100 μM $CuSO_4$. The Sup35N-PrP120-230 construct was not able to nucleate [*PSI*$^+$], whereas the Sup35N-PrP90-144, Sup35N-PrP90-159 and Sup35N-PrP90-171 constructs exhibited increased [*PSI*$^+$] formation, compared to Sup35N-PrP120-230. Quantitative data are shown in Table 3-1. (B) and (C) Sup35NM fused to PrP90-159 (B) or to PrP23-230 (C) can promote formation of [*PSI*$^+$] in a [*psi*$^-$ *pin*$^-$] strain after overexpression. On panels A, the images from –Ade plates are shown, obtained without (left column on panel A) or with (panels B and C, and right column on panel A) pre-incubation in the presence of additional (100 μM) $CuSO_4$.

*3.3.7 Biochemical detection of [*PSI$^+$*] aggregates by Sup35N fused to PrP*

By using semi-denaturing detergent agarose gel electrophoresis (SDD-AGE), we have demonstrated that the chimeric proteins containing PrP90-230 produced detergent-resistant polymers in the yeast cells lacking pre-existing prions (Figure 3-12A) as is typical of yeast prions and amyloids[32] and promoted the immobilization of endogenous Sup35

protein into an aggregated fraction (Figure 3-12B). Thus, phenotypically detectable [*PSI*$^{+}$] formation coincides with physical aggregation of the inducer protein and immobilization of the inducee protein into aggregates. Also, the deletion of a region between amino acid residues 90 and 119 that previously knocked out [*PSI*$^{+}$] nucleation by the chimeric Sup35N-PrP protein in yeast (Figure 3-11A and Table 3-1) essentially eliminates the immobilization of full-size Sup35 protein into aggregates in the yeast cells as detected by SDD-AGE (Figure 3-12). C-terminal truncations of mouse PrP at positions 159 and 171 that previously increased [*PSI*$^{+}$] nucleation by the chimeric Sup35N-PrP proteins in yeast (Figure 3-11A and Table 3-1) immobilized Sup35 into amyloid aggregates (Figure 3-12C).

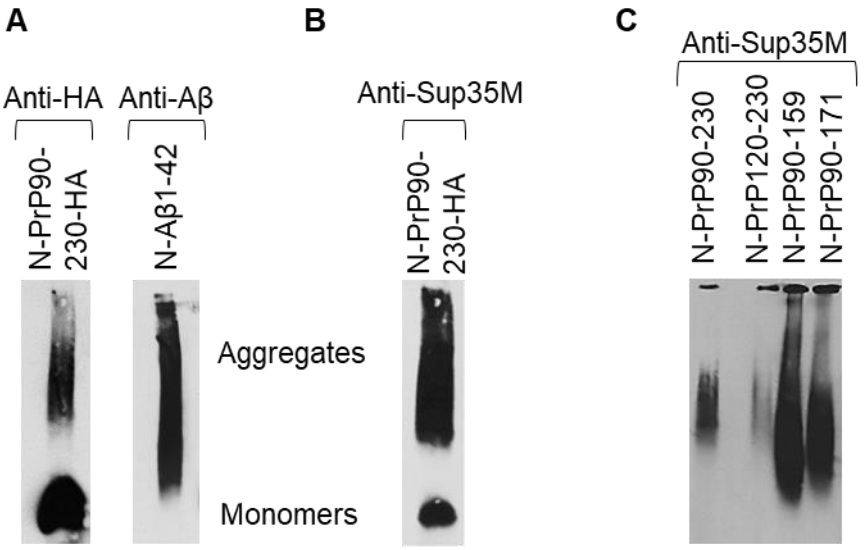

Figure 3-12. Biochemical detection of aggregation promoted by chimeric proteins in yeast. (A), (B), and (C) Cell lysates of cultures expressing chimeric proteins Sup35N-PrP90-230-HA or Sup35N-PrP90-230 derivatives in the presence of 100 μM $CuSO_4$ analyzed by semi-denaturing detergent agarose gel electrophoresis (SDD-AGE). On panel A, monomers and high molecular weight aggregates of chimeric proteins were detected by the anti-HA antibody for the HA-tagged Sup35N-PrP90-230. On panel B, immobilization of the endogenous Sup35 protein into an aggregated fraction in the presence of Sup35N-PrP90-230 (but not in the presence of control Sup35N) is detected using the anti-Sup35M antibody. On panel C, Sup35N-PrP120-230 construct cannot promote immobilization of endogenous Sup35 protein into an aggregated fraction, whereas the Sup35N-PrP90-159 and Sup35N-PrP90-171 constructs increase immobilization of Sup35 into an aggregated fraction, compared to Sup35N-PrP90-230. Equal protein amounts were loaded in each case; monomeric fractions are not shown.

3.3.8 Protein expression levels of Sup35N-PrP derivatives

One possible explanation for chimeric constructs, as well as for alterations of PrP or Aβ to influence [*PSI*$^{+}$] nucleation could be through altering levels of chimeric proteins. To investigate this possibility, we have compared levels of proteins accumulated in yeast cells at the same concentrations of $CuSO_4$. As described previously[82], and confirmed by us (Figure 3-13A), Sup35N is accumulated at low levels in yeast, despite the fact that it has a higher prion-inducing activity in comparison to Sup35NM and Sup35. This is probably due to the high misfolding capability and proteolytic instability of Sup35N. The Sup35N-PrP90-230 chimeric protein was produced at higher levels compared to Sup35N (Figure 3-13A). However, this could not explain the increased prion-nucleating activity of Sup35N-PrP90-230, because the Sup35N-PrP120-230 derivative, not capable of prion nucleation, was produced at about the same level as Sup35N-PrP90-230 (Figure 3-13B). Moreover, the C-terminal truncated derivatives of Sup35N-PrP, that exhibited increased [*PSI*$^{+}$] nucleation, were in fact accumulated at lower levels compared to Sup35N-PrP90-230 (Figure 3-13B). Overall, our data show that while cellular levels of proteins used in this work could vary in some cases, the differences in prion nucleation cannot be explained by differences in protein abundance.

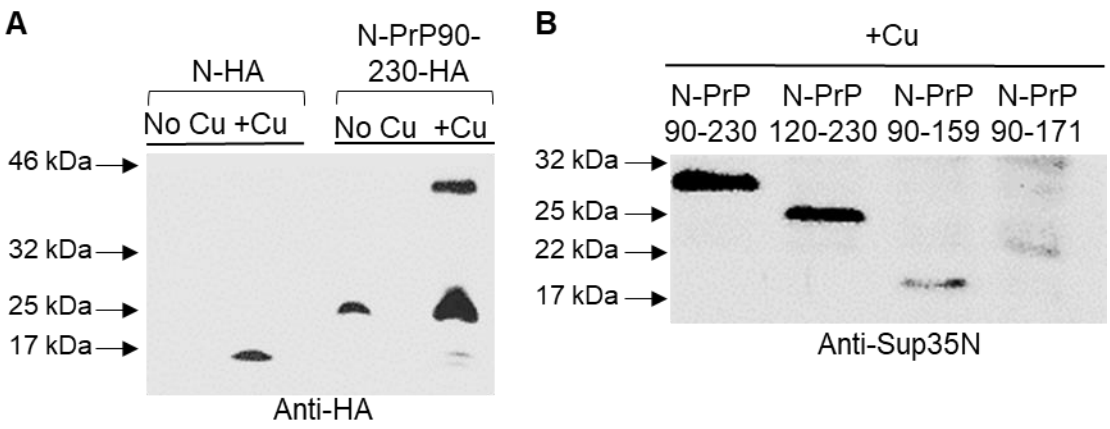

Figure 3-13. Protein expression levels of Sup35N-PrP derivatives. (A) Detection of the Sup35N and Sup35N-PrP90-230 proteins, tagged with HA, by using SDS-PAGE and Western blot with anti-HA antibody. Sup35N-PrP90-230 is accumulated at higher levels, compared to Sup35N. The upper band in the right lane corresponds to the dimer, presumably formed via disulfide bonds, as it is sensitive to β-mercaptoethanol (data not shown). (B) Comparison of the levels of Sup35N-PrP90-230, Sup35N-PrP120-230, Sup35N-PrP90-144, and Sup35N-PrP90-171 as detected by SDS-PAGE and Western blot with anti-Sup35N antibody. The Sup35N-PrP90-230 and Sup35N-PrP120-230 proteins are accumulated at similar levels. This result is also confirmed by using the anti-PrP (4H11) antibody (data not shown). The C-terminal deletion constructs are produced at lower levels, compared to Sup35N-PrP90-230 and Sup35N-PrP120-230. In all cases, protein amounts were normalized by the Bradford assay and/or Coomassie staining. On all panels, "+Cu" refers to cultures growing in the presence of 100 μM $CuSO_4$.

3.3.9 Analysis of [PSI$^+$] strains induced by Sup35N-PrP derivatives

The Sup35 protein can produce a variety of prion variants or "strains" which presumably correspond to various amyloid structures[34,83]. These strains can be differentiated from each other based on both their phenotypic manifestations and biochemical patterns. "Stronger" strains are characterized by higher levels of nonsense codon readthrough (leading to better growth on –Ade medium and lighter color on complete medium in the case of *ade1-14* reporter) and by higher mitotic stability compared to "weaker" strains. This is because "stronger" strains are generated by amyloid fibrils with a less rigid amyloid core that are more efficiently fragmented by the yeast chaperone machinery and therefore produce larger number of oligomeric "seeds", making immobilization of newly synthesized

Sup35 and proliferation of prion state more efficient[85]. Once established, the prion strain typically faithfully reproduces its observable characteristics.

In order to determine if mammalian amyloidogenic proteins influence the parameters of prion “strains” produced in yeast, we compared spectra of prion strains generated in the presence of different inducing constructs. For this purpose, [*PSI*$^{+}$] isolates were divided into three groups designated as “strong”, “intermediate” and “weak” strains on the basis of growth on –Ade medium and color on complete (YPD) medium. Strain patterns were scored after elimination of the inducing plasmid, in order to exclude a possibility of that the continuous presence of a chimeric construct influences the phenotypic manifestation of a [*PSI*$^{+}$] strain. Data are shown on Figure 3-14A and Appendix Figure A, and in Table 3-3. Sup35N-PrP90-230 induced preferentially “strong” strains, the constructs with some deletion PrP derivatives, such as Sup35N-PrP90-159 and Sup35N-PrP90-171 induced preferentially or exclusively “intermediate” strains.

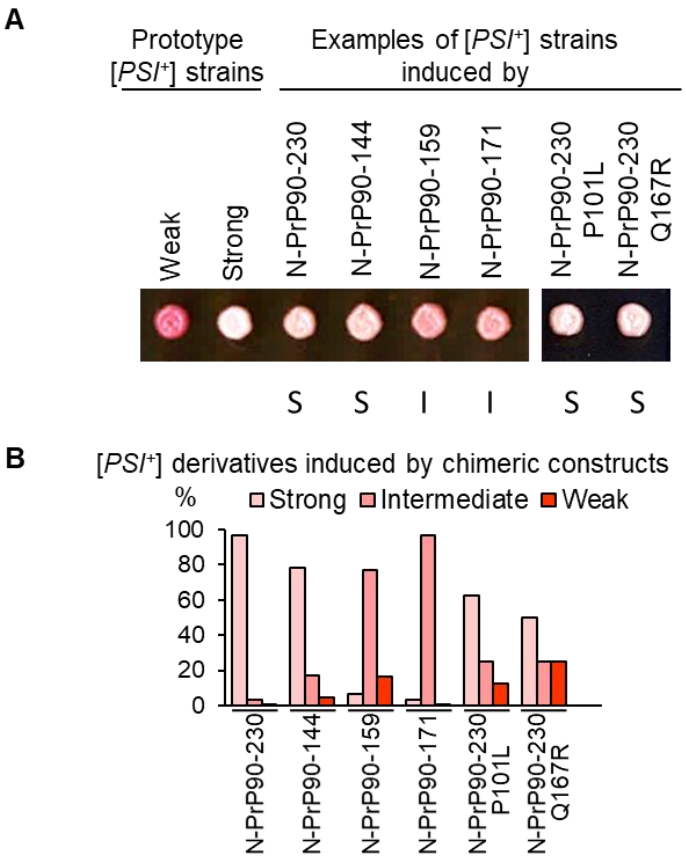

Figure 3-14. Spectra of prion strains induced by various Sup35N-PrP derivatives. (A) [*PSI*$^+$] strains were distinguished by color on YPD and amount of growth on –Ade. Strong [*PSI*$^+$] appeared white or white-pink on YPD and grew after 2 days on -Ade; intermediate [*PSI*$^+$] appeared solid pink on YPD and grew after 4 days on -Ade; weak [*PSI*$^+$] appeared red-pink on YPD and grew after 7 days on -Ade. Previously published prototype strains OT56 (for the strong [*PSI*$^+$] prion) and OT55 (for the weak [*PSI*$^+$] prion) are shown for the comparison to representative strong (S), weak (W) and intermediate (I) isolates, nucleated by the chimeric constructs (as indicated) and tested after the loss of a prion-inducing plasmid. YPD plates were incubated for 4 days at 30°C, followed by 3 days of refrigeration at 4°C for the better color development. (B) Percentages of strong, intermediate, and weak [*PSI*$^+$] strains induced by wild type and altered Sup35N-PrP derivatives in a [*psi*$^-$ *pin*$^-$] strain. More detailed information, including images for multiple isolates, data for the constructs containing point mutations, actual numbers and errors is presented in Appendix Figure A and Table 3-3.

Table 3-3. Numbers and percentages* of [*PSI*$^+$] strains induced by various PrP-based chimeric constructs

Inducer	Strong [*PSI*$^+$]	Intermediate [*PSI*$^+$]	Weak [*PSI*$^+$]	Total number of [*PSI*$^+$] isolates checked
Sup35N-PrP90-230	31 96.9 (+/-3.0)%	1 3.1 (+/-3.0)%	0 0 (+3.0)%	32
Sup35N-PrP90-144	18 78.3 (+/-8.6)%	4 17.4 (+/-7.9)%	1 4.3 (+/-4.2)%	23
Sup35N-PrP90-159	2 6.7 (+/-4.5)%	23 76.6 (+/-7.7)%	5 16.7 (+/-6.8)%	30
Sup35N-PrP90-171	1 0 (+3.4)%	27 100 (-3.4)%	0 0 (+3.4)%	28
Sup35N-PrP90-230 P101L	5 62.5 (+/-17.1)%	2 25 (+/-15.4)%	1 12.5 (+/-11.7)%	8
Sup35N-PrP90-230 Q167R	4 50 (+/-17.7)%	2 25 (+/-15.3)%	2 25 (+/-15.3)%	8

*****Errors, calculated according to multinomial distribution (based on ref. 68), are shown in parentheses.

3.4 Discussion

*[*PIN$^+$*] independent [*PSI$^+$*] nucleation.* Efficient prion nucleation by the overproduced yeast Sup35 protein or its PrD-containing fragments typically requires the presence of another (usually QN-rich) protein in an aggregated form[37,38,39]. A fusion of some Sup35 PrD-containing derivatives to extended polyQ tracts, resembling those associated with HD in humans, or to a yeast prion forming protein Rnq1 promotes nucleation of the Sup35 prion even in the absence of pre-existing Q/N rich yeast prions[62,85]. However, expanded polyQ constructs and QN-rich proteins were also reported to promote Sup35 aggregation *in trans*[37],, so that an addition of a polyQ or another QN-rich region to the QN-rich Sup35 PrD could be interpreted as an expansion of Sup35 PrD. Our new data demonstrate (to our knowledge, for the first time) that a fusion of Sup35 PrD-containing region (Sup35N or Sup35NM) to a non-QN-rich mammalian protein (or protein domain) with proven

amyloidogenic properties is sufficient for nucleating the formation of Sup35-based prions in yeast cells lacking known pre-existing prions. An apparent explanation for this result is that mammalian proteins nucleate an amyloid in yeast, thus promoting amyloidization of the attached yeast prion domain (Figure 3-15). This leads to immobilization of full-length endogenous yeast protein into prion aggregates, thus allowing for phenotypic detection of a yeast prion. Importantly, a covalent attachment of mammalian "inducer" to Sup35N (or NM) is required for prion nucleation, as mammalian non-QN-rich amyloidogenic protein do not promote [*PSI*$^{+}$] induction *in trans* (Figure 3-2). As expected, the Sup35N-based chimeric proteins are more efficient in prion nucleation than the Sup35NM-based chimeric proteins, apparently due to an anti-nucleation effect of the M region of Sup35, which contains stretches of potentially repulsive charged residues. This explains why the previous work by Choe group[86] failed to detect [*PSI*$^{+}$] induction by the Sup35NM-PrP-GFP chimeric protein in the [*pin*$^{-}$] cells. Indeed, the Sup35NM-PrP90-230 chimeric protein also failed to nucleate [*PSI*$^{+}$] in our hands (Figure 3-4C), although [*PSI*$^{+}$] induction was detected for the Sup35N-PrP90-230 construct (Fig. 3-4A).

*Role of protein amyloidogenicity in [*PSI^{+}*] nucleation.* Importantly, non-amyloid protein multimerization is not sufficient to trigger the formation of amyloid nuclei at a level comparable to amylodogenic oligomerization, as shown by the lack of [*PSI*$^{+}$] induction in the presence of chimeric constructs, producing non-amyloidogenic multimeric proteins such as such as Ade2 and LacZ(Figure 3-6A,B). Fusions of Sup35N with mammalian amyloidogenic proteins are characterized by higher protein abundance at the same levels of expression, compared to proteolytically unstable Sup35N (Figure 3-13). However, the increased frequency of prion nucleation by Sup35N-based chimeric proteins is not simply due to an increase in the abundance of chimeric constructs. This shows that the increased prion nucleation by chimeric constructs is a result of their amyloidogenic properties,

leading to the initiation of the self-assembly into an amyloid form.

Sequence requirements for prion nucleation by PrP. The region between residues 90 and 119 of PrP, that is known to be essential for the susceptibility to prion infection in mammals [], is also required for prion nucleation in yeast, while the N-terminal region of PrP (23-89) is dispensable for both (Figure 3-10). Mutation P101L, associated with heritable prion disease in mammals[49,55] increased, while mutation Q167R, inhibiting prion replication in mammals decreased PrP-dependent prion nucleation in the yeast assay. Increased prion nucleating ability of the fragments lacking the C-proximal region of PrP (Figure 3-11A) agrees with previous reports linking C-proximal PrP truncations to a heritable neurological disease in humans[71] and supports a notion that this disease is likely to be prion-like in nature. One possible explanation for this effect is that the α-rich C-proximal domain of PrP stabilizes the native conformation and therefore antagonizes the initiation of the cross-β (prion) conformation[71]. While the structural organization of PrP in a prion form remains a matter of debates (*e. g.*, our data agree with models locating cross-β interactions within the region 90-170, suggesting the retention of the native secondary structure by the C-terminal region of PrP[77] and predict that the proposed β-structure at positions 160–164 is dispensable for prion initiation. However, our data do not necessarily contradict a possibility of further expansion of the amyloid core to the C-proximal region as shown for some PrP-based amyloids[87,88]. Most importantly, our yeast assay provides a tool that could be employed to further decipher sequential and structural requirements for initiation of PrP polymerization and conformational conversion.

*The impact of a nucleating construct on spectra of induced [*PSI$^+$*] "strains".* Both yeast[32] and mammalian[89-91] prion and amyloid proteins are known to form various variants or "strains" that differ from each other by phenotypic and biochemical characteristics and are apparently controlled by distinct protein conformations. Interestingly, we have found out

that the spectra of [*PSI*$^{+}$] strains induced by different chimeric constructs differ from each other (Figure 3-14). One possible explanation for these data is the formation of distinct initial nuclei by different attached regions of chimeric proteins, followed by an expansion of the amyloid region to different regions of the attached Sup35N domain. Such a mechanism would correspond to a "deformed templating" model previously proposed for strain conversions in PrP prions[92]. In this scenario, the spectra of [*PSI*$^{+}$] strains might corroborate to the differences in the "hybrid" templates formed by the fusion proteins. An alternative explanation is that certain strain conformations formed by Sup35N are more compatible, while other strain conformations are less compatible with an amyloid conformation formed by a specific mammalian amyloidogenic protein physically attached to the same molecule.

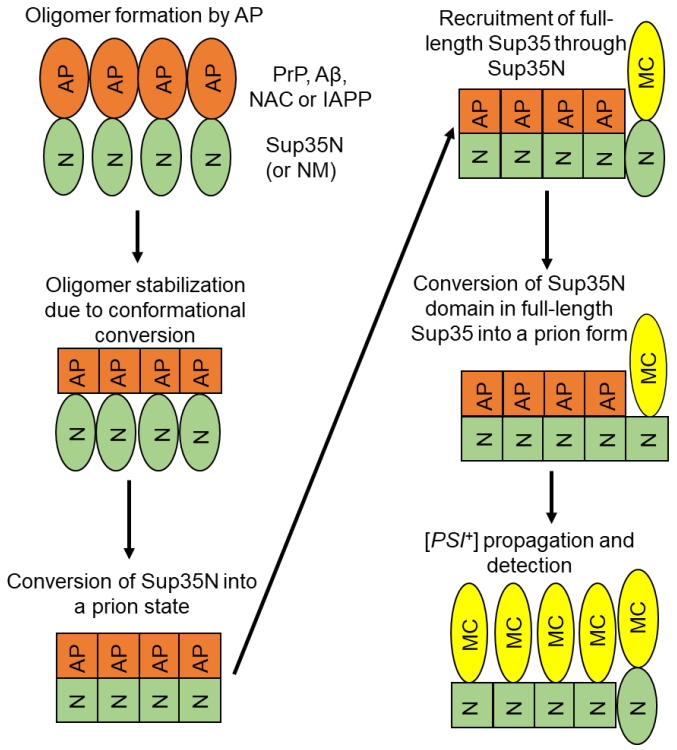

Figure 3-15. Model for [*PSI*$^{+}$] nucleation by mammalian amyloidogenic proteins. N, M and C – domains of Sup35, AP – mammalian amyloidogenic protein (PrP, Aβ, NAC region of α-synuclein, IAPP otherwise called amylin, or myocilin). Non-prion isoforms are designated as ellipses, prion isoforms – as squares.

3.5 Conclusions

- Mammalian amyloidogenic proteins did not promote [*PSI*$^{+}$] nucleation *in trans.*

- Mammalian non-QN-rich amyloidogenic proteins or their amyloidogenic regions Q/N rich nucleated the Sup35 prion in yeast in the absence of pre-existing prions, when fused to the prion domain of Sup35 protein.

- Non-amyloidogenic proteins (including those forming non-amyloid multimers) did not nucleate [*PSI*$^{+}$] when fused to the prion domain of Sup35.

- [*PSI*$^{+}$] induction by Sup35N-PrP chimera was not due to the induction of [*PIN*$^{+}$]

- Anti- or pro-amyloidogenic alterations in PrP respectively antagonized or promoted prion nucleation in yeast

- Sup35N-PrP derivatives that nucleated [*PSI*$^{+}$] also produced detergent-resistant prion polymers in the yeast cells and promoted the immobilization of endogenous Sup35 into an aggregated fraction.

- Different Sup35N-PrP chimeras induced different spectra of prion strains in yeast

CHAPTER 4. MUTATIONAL ANALYSIS OF AMYLOID BETA IN YEAST

This chapter includes data published in Journal of Biological Chemistry.

Chandramowlishwaran, P., Sun, M., Casey, K. L., Romanyuk, A. V., Grizel, A. V., Sopova, J. V., Rubel, A. A., Nussbaum-Krammer, C., Vorberg, I. M., and Chernoff, Y. O. (2018) Mammalian amyloidogenic proteins promote prion nucleation in yeast. *Journal of Biological Chemistry*. 293:3436-3450

4.1 Summary

In this chapter, we employed the yeast model introduced in Chapter 3 to investigate the effects of sequence alterations in Aβ peptide (associated with Alzheimer's disease, (AD) and of certain chemicals previously linked to AD on prion nucleation by chimeric Aβ1-42-based constructs in yeast. Yeast assay confirms that the more aggregation-prone and more pathogenic Aβ derivative, Aβ1-42 is more efficient in prion nucleation than is the less aggregation-prone and less pathogenic Aβ derivative, Aβ1-40, confirming the previously reported differences in the aggregation of Aβ1-40 and Aβ1-42 in humans. A triple mutation (F19S, F20S, I31P) or even a single mutation I31P in Aβ1-42 knocking cross-β amyloid structures according the most recent structural models entirely abolishes prion nucleation in the yeast assay. In contrast to Sup35N-Aβ1-42 chimera, Sup35N-Aβ1-40 chimera or Sup35N-Aβ1-42 with the triple mutation could not aggregate or immobilize the endogenous Sup35 into an aggregated fraction. The mutation D23N, associated with familial AD, showed increased nucleation as compared to wild type Aβ1-42, while, substitutions K28E or D23K respectively decreased or increased prion nucleation by Sup35N-Aβ1-42 in yeast. Mutations in Aβ1-42 predicted to have low or high amyloidogenicity by a computational model for disease-related amyloids that invoke β arches composed of strand-turn-strand motifs in which the two β strands interact via their side chains, respectively demonstrated decreased or increased nucleation by Sup35N-Aβ1-42 in yeast. Toxicological metal ions previously suspected to promote AD, such as Li, Cd, and As, as well as neuronal metal ions like Zn and Cu, increased prion nucleation

in the presence of Sup35N-Aβ1-42, indicating the applicability of our yeast prion nucleation assay for testing the effects of chemical agents on the amyloid properties of Aβ1-42. Overall, our data confirm that the ability of Aβ1-42 to promote prion nucleation in yeast depends on the same parameters that control Aβ1-42 oligomerization and aggregation in humans and *in vitro*, and that the yeast assay can be used for dissecting the sequence elements and environmental factors influencing amyloid nucleation by Aβ1-42.

4.2 Specific materials and methods

4.2.1 Materials

The strains, plasmids, and primers used in this study are listed in Appendix Tables A, B, and C respectively. Sup35C antibody used in this study is described in Chapter 2.

4.2.2 Methods

Standard protocols were used for DNA isolation, gel electrophoresis, restriction digestion, gel extraction, ligation, and bacterial transformation and are described in Chapter 2. Standard yeast media and standard procedures for yeast cultivation, phenotypic analysis, and transformation were used and are described in Chapter 2. The plate assay for [*PSI*$^+$] nucleation and semi-quantitative/quantitative [*PSI*$^+$] measurements are described in Chapter 2. The protocol for protein analysis including SDS-PAGE for measuring protein levels and SDD-AGE for characterizing the amyloid aggregates are described in Chapter 2. The scheme for mutations in the region coding for Aβ1-42 were generated using site-directed mutagenesis and are described in Chapter 2.

4.2.2.1 Scheme of screening assay for agents influencing [*PSI*$^+$] nucleation

In the initial plate assay, a chemical to be tested was absorbed on the sterile paper filter and placed in the middle of the freshly-made lawn of the yeast [*psi*$^-$ *pin*$^-$] reporter strain, bearing Sup35N-Aβ construct and prepared on a petri dish with the medium inducing expression of the chimeric Sup35N-Aβ1-42 construct (e. g. galactose for the P_{GAL} promoter). Toxicological compounds, such as Cd and As salts or even biologically relevant ions at high concentrations, generate a halo of growth inhibition around the filter in these conditions. This confirms that compound is taken up by the yeast cells. After the lawn is grown, it was replica plated onto –Ade medium, where prion formation can be detected by growth due to nonsense-suppression of the *ade1-14* reporter (see Figure 4-1). We used H_2O as the experimental control and experimental metal ion containing solvents such as 300μM $CuSO_4$, 300μM LiCl, 300μM $ZnCl_2$, 150μM $AsCl_2$, and 100μM $CdCl_2$. The concentrations for the nucleation experiment was adjusted based on the toxicity of the compound being tested. As and Cd generated toxicity and thus their concentrations were lowered until they didn't form a halo of inhibition after they were added to the filter paper disc in the presence of yeast cells.

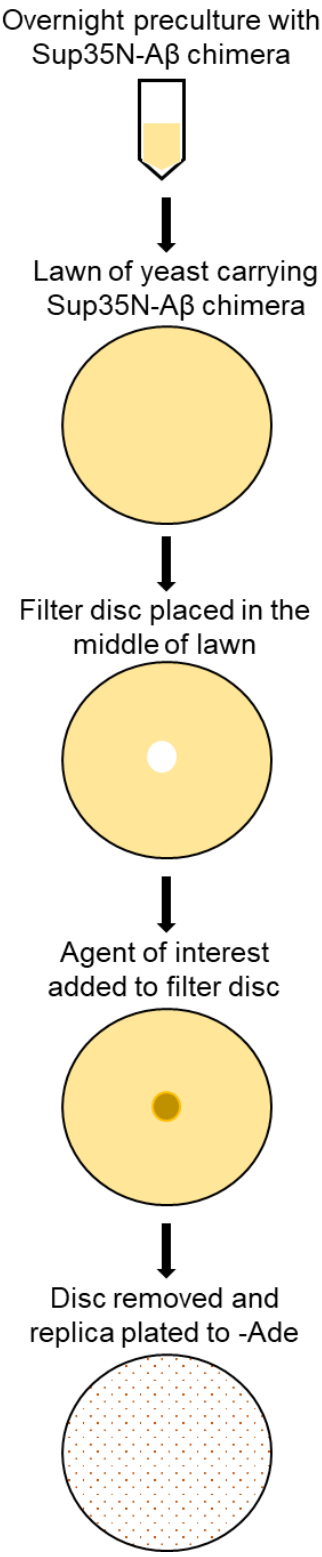

Figure 4-1. Scheme of plate assay to check for agents that influence [*PSI*$^{+}$] nucleation by Sup35N-Aβ chimeric protein

4.2.2.2 ArchCandy algorithm for prediction of Aβ mutations

The mutations in Aβ with a high or low amyloidogenic score to predict amyloid forming potential or lack thereof, was based on the ArchCandy-1.0 program that detects regions in protein sequences that have a potential to form amyloids[93]. The scores for the Aβ mutants were generated and provided by Dr. Andrey Kajava at Montpellier University, France as a collaborative project. The core structural element of a majority of naturally-occurring and disease-related amyloid fibrils is a β-arcade representing a parallel and in register stacks of β-strand-loop-β-strand motifs called β-arches[93]. "ArchCandy" was developed based on an assumption that protein sequences that are able to form β-arcades are amyloidogenic. The amyloidogenicity scores of the mutations H13L, A21E D23A, G25V, K28E and F19K are listed here. The mutants were predicted to have lower amyloidogenicity based on a score of 0.549 using the algorithm explained previously. The mutants tested were Aβ(1-42) K28E with the amino acid sequence DAEFRHDSGYEVHHQKLVFFAEDVGSNEGAIIGLMVGGVVIA), Aβ(1-42) G25V with the amino acid sequence DAEFRHDSGYEVHHQKLVFFAEDVVSNKGAIIGLMVGGVVIA), and Aβ(1-42) F19K with the amino acid sequence (DAEFRHDSGYEVHHQKLVKFAEDVGSNKGAIIGLMVGGVVIA). The mutants were predicted to have higher amyloidogenicity based on a score of 0.763. The mutants tested were Aβ(1-42) A21E, D23A with the amino acid sequence (DAEFRHDSGYEVHHQKLVFFEEAVGSNKGAIIGLMVGGVVIA) and Aβ(1-42) H13L with the amino acid sequence (DAEFRHDSGYEVLHQKLVFFAEDVGSNKGAIIGLMVGGVVIA).

4.3 Results

A unique feature of our experimental system is that *in vivo* (inside a living organism) protein misfolding and disease formation of human proteins, triggering the amyloid nucleation (earliest formation or the very first step) process, can be induced at our will by increasing the level of production of a chimeric protein. This somewhat mimics a proposed scenario of Alzheimer's disease (AD) development in humans, where increased production of Alzheimer's protein is implicated in the initial amyloid formation.

In chapter 3, we overproduced the human amyloid β peptide (Aβ), associated with AD, in a yeast strain lacking pre-existing prions ([*pin*$^-$ *psi*$^-$]) either individually or simultaneously with separately expressed Sup35N (Figure 3-2). Aβ1-42 or Aβ1-42-GFP could not induce [*PSI*$^+$] formation, both at normal levels of Sup35 and in the presence of excess Sup35N (Figure 3-3A, B). However, Aβ1-42 promoted [*PSI*$^+$] nucleation when attached to the Sup35 prion domain (Figure 3-4A). The Ade$^+$ colonies induced by the Aβ-based chimeric constructs in the [*pin*$^-$] strain retained suppression after the loss of the inducing plasmid and were curable by serial passages on medium containing an antiprion agent guanidine hydrochloride, GuHCl. These data confirmed that the majority of these colonies arise from the conversion of the endogenous Sup35 protein into a prion form, [*PSI*$^+$].

Next, we checked if alterations (deletions or mutations) in Aβ1-42 known to influence prion propagation and disease in mammals have similar effects in yeast. Using *in vitro* models as well as the most recent structural model of Aβ1-42 polymers models[94,95] demonstrating the secondary structure of Aβ(1–42) molecule which consists of two molecules per Aβ(1–42) polymer unit and comprises five in-register parallel intermolecular β-strands [i.e., 2–6 (β1), 15–18 (β2), 26–28 (β3), 30–32 (β4), and 39–42 (β5)]., we mapped the locations of deletions and mutations in Aβ(1–42), that are known or predicted to influence the

aggregation patterns of Aβ(1–42). The alterations made in Aβ (1–42) are indicated as grey dotted lines (for deletions) and orange dotted lines (for point mutations). The mutations in red indicate those were predicted by ArchCandy algorithm (refer Methods) to have lower or higher amyloidogenicity based on a β arcade model of disease related amyloids; the mutations in green indicate those that were based on *in vitro* models or recent structural models; the mutation in purple indicates a familial AD Iowa mutation.

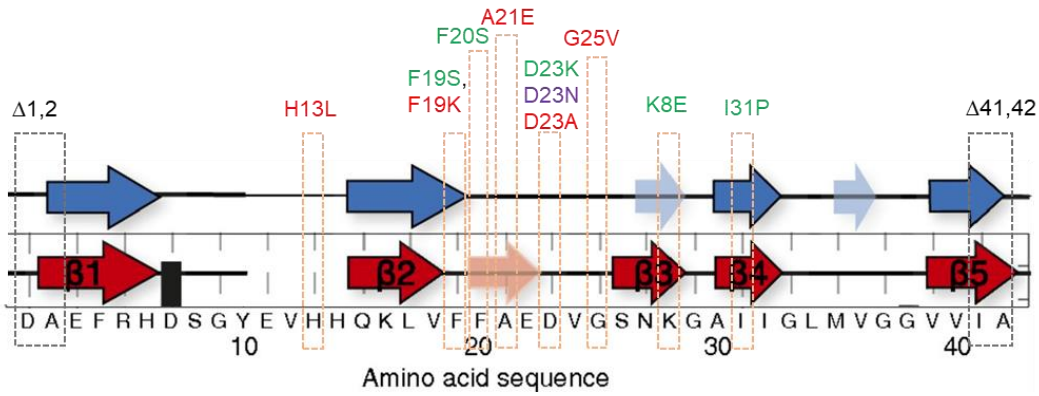

Figure 4-2. The location of alterations in Aβ(1–42) based on the secondary structure of Aβ(1–42) molecule. The model is based on the latest structure of a polymorph of Aβ (1–42) amyloid fibril mostly based on solid-state NMR (as per ref. 95, 96). The alterations made in Aβ(1–42) are indicated as dotted lines in different colors (refer text above).

4.3.1 Effects of truncations in Aβ1-42 on [PSI⁺] nucleation by Sup35N-Aβ1-42

Several variants of Aβ peptide exist in humans, of which Aβ1-42 and Aβ1-40 (lacking the last two amino acid residues) are the most abundant ones[96]. Of these two, Aβ1-42 is considered to be the most amyloidogenic and most pathogenic form in humans[97]. In yeast, Sup35N-Aβ1-40 nucleated [*PSI*⁺] much less efficiently than did Sup35N-Aβ1-42 (Figure 4-3A), while Sup35NM-Aβ1-40 did not nucleate [*PSI*⁺] at all (Figure 4-3B). Notably, removal of the two N-terminal amino acid residues of Aβ within the chimeric construct did not inhibit [*PSI*⁺] nucleation (Figure 4-3C), in an agreement with structural models placing

the N-terminal region of Aβ outside of amyloid core[94,95].

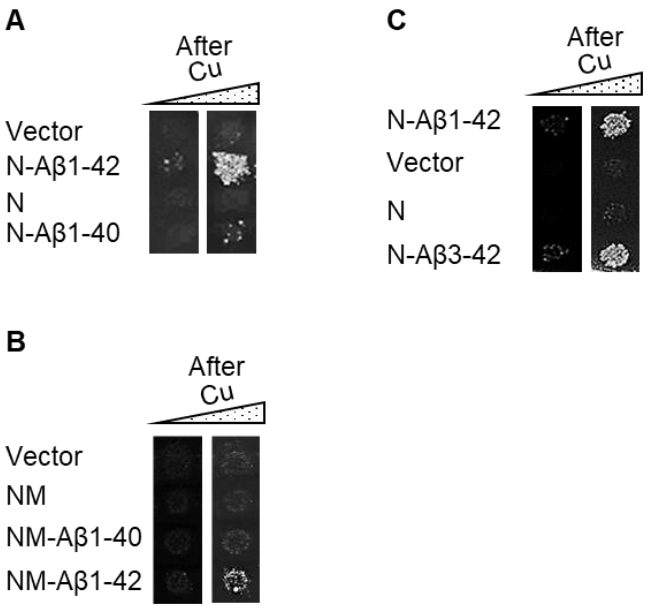

Figure 4-3. [*PSI*$^+$] nucleation by chimeric constructs with various Aβ truncations in yeast. (A) The Sup35N-Aβ1-40 construct shows decreased [*PSI*$^+$] induction in a [*psi*$^-$ *pin*$^-$] strain, compared to Sup35N-Aβ1-42. (B) The Sup35NM-Aβ1-40 construct does not induce [*PSI*$^+$] formation in a [*psi*$^-$ *pin*$^-$] strain. [*PSI*$^+$] induction by Sup35NM-Aβ1-42 is shown as a positive control. (C) The Sup35N-Aβ3-42 construct induces [*PSI*$^+$] formation in a [*psi*$^-$ *pin*$^-$] strain at levels comparable to Sup35N-Aβ1-42. On panels A through C, the images from –Ade plates are shown, without (left column) or with (right column) pre-incubation on the medium with additional 100 μM $CuSO_4$. For quantitative data, see Table 4-1.

Table 4-1. Frequencies of [*PSI*$^+$] induction by Aβ-based chimeric and control plasmids

Inducer	**Frequency (+/- standard deviation) of Ade$^+$ colonies per 10,000 cells after 100 μM $CuSO_4$**	
	0 hrs.	**24 hrs.**
Sup35N-Aβ1-42	1.19+/-0.16	1178+/-208
Sup35N-Aβ1-40	0.09+/-0.08	2.0+/-0.9
Sup35N-Aβ1-42*** (F19S, F20S, I31P)	0.09+/-0.05	0.36+/-0.28
Sup35NM	0.07+/-0.06	0.13+/-0.04
Sup35NM-Aβ1-42	0.11+/-0.03	30+/-7
Sup35NM-Aβ1-42*** (F19S, F20S, I31P)	0.01+/-0.02	0.04+/-0.03

4.3.2 Effects of mutations in Aβ1-42 on [PSI$^+$] nucleation by Sup35N-Aβ1-42

We have also generated several mutations at the positions of Aβ1-42 known to influence amyloid formation[98,99,100].

4.3.2.1 Based on an *in vitro or a* familial AD model

Previous *in vitro* experiments and structural data identified positions 19, 20 and 31 as being important for amyloid formation by Aβ[94,95] and located within intramolecular cross-β sheets of Aβ1-40 polymers[95]. However, according to the most recent structural model of Aβ1-42 polymers[95] only position 31 is located within one of the β-strands, while positions 19 and 20 are involved in hydrophobic interactions. Indeed, the substitution I31P, breaking the proposed β4-strand[95], greatly decreased [*PSI*$^+$] nucleation by Sup35N-Aβ1-42, while the substitution F19S caused only a mild decrease, and the substitution F20S had almost no effect (Figure 4-4A). Notably, the triple mutation F19S, F20S, I31P entirely abolished [*PSI*$^+$] nucleation by both Sup35N-Aβ1-42 (Figure 4-4A, Table 4-1) and Sup35NM-Aβ1-42 (Table 4-1). On the contrary, chimeric constructs with a substitution D23N, a so-called "Iowa mutation" associated with the heritable form of AD[14], significantly increased [*PSI*$^+$] nucleation in yeast (Figure 4-4B). These data confirm that effects Aβ alterations in the yeast model parallel those detected *in vitro* or in humans.

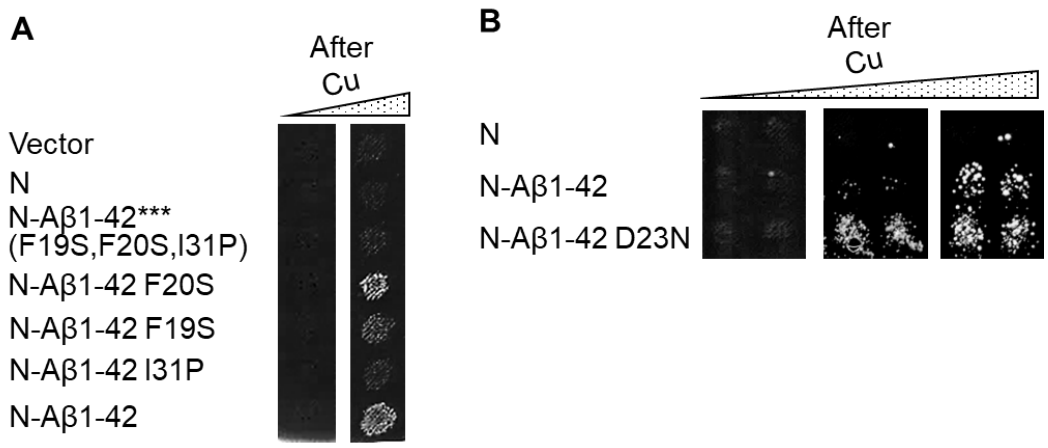

Figure 4-4. [*PSI*$^+$] nucleation by Aβ1-42 with mutations from *in vitro* data and a familial AD model, fused to Sup35N (A) Effects of base substitutions at positions 19, 20 and 31 of Aβ, and of a combination of these substitutions on [*PSI*$^+$] induction by the chimeric Sup35N-Aβ1-42 constructs in a [*psi*$^-$ *pin*$^-$] strain, compared to wild type Sup35N-Aβ1-42. (B) The D23N substitution increases the ability of Sup35N-Aβ1-42 to induce [*PSI*$^+$] formation in a [*psi*$^-$ *pin*$^-$] strain. Images from –Ade plates are shown, obtained after pre-incubation on the medium with additional 0, 10, or 50μM $CuSO_4$, from left to right. For quantitative data for some of the chimeras, see Table 4-1.

4.3.2.2 Based on structural and computational AD models

Based on the recent structural models for Aβ1-42[94,95] fibril including the high-resolution structures of Aβ1-42 amyloids based on solid-state NMR (Figure 5-2), a substitution K28E would affect the β3 strand of Aβ1-42 fibril (Figure 4-2). This was contrary to previous solid-state NMR studies of Aβ1-40 that identified the existence of a salt bridge between the side chains of residues Asp23 and Lys28 in the Aβ1-40 fibril[101,102], considered to be one of the hallmarks of Aβ aggregation and found to be present in Aβ1-42 amyloid fibrils. To reproduce the structural data demonstrated by the latest solid-state NMR studies for Aβ1-42 in yeast, we made substitutions K28E as well as a substitution D23K that would change the charge on Asp23 to that of Lys28. Furthermore, we also made a reciprocal mutation of D23K, K28E that would change the charges on Asp23 and Lys28 but would restore the interactions between them and stabilize the Aβ fibril if they formed a salt-bridge in the first place. The substitution K28E significantly decreased [*PSI*$^+$] nucleation by Sup35N-Aβ1-

42. On the contrary, the substitution D23K showed slightly increased [*PSI*$^{+}$] nucleation compared to Sup35N-Aβ1-42. However, the reciprocal substitution D23K, K28E showed an increased [*PSI*$^{+}$] nucleation compared to Sup35N-Aβ1-42 with substitution K28E but less than Sup35N-Aβ1-42 or Sup35N-Aβ1-42 with D23K substitution.

Also, based on a recent computational model of disease-related amyloids[93] that suggest that complexes of 2 or more β arches, a structural motif in amyloid proteins may form nucleation complexes for amyloid fibrillogenesis *in vivo,* we made mutations in Aβ1-42 that were predicted to have a high or low amyloidogenicity score depending on their formation of β arches, and fused them to Sup35N. As per the ArchCandy algorithm for predicting the formation of β arches, substitutions H13L and A21E, D23A were predicted to have a high amyloidogenicity score and substitutions G25V, F19K, and K28E were predicted to have a low amyloidogenicity score in comparison to Aβ1-42 without any mutations. In comparison to Sup35N-Aβ1-42 without any alterations, the substitutions A21E, D23A slightly increased [*PSI*$^{+}$] nucleation by Sup35N-Aβ1-42. On the contrary, the substitutions F19K and K28E greatly decreased [*PSI*$^{+}$] nucleation by Sup35N-Aβ1-42 while the substitutions H13L and G25V showed comparable levels of [*PSI*$^{+}$] nucleation to Sup35N-Aβ1-42, although they do demonstrate slight differences in [*PSI*$^{+}$] nucleation compared to Sup35N-Aβ1-42 in terms of growth on -Ade but they had to be detected within 5 days of incubation (short period of incubation) on -Ade media and was hard to accurately demonstrate in this format of plate assay.

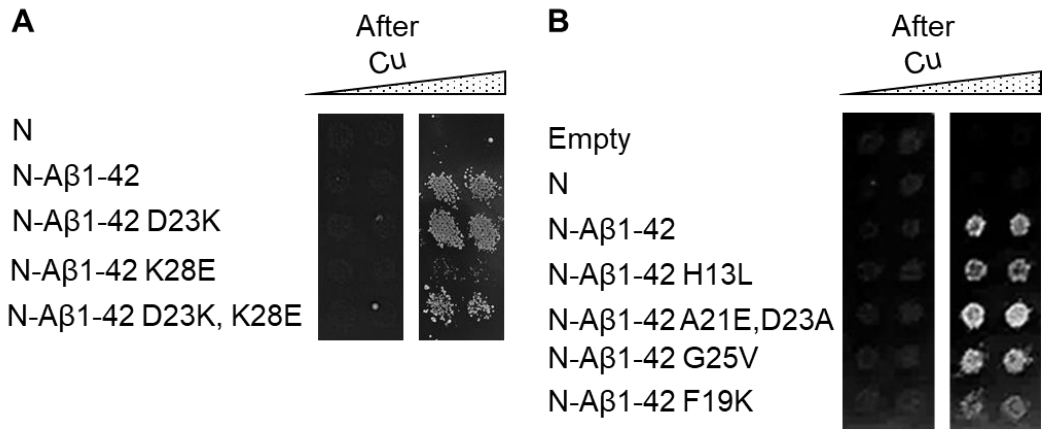

Figure 4-5. [*PSI*$^+$] nucleation by Aβ1-42 with mutations from *structural models*, fused to Sup35N. (A) A D23K substitution slightly increases the ability of Sup35N-Aβ1-42 to induce [*PSI*$^+$] formation in a [*psi*$^-$ *pin*$^-$] strain while K28E substitution has an opposite effect on [*PSI*$^+$] induction. However, a reciprocal substitution of D23K, K28E restores the ability of Sup35N-Aβ1-42 to induce [*PSI*$^+$]. Sup35N-Aβ1-42 is used as a control. (B) Effects of substitutions at different positions of Aβ, on [*PSI*$^+$] induction by the chimeric Sup35N-Aβ1-42 constructs in a [*psi*$^-$ *pin*$^-$] strain, compared to wild type Sup35N-Aβ1-42. On panels A and B, the images from –Ade plates are shown, without (left column) or with (right column) pre-incubation on the medium with additional 100 μM $CuSO_4$.

*4.3.3 Biochemical detection of [*PSI$^+$*] aggregates by Sup35N fused to Aβ1-42 derivatives*

By using semi-denaturing detergent agarose gel electrophoresis[69] (SDD-AGE), we have demonstrated that the chimeric proteins containing Aβ1-42 produced detergent-resistant polymers in the yeast cells lacking pre-existing prions (Figure 4-6A) as is typical of yeast prions and amyloids[32] and promoted the immobilization of endogenous Sup35 protein into an aggregated fraction (Figure 4-6B). Thus, phenotypically detectable [*PSI*$^+$] formation coincides with physical aggregation of the inducer protein and immobilization of the inducee protein into aggregates. The Sup35N-Aβ1-40 construct (Figure 4-6A) and Sup35N-Aβ1-42 triple mutant (F19S, F20S, I31P; Figure 4-4B) neither formed detergent-resistant polymers at detectable levels nor immobilized Sup35 into an aggregated state, according to SDD-AGE. Overall, our data show that effects of Aβ alterations of [*PSI*$^+$]

nucleation in yeast parallel their effects shown in humans or *in vitro*, and/or predicted from structural models.

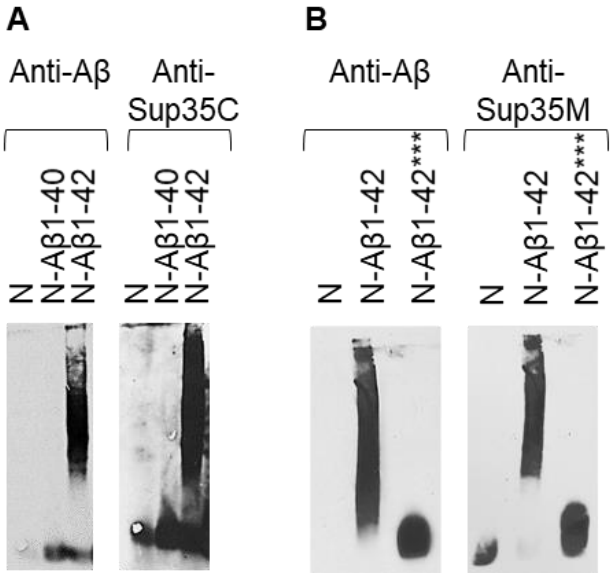

Figure 4-6. Biochemical detection of the effects of Aβ alterations on protein aggregation in yeast. Cultures were grown in the presence of 100 μM $CuSO_4$. (A) In contrast to Sup35N-Aβ1-42, the Sup35N-Aβ1-40 construct does not efficiently aggregate (left image) and does not immobilize endogenous Sup35 into an aggregated fraction (right image). The small Aβ monomers are not seen on the left image as they have run out of the gel. (B) The Sup35N-Aβ1-42 protein with triple F19S, F20S, I31P substitution does not aggregate (left image) and does not immobilize endogenous Sup35 when probed with into an aggregated fraction (right image). The image for N-Aβ1-42 (on the left) and the images for N and N-Aβ1-42 (on the right) in panel B are the same images that were shown on Fig 3, A and B, respectively. These images are repeated here as positive (N-Aβ1-42) and negative (N) controls.

4.3.4 Protein expression levels of Sup35N-Aβ1-42 derivatives

One possible explanation for chimeric constructs, as well as for alterations of Aβ to influence [*PSI*$^+$] nucleation could be through altering levels of chimeric proteins. To investigate this possibility, we have compared levels of Sup35N-Aβ1-42-based chimeric proteins accumulated in yeast cells at the same concentrations of $CuSO_4$. The prion-inducing Sup35N-Aβ1-42 construct was accumulated at the same levels as prion non-inducing Sup35N-Aβ1-40 and Sup35N-Aβ1-42 triple F19S, F20S, I31P mutant (Figure 4-

7A, B) respectively. The [*PSI*$^{+}$]-inducing Sup35NM-Aβ1-42 construct was accumulated at the same level as non-inducing Sup35NM-Aβ1-40 construct, and both were less abundant than the non-inducing control, Sup35NM (Figure 4-7C). Overall, our data show that while cellular levels of proteins used in this work could vary in some cases, the differences in prion nucleation cannot be explained by differences in protein abundance.

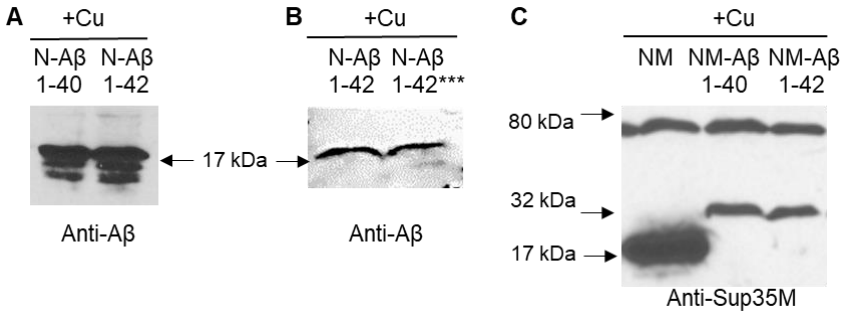

Figure 4-7. Detection of chimeric proteins in yeast. (A) Comparison of the levels of Sup35N-Aβ1-40 and Sup35N-Aβ1-42 constructs as detected by SDS-PAGE and Western blot with anti-Aβ (6E10) antibody. Both proteins are accumulated at similar levels. (B) Comparison of the levels of Sup35N-Aβ1-42 and Sup35N-Aβ1-42*** (triple F19S, F20S, I31P substitution) constructs as detected by SDS-PAGE and Western blot with anti-Aβ (6E10) antibody. Both proteins are accumulated at similar levels. (C) Comparison of the levels of Sup35NM, Sup35NM-Aβ1-40, and Sup35NM-Aβ1-42 constructs as detected by SDS-PAGE and Western blotting with anti-Sup35M antibody. Chimeric protein are accumulated at similar levels, which are lower than the level of accumulation of Sup35NM. In all cases, protein amounts were normalized by the Bradford assay and/or Coomassie staining. On panel E, the upper band corresponding to full-length Sup35 protein also serves as a loading control. On all panels, "+Cu" refers to cultures growing in the presence of 100 µM $CuSO_4$.

4.3.5 Analysis of [PSI^{+}] strains induced by Sup35N-Aβ1-42 derivatives

As explained in Chapter 4, the Sup35 protein can produce a variety of prion variants or "strains" which presumably correspond to various amyloid structures that can be differentiated from each other based on both their phenotypic manifestations and biochemical patterns[32]. Once established, the prion strain typically faithfully reproduces its observable characteristics. To determine if mammalian amyloidogenic proteins influence the parameters of prion "strains" produced in yeast, we compared spectra of prion strains

generated in the presence of different inducing constructs. For this purpose, [*PSI*$^{+}$] isolates were analyzed as described for Sup35N-PrP derivatives in Chapter 3. Data are shown on Figure 4-8, Appendix Figure A, Table 4-2. While Sup35N-Aβ1-42 exclusively "strong" strains and Sup35N-Aβ1-40 produced [*PSI*$^{+}$] isolates of all three classes. Some point mutations changed a spectrum of the induced [*PSI*$^{+}$] strains. The Sup35N-Aβ1-42 construct with mutation D23N induced preferentially intermediate [*PSI*$^{+}$] isolates, while construct with the mutation K28E construct induced preferentially weak and intermediate [*PSI*$^{+}$] isolates. These results indicate that the preferable type of a yeast prion strain, in part, depends on the mammalian amyloidogenic protein used in the inducing construct.

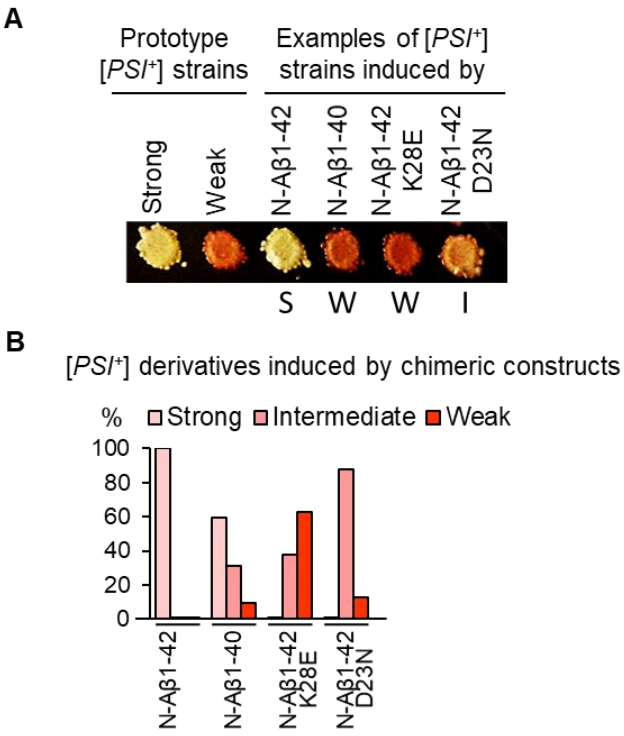

Figure 4-8. Spectra of prion strains induced by various Sup35N-Aβ derivatives. (A) [*PSI*$^{+}$] strains were analyzed as shown in Figure 3-14. (B) Percentages of strong, intermediate, and weak [*PSI*$^{+}$] strains induced by wild type and altered Sup35N-Aβ derivatives in a [*psi*$^{-}$ *pin*$^{-}$] strain. More detailed information, including images for multiple isolates, data for the constructs containing point mutations, actual numbers and errors is presented in Appendix figure A and Table 4-2

Table 4-2. Numbers and percentages* of [*PSI*$^+$] strains induced by various Aβ-based chimeric constructs

Inducer	**Strong [*PSI*$^+$]**	**Intermediate [*PSI*$^+$]**	**Weak [*PSI*$^+$]**	**Total number of [*PSI*$^+$] isolates checked**
Sup35N-Aβ1-42	32 100 (-3.0)%	0 0 (+3.0)%	0 0 (+3.0)%	32
Sup35N-Aβ1-40	19 59.4 (+/-8.7)%	10 31.2 (+/-8.2)%	3 9.4 (+/-5.1)%	32
Sup35N-Aβ1-42 K28E	0 0 (+10.5)%	3 37.5 (+/-16.5)%	5 62.5 (+/-15.7)%	8
Sup35N-Aβ1-42 D23N	0 0 (+10.5)%	7 87.5 (+/-10.5)%	1 12.5 (+/-10.5)%	8

*4.3.6 [*PSI$^+$*] nucleation by Sup35N-Aβ1-42 in the presence of metal ions*

First, we used a modified yeast-based plate assay (Figure 4-1). for testing compounds that were previously linked or suspected to be linked to AD. These included metal ions suspected in AD (e. g. Cd, As, Pb, Al, Cu, Fe, Li and Zn) [104,105], out of which Al, Cu, Fe, and Zn are neuronal metal ions and the rest are toxicological metal ions. Our pilot experiments have indeed demonstrated that in plate assays, some metal ions (specifically, Zn, Li, Cd, and As, and to a lesser extent, Fe) increased formation of Ade+ colonies in the presence of Sup35N-Aβ1-42 when compared to a control (H2O) (Figure 4-9).

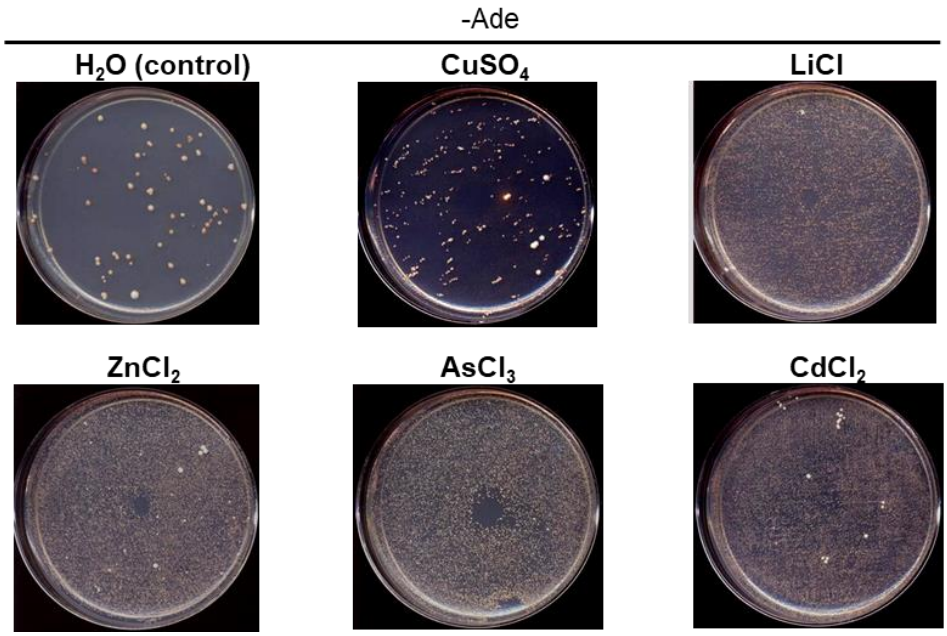

Figure 4-9. Identification of metal ions influencing [*PSI*$^{+}$] nucleation by Aβ1-42 fused to Sup35N in yeast. Yeast cells bearing Sup35N-Aβ1-42 under the P_{GAL} promoter in a [*psi*$^{-}$ *pin*$^{-}$] strain, were incubated on the galactose medium in the presence of H_2O (control) or presence of 300μM $CuSO_4$, 300μM LiCl, 300μM $ZnCl_2$, 150μM $AsCl_2$, and 100μM $CdCl_2$. and velveteen replicated plated into –Ade media for [*PSI*$^{+}$] detection.

4.4 Discussion

Amino acid residues influencing prion nucleation by Aβ. In the case of Aβ peptide, data from the yeast assay are also in a good agreement with existing results obtained in other systems. For example, the Aβ40 peptide lacking the two C-terminal hydrophobic amino acids, I41 and A42, is considered to be less aggregation-prone and is a typically non-pathogenic Aβ isoform in humans[98]. This peptide is drastically inefficient in prion nucleation in the yeast assay, compared to the highly amyloidogenic and presumably pathogenic Aβ1-42 (Figure 4-3A, B). While previous structural studies used the *in vitro* produced Aβ1-40 polymers[101,102] the high-resolution structures of Aβ1-42 amyloids, mostly based on solid state NMR have also been reported recently[94,95]. These structures include two molecules per polymer unit, and five β intermolecular sheets spanning residues 2-6

(β1), 15-18 (β2), 26-28 (β3), 30-32 (β4), and 39-42 (β5) per each “half” of the fibril (Figure 4-2, 4-10). The anti-nucleation effects (Figure 4-4A, 4-5B) of substitutions I31P (breaking a β4 strand) and F19S as well as F19K (disrupting hydrophobic interactions with the β2 strand) in the yeast assay are in good agreement with the published structural models (Figure 4-10). Likewise, the pro-nucleation effect (Figure 4-4B) of the D23N substitution, corresponding to so called “Iowa mutation”, a heritable case of AD[72], is also in a good agreement with the models. This substitution removes one of negatively charged residues presumably facing the solvent that might increase an aggregation propensity. To confirm the previous models that implicate a salt bridge between Asp23 and Lys28, we originally hypothesized that the substitution D23K that reverses the charge would knock out nucleation as does K28E, while a double substitution D23K, K28E involving a charge reversal would restore the salt bridge and thus restore prion nucleation. Though, substitution K28E demonstrated an anti-nucleation effect (Figure 4-5A) and the reciprocal mutation D23K, K28E restored prion nucleation to a significant extent (Figure 4-5A, affecting the β3 strand), D23K in fact increased prion nucleation on its own (Figure 4-5A), thus not lending support to the models suggesting the formation of a salt-bridge between Asp23 and Lys28[95,102].However, our data still demonstrates that residues K28 and D23 have an important role in the formation of the Aβ (1–42) amyloid fibril and the anti-nucleation effect of chimera with K28E indeed experimentally verified the latest structural models for Aβ(1–42)[95,96]. The solvent-exposed charged residue D23 is located within the sequence segment F19–K28 and has been identified to be of great significance for the enhanced toxicity of familial mutations in Aβ(1–40) and shows structural variability with typically one or two short β-sheets and likewise, the substitutions D23N or D23K or D23A (one of the mutations in A21E, D23A mutant) increased nucleation in our assay, and potentially enhances the stacking of the Aβ molecular out to the next layer along the fibril axis and also enables interactions with solvents or chemical agents like metal ions that

can stabilize the Aβ fibril by rapidly increasing Aβ aggregation. In the case of substitution K28E, the mutation disrupts the hydrophobic interactions with the β2 strand, as demonstrated by decreased nucleation (Figure 4-5A). Moreover, a salt bridge has been observed between the side chain of K28 and the C terminus of Aβ(1–42) and this fits with our data demonstrating decreased nucleation by K28E, potentially disrupting the interactions between K28 and the C-terminus (Figure 4-10). While residues 15–42 are packed densely, the N-terminal segment of residues 1–14 is not entirely rigid and has been shown by NMR studies to contain Cu coordination mode which involves three histidines (His6, His13 and His14)[103]. His13 is also a crucial residue in the zinc ion-induced aggregation of Aβ[103]. The histidine restudies, specifically His13 coordinate the binding of Aβ peptide to metals. H13L, although not reproducing the pro-nucleation effect predicted by ArchCandy algorithm in our assay (Figure 4-5B) potentially demonstrates such an effect after binding to metal ions that can speed up aggregation and stabilize the Aβ fibril.

Additionally, the amyloidogenicity score given by ArchCandy are for mutations in Aβ peptide and not in the Sup35N-Aβ chimera. Potentially, generating amyloidogenicity scores based on the formation of β-arcades in Sup35N-Aβ chimera rather than Aβ peptide might work better for the purpose of checking prion nucleation by Aβ mutations using our assay since Aβ is physically fused to Sup35N and thus potentially forms a hybrid template that changes the conformation of the amyloid fibril formed as a result.

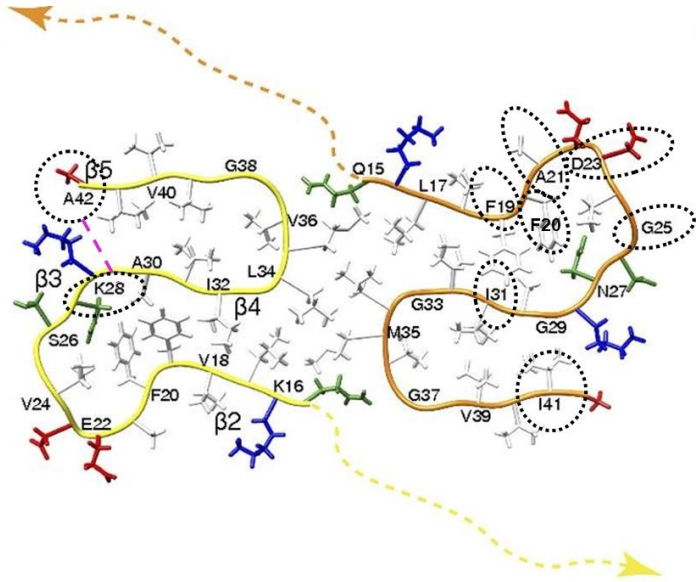

Figure 4-10. The location of mutations in the 3D structure of Aβ(1–42) fibrils (as per ref. 95). The Aβ(1–42) amyloid fibrils is composed of two molecules per subunit, which are symmetric with respect to the central axis of the fibril. The backbone of the two symmetric molecules are shown as yellow and orange spines. The 3D structure of the N-terminal residues 1–14 (dotted yellow lines), the side chains of the positively charged residues (red), the negatively charged (blue), the hydrophobic residues (white), and polar residues (green). Every second residue is labeled with the one-letter amino acid code. The location of mutations on the 3D structure of Aβ(1–42) fibrils are shown as black dotted lines. A potential salt bridge between residue K28 and the C-terminus of Aβ(1–42) is shown as pink dotted lines.

*The impact of a nucleating construct on spectra of induced [*PSI$^+$*] "strains".* As explained in Chapter 3, Both yeast and mammalian prion and amyloid proteins are known to form various variants or "strains" that differ from each other by phenotypic and biochemical characteristics and are apparently controlled by distinct protein conformations. Similar to the prion strains formed by Sup35N-PrP90-230 derivatives in Chapter 4, we have found out that the spectra of [*PSI*$^+$] strains induced by different Aβ-based chimeric constructs also differ from each other (Figure 4-8) either due to the formation of distinct initial nuclei by different attached regions of chimeric proteins, followed by an expansion of the amyloid region to different regions of the attached Sup35N domain via "deformed templating" model[92]. In this scenario, the spectra of [*PSI*$^+$] strains might corroborate to the differences in the "hybrid" templates formed by the fusion proteins or a preference by Sup35N for

certain strain conformations by specific mammalian amyloidogenic proteins physically attached to Sup35N.

Potential applications of the yeast prion nucleation assay – identification of metals that influence Aβ nucleation. Initial prion nucleation by mammalian proteins is the crucial step triggering the subsequent amyloid formation and pathogenicity of Aβ and potentially other disease-related amyloidogenic proteins as demonstrated in Chapter 4. We have used the nucleation assay to search for chemical factors and conditions specifically modulating the process of initial amyloid nucleation in both a general and a protein-specific manner. Using a modified prion nucleation assay, we have screening for both neuronal metal ions that can trigger Aβ via dysregulation of brain metal homeostasis[104] as well as toxicological metal ions[104,105] that potentially trigger or accelerate Aβ aggregation by acting as an environmental contaminant (Figure 4-9). So far, systematic *in vivo* information about the role of metals in Aβ aggregation is lacking. While Aβ can bind metals, and some metals influence Aβ aggregation *in vitro*, it remains unclear whether or not this occurs at concentrations having physiological relevance. Moreover, metals also exhibit broad effects on Aβ production and degradation, as well as on the functioning of the human organism and brain at various levels. It is therefore unclear if metal effects in AD are related to the initial amyloid formation or its consequences. Using physiological concentrations of metal ions (150 to 300μM) in non-toxic solvents, we have shown that Zn, Li, As, Cd, as well as Cu to an extent significantly increase nucleation by Aβ-based chimeric constructs in yeast (Figure 4-9). While some of these metal ions like As and Cd cause toxicity to yeast at high concentrations, they could be tested at lower concentrations without causing cytotoxicity. The major problem with the systematic studies of the impact of environmental factors on amyloidosis is the lack of rapid experimental assays allowing for the detection of potentially amyloidogenic agents through their effects on the initial

amyloid formation in living cells. We have developed such an assay that would allow identification of true amyloidogenic agents, paving the way for further characterization of the molecular mechanisms of their action and determining the potential risks. This may pave the way for the development of both therapeutic and prophylactic treatments for amyloid diseases that address a triggering mechanism of the disease, initial amyloid nucleation. The major advantage of our system in comparison to previously proposed yeast-based and cell-based assays is that our assay does not require the chimeric fusion protein to propagate a prion state in yeast. Prion detection is achieved by transferring the amyloid state to the endogenous yeast Sup35 protein, so that even transient amyloid formation by a chimeric construct is then fixed and amplified by conversion of an endogenous yeast protein into a prion. Furthermore, non-amyloid multimeric proteins are apparently not capable of nucleating prion formation at high efficiency in our system, making it possible to use this assay for identifying new potentially amyloidogenic proteins or domains, originated from various organisms, including humans. The rapid and easy phenotypic detection of prion nucleation in yeast makes our assay amenable to high-throughput approaches.

4.5 Conclusions

- The ability of Aβ1-42, fused to Sup35N, to promote amyloid nucleation in yeast was decreased by the removal of two C-terminal amino acids (converting Aβ1-42 to less amyloidogenic Aβ1-40)

- A familial pro-AD mutation, D23N increased prion nucleation by Sup35N-Aβ1-42 in yeast.

- Amino acid substitutions K28E or D23K respectively decreased or increased prion nucleation by Sup35N-Aβ1-42 in yeast, while a double reciprocal mutation D23K, K28E demonstrated prion nucleation comparable to that of Sup35N-Aβ1-42.

- The ability of Aβ1-42, fused to Sup35N, to promote amyloid nucleation in yeast was abolished by amino acid substitutions that alter structural properties of Aβ, important for amyloid formation.

- Sup35N-Aβ1-42 formed SDS-resistant amyloid aggregates and immobilized endogenous Sup35 into an aggregated fraction, while Sup35N fused to Aβ1-40 or Aβ1-42 triple mutant was unable to do so.

- Sup35N-Aβ1-42 with different alterations induced different spectra of prion strains in yeast

- Some metal ions suspected to promote AD, increased prion nucleation in the presence of Sup35N-Aβ1-42 in the yeast assay.

CHAPTER 5. GENERATION AND PROPAGATION OF Aβ- and TAU-DEPENDENT PRION STRAINS IN YEAST

This chapter includes the work in preparation for publication and portions of it were performed in collaboration with David Lynn and Lary Walker at Emory University.

5.1 Summary

While previous chapters were dealing with prion nucleation, in Chapter 5 we established a yeast model for studying prion propagation by amyloid β (Aβ) or microtubule binding protein tau (tau), two human proteins associated with Alzheimer's disease (AD) in the case of Aβ and tau as well as frontotemporal dementia in the case of tau. We have constructed chimeric proteins, in which the prion domain (PrD) or an aggregation prone portion of the PrD of Sup35 was replaced by human Aβ or the microtubule binding repeat domains of human tau and have shown that such a chimeric protein was functional in translational termination and could spontaneously switch to the partially non-functional polymeric state, thus generating and propagating a prion isoform. The formation of such a prion by Aβ was promoted by transfecting yeast cells with *in vitro* generated Aβ1-42 or Aβ1-40 aggregates. Remarkably, the prion isolates formed by the Aβ-based chimeric protein demonstrated different phenotypic stringencies, indicating the existence of different Aβ-based prion strains, thus mimicking the phenotypic diversity seen in AD. Thus, our data establishes a yeast model for studying Aβ- and tau-dependent propagation of prion strains in yeast and provides a unique opportunity for applying high resolution genetic and biochemical techniques to studying Aβ or tau strains generated in humans and *in vitro*. Additionally, this model also enables the systematic study of the possibility of a direct cross-seeding of tau by Aβ that has not been addressed in cellular models thus far.

5.2 Specific materials and methods

5.2.1 Materials

5.2.1.1 Strains

The *S. cerevisiae* strains used in this study are shown in Appendix Table A. GT2126 was constructed by a direct plasmid shuffle (Figure 5-1). The plasmid Aβ1-42-NR-MC with a constitutive SUP35 promoter was transformed into GT671 and Sup35 plasmid with a *LEU2* marker was shuffled out. GT2180 was constructed in a similar manner by using GT651 as the donor strain. GT2265 is the MAT**a** derivative of GT2180 and was generated by inducing the mating type switch in the presence of plasmid YRpHO[106]. GT2266 was constructed by transforming the Aβ1-42-NR-MC plasmid with a constitutive SUP35 promoter and a *URA3* marker into GT2180 and the Aβ1-42-NR-MC plasmid with a constitutive SUP35 promoter and a *LEU2* marker was lost. The Sup35MC plasmid with a *LEU2* marker was transformed into GT2266, and the Sup35MC plasmid with a *URA3* marker was shuffled out by counter selection on 5-FOA media. GT81-1C and GT409 (Appendix Table A) were employed for the comparisons to [*PSI*$^{+}$] strains induced by chimeric constructs in SDD-AGE experiments.

5.2.1.2 Plasmids and primers

The *S. cerevisiae* - *E. coli* shuttle plasmids used in this study and primers used in plasmid constructions are shown in Appendix Tables B and C respectively. The chimeric genes coding for Aβ-Sup35MC or tau repeat domain (RD) encompassing amino acids 244 to 372 as well as tau RD with a double point mutations, P301L, V337M, under P_{CUP1} with a *URA3* marker was constructed by inserting the PCR-amplified BamHI-BglII fragment that codes for the region 1-42 of Aβ42 from the plasmids pcDNA3.1(+)-Aβ42 (kindly provided by Dr.

K. Ugen, University of South Florida) containing the human Aβ1-42-coding sequence, or the repeat domain 244-372 of tau from the plasmids pcDNA3.1(+)-tau-RD-wild-type and pcDNA3.1(+)-tau-RD-P301L, V337M mutant (kindly provided by Dr. Marc Diamond, Washington University, St. Louis) containing the human tau 244-372-coding sequence, into the pmCUP1-Sup35MC vector at the position following the P_{CUP1} promoter.

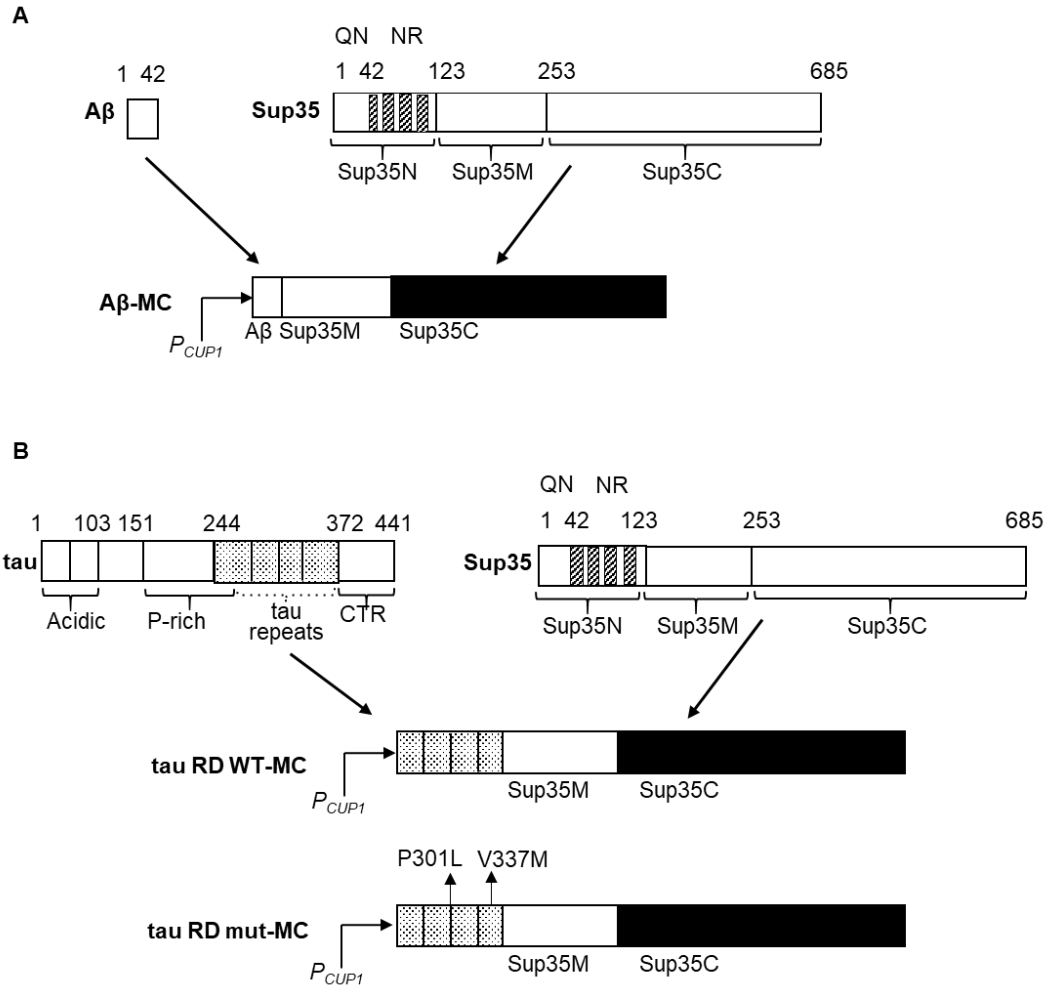

Figure 5-1. Scheme of construction of chimera Aβ-MC and tau-MC under the copper-inducible promoter, P_{CUP1}. (amino acid positions not to scale). Sup35N terminus or "prion domain" is composed of NQ region (rich in asparagine and glutamine) and NR region (oligopeptide repeats). The region coding for the prion domain of Sup3N was substituted with the region coding for human Aβ1-42 or for human microtubule binding repeat domain (RD) of wildtype tau or tau RD with P301L, V337M base substitutions.

The chimeric gene coding for Aß42-Sup35NR-MC under a constitutive SUP35 promoter with a *URA3* marker was constructed in two steps. The first step involved the construction of Sup35 plasmid under a constitutive SUP35 promoter in the backbone of a pmCUP1-based plasmid. This plasmid was constructed via replacing the fragment containing *SUP35* and the *SUP35* promoter in the pRS316 backbone that was excised by using restriction endonucleases, XhoI and SacI, with the fragment containing P_{CUP1} in pmCUP1 vector. Aß42-Sup35-NR-MC plasmid under a constitutive SUP35 promoter was constructed by replacing the *SUP35* fragment that codes for the region 1-42 of Sup35 from the previously constructed Sup35 plasmid in the P_{CUP1} backbone, with the PCR-amplified BamHI-PstI fragment containing the *Aß42* fragment from the plasmid pcDNA3.1(+)-Aβ42 containing the human Aβ1-42-coding sequence. A Kozak sequence followed by an initiating methionine was added to C-terminus of BamHI restriction enzyme in the forward oligonucleotide primer (refer primer sequence in Appendix Table C), to construct Aβ1-42-containing chimeras.

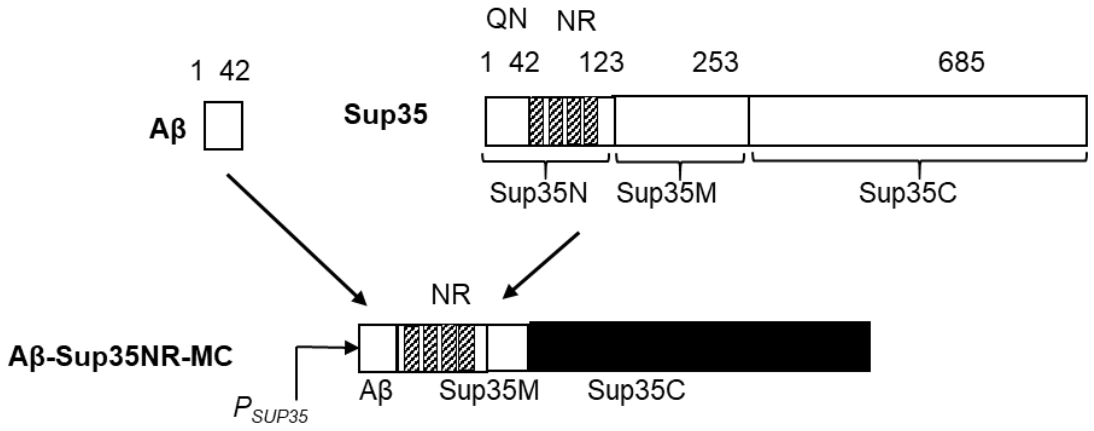

Figure 5-2. Scheme of construction of chimera Aβ-NR-MC under the endogenous *S. cerevisiae SUP35 promoter* (P_{SUP35}) (amino acid positions not to scale). The region coding for the first 42 amino acids of Sup35N was substituted with the region coding for human Aβ1-42.

Aβ-NR-MC plasmid under the endogenous *SUP35 promoter* with a *LEU2* marker was constructed via replacing the XhoI-SacI fragment containing the *Aß42-NR-MC* and constitutive SUP35 promoter from the Aß42-NR-MC plasmid with a URA3 marker and inserted into pRS415 vector at the position following the XhoI restriction site. All the regions that underwent PCR amplification as well as immediate flanking regions were verified by sequencing, performed at Eurofins MWG Operon (Huntsville, AL). Isolation of plasmid DNA from bacteria was performed according to standard procedures.

5.2.1.3 Antibody

Sup35C antibody used in this study is described in Chapter 2.

5.2.1.4 *In vitro* aggregated Aβ1-42 and Aβ1-40 seeds

Aβ42 seeds were prepared by Aditi Sharma from Andreas Bommarius Research Lab (School of Chemical and Biomolecular Engineering, Georgia Tech) using lyophilized Aβ1-42 purchased from GenicBio. 1 mg of synthetic Aβ42 was equilibrated to a room temperature for at least 30 min in a desiccator. The peptide was resuspended in 1ml of NH_4OH (10% v/v) to a final concentration of 1mg/ml, followed by incubation at room temperature for 10 min. The peptide was sonicated in a sonicator for 5 min and 100µl of the solution was aliquoted into ten 1.5ml centrifuge tubes. Small holes were made on the lids of the tubes and the tubes were flash frozen in liquid nitrogen and quickly placed in a lyophilizer to lyophilize the samples for ~12 hrs., followed by storage at -80°C. To use the frozen peptides for conducting experiments, one aliquot was taken out from -80°C and resuspended in 50µL of 1mM NaOH and diluted 10-fold with 1M phosphate buffer saline (PBS). The protein concentration was measured by Micro Bicinchoninic Acid (microBCA) and ensured that the measurement was ~40µM and appropriately diluted as required with buffer containing 1µM Thioflavin T. The solution containing Aβ was filtered with 0.2µ filter

to remove oligomers or large molecular weight aggregates before use. The Aβ solution was pipetted into a 96 well plate and the volume per well was 200µl. The plate was placed in a Biotek Synergy H4 Multi-mode plate reader and the fluorescence was measured with an excitation wavelength of 440nm and an emission wavelength of 480nm at a temperature of 25°C. Readings were recorded every 5-10 min with continuous shaking at the medium setting (18Hz frequency, 0.022-inch amplitude). An aggregation cycle was approximately completed in 16 hrs. and the aggregates samples were stored in 1.5ml centrifuge tubes at -20°C for storage and taken out from the freezer and thawed in ice for 30 min to be used for the transformation step in the transfection procedure.

Aβ40 seeds were obtained by continuous shaking of Aβ40 monomers at room temperature at 100 rpm. Aβ40 monomers were synthesized using a microwave peptide synthesizer (CEM Corporation) by a collaborator, Noel Xiang' An Li from David Lynn Research Lab (Biological Chemistry Department, Emory University).

5.2.2 Methods

Standard protocols were used for DNA isolation, gel electrophoresis, restriction digestion, gel extraction, ligation, and bacterial transformation[68] and are described in Chapter 2. Standard yeast media and standard procedures for yeast cultivation, phenotypic analysis, and transformation were used and are described in Chapter 2. The schemes and description of plasmid shuffle experiments and analysis of colonies are described in the results section for each experiment.

5.3 Results

5.3.1 Identification and characterization of [Aβ+] strains in yeast

The *S. cerevisiae* Sup35 protein can be divided into three major domains as follows: (i) an N-proximal prion-forming domain (Sup35N), or PrD, (ii) a middle domain (Sup35M) promoting protein solubility and (iii) a C-proximal release factor domain (Sup35C) essential for translational termination and cell viability. The Sup35 prion domain is composed of three regions: (i) QN-rich region (QN), located before aa position 40, (ii) a region of imperfect oligopeptide repeats (NRs) and, (iii) region 97–123 that does not have a specific sequence pattern[32]. In Chapter 3 and 4, we confirmed that transient overproduction of a fusion of mammalian amyloid proteins like Aβ1-42 peptide to the C-terminus of Sup35N fragment promoted the *de novo* nucleation of [*PSI*$^{+}$] in the absence of pre-existing prions. pmCUP1-Sup35N-Aβ1-42 also formed SDS-resistant amyloid aggregates when analyzed by SDD-AGE, thus confirming Aβ polymerization and immobilization of endogenous Sup35 protein in yeast.

Here, we employed a similar experimental strategy to check if Aβ1-42 can form its own prion and propagate various strains in yeast. Previous studies showed that the replacement of the Sup35 prion domain (Sup35N) by Aβ42[45] causes a termination defect and results in protein oligomerization. Thus, this model could not be applied for specifically studying Aβ-based strains. To order to do so, Aβ had to be maintained in non-polymerized form and switched to the polymerized form in a controlled manner. In this study, we reproduced the results obtained previously and employ a modified strategy to switch Aβ from a non-polymerized form to a polymerized form to check for the formation of [*Aβ*$^{+}$] strains generated and propagated by a Aβ-based protein.

5.3.1.1 Phenotypic detection of Aβ-MC chimeric protein in yeast

To develop a yeast model for studying Aβ-dependent prion strains without the prion domain of Sup35, a centromeric plasmid with a *URA3* marker (Appendix Table A), expressing a chimeric protein containing the region coding for Aβ1-42 fused to the N terminus of Sup35MC, lacking the prion domain Sup35N, was constructed and placed under a copper inducible promoter (P_{CUP1}) (Figure 5-1). Initially, a yeast strain expressing only pmCUP1-Aβ-MC was constructed using a plasmid shuffle procedure (Figure 5-3). A *S. cerevisiae* [*psi*$^-$] ***sup35Δ*** strain with the SUP35 gene on a *LEU2* plasmid was transformed by *URA3* plasmids bearing [*Aβ1-42-MC*] or [*Aβ1-42-NR-MC*]. Transformants were obtained on medium lacking uracil and leucine (−Ura, Leu) that is selective for both plasmids and checked for suppression of the *ade1-14* reporter on both medium lacking only adenine (−Ade) and medium lacking uracil, leucine, and adenine (−Ura, Leu, Ade). These media were used to determine whether the newly introduced Aβ1-42-MC chimeric protein is immediately converted into a non-functional form or if it remained functional. In parallel, transformants were streaked out on −Ura medium and replica plated to −Leu medium, to identify the Ura+ Leu- colonies that lost the original *LEU2* plasmid. Only one Ura+ Leu- colony was analyzed from each individual transformant, to ensure independence of all colonies from each other.

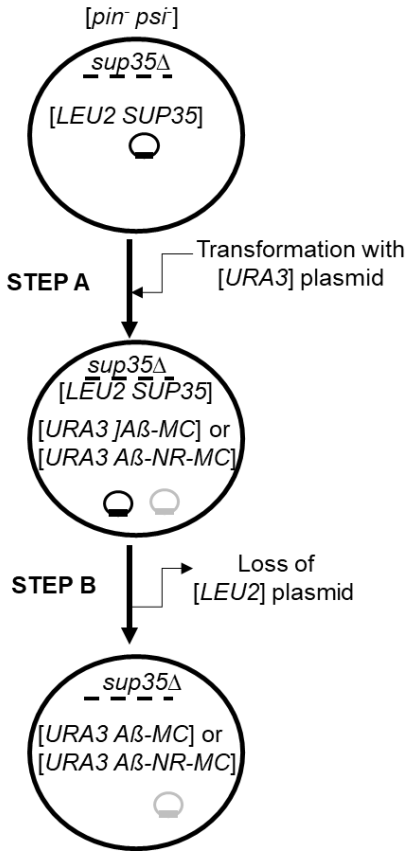

Figure 5-3. Construction of the *S. cerevisiae* strains expressing [*Aß-MC*] *or* [*Aß-NR-MC*] *proteins.*

To detect [*PSI*$^{+}$] formation, we employed the *ade1–14* (UGA) reporter. The [*psi*$^{-}$] strains bearing this reporter are Ade- (i.e. they do not grow on medium lacking adenine) and only rarely produce spontaneous Ade^{+} colonies, in part due to reversions or suppressor mutations. The conversion of endogenous Sup35 into a prion form leads to a termination defect and read-through of ade1–14, resulting in an Ade^{+} phenotype. Before induction, Aβ-Sup35MC construct, demonstrated nonsense suppression as indicated by growth on -Ade (Figure 5-4). This showed that the Sup35MC in the chimera was poorly functional in terminating translation, thus resulting in protein polymerization even at background levels of expression. After overexpression with 100μM $CuSO_4$, the nonsense suppression was not eliminated as demonstrated by growth on -Ade, despite an addition

of 100μM $CuSO_4$ to -Ade media to increase the abundance of Sup35MC to improve the functionality of the chimera. The control, Sup35MC construct, was functional in terminating translation. This confirmed that chimeric Aβ-Sup35MC constructs are partly non-functional in termination of translation in yeast.

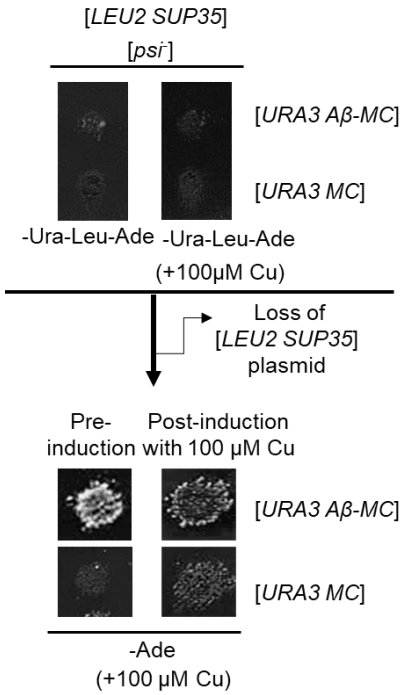

Figure 5-4. Phenotypic detection of nonsense suppression by Aβ-MC chimeric protein. The [*psi- pin-*] strain simultaneously expressing both Sup35 protein and Aβ-MC chimeric protein, do not cause nonsense suppression. After losing [*LEU2 SUP35*] by plasmid shuffle procedure (Figure 5-3), [*URA3 Aβ-MC*] plasmid without complete Sup35 is defective in terminating translation and causes nonsense suppression, before or after induction with 100μM $CuSO_4$, despite an addition of 100μM $CuSO_4$ to increase an abundance of Aβ-MC protein.

5.3.1.2 Phenotypic analysis of Ade^+ colonies formed by Aβ-NR-MC chimeric protein in yeast

The instant polymerization of Aβ-Sup35MC construct made the controlled formation of Aβ-dependent prion strains impossible. To circumvent this, we constructed another plasmid

in which only the QN-rich region encompassing the first 42 amino acids of Sup35N is replaced by $A\beta_{42}$, while retaining region of oligopeptide repeats (NRs) in Sup35N region and placed under the P_{SUP35} constitutive promoter (Figure. 5-2). pmSUP35-Aβ-NR-MC plasmid and a control, pmCUP1-Sup35MC plasmid were simultaneously transformed into [*psi*$^-$ *pin*$^-$] strain GT671 with genomic SUP35 gene deleted, and bearing a Sup35-expressing plasmid (pASB2, with the *LEU2* marker). Then, the original Sup35-expressing plasmid was lost from the strain by counter selecting on –Ura and –Leu media. Next, 8 individual colonies bearing only the P_{SUP35}-*Aβ-NR-MC* plasmid were patched on -Ura and replica plated to –Ade media to check for nonsense suppression. The chimeric protein was completely functional in terminating translation as indicated by a lack of growth on -Ade, similar to the control P_{SUP35}-*MC* plasmid (Figure 5-5A). After an incubation period of 20 days, all the patches produced Ade$^+$ papillae (Figure. 5-5A and Table 5-1). The *de novo*-formed Ade$^+$ papillae were individually picked from the original -Ura plate and streaked on to complete YPD medium to check for color and -Ade medium to check for growth. The Ade$^+$ isolates produced colonies of different phenotypic stringencies and different levels of growth on YPD and -Ade respectively. The Ade$^+$ colonies were divided into three groups designated as “strong”, “intermediate” and “weak” strains based on growth on –Ade medium and color on YPD medium (Figure 5-5B and Table 5-1). The vast majority of Ade$^+$ colonies induced by the Aβ-based chimeric construct were curable by serial passages on medium containing an antiprion agent guanidine hydrochloride, GuHCl. This indicated that the GuHCl-curable nonsense suppression state was stably maintained by daughter cells.

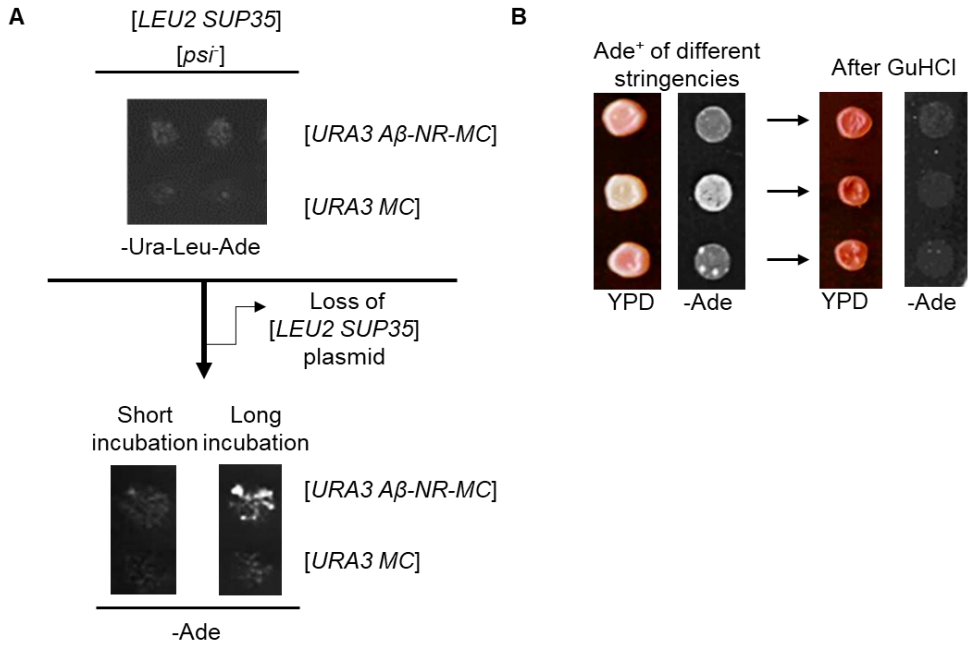

Figure 5-5. Phenotypic detection of Ade$^+$ colonies formed by Aβ-NR-MC chimeric protein. A - The [*psi$^-$ pin$^-$*] strain simultaneously expressing both Sup35 protein and Aβ-NR-MC chimeric protein remains functional in terminating translation. After losing [*LEU2 SUP35*] by plasmid shuffle procedure (Figure 5-3), the Aβ-NR-MC chimeric protein confers an Ade$^-$ phenotype after 10 days ("Short incubation"), indicating full functionality. After an incubation period of 20 days ("Long incubation"), [*URA3 Aβ-NR-MC*] spontaneously forms Ade$^+$ colonies. B – The colony purified Ade$^+$ papillae exhibited different phenotypic stringencies and lost the ability to grow on –Ade medium after 20-40 generations in the presence of guanidine hydrochloride (GuHCl), an agent antagonizing propagation of yeast prions.

Table 5-1. Curability of Ade$^+$ colonies generated by Aβ-NR-MC spontaneously and by transfection

Origin of Ade$^+$ colonies	**Phenotypic stringency**	**Number of colonies curable by GuHCl**	**Number of colonies not curable by GuHCl**	**Total number of Ade$^+$ isolates tested**
Spontaneous	Strong	3	4	7
	Intermediate	11	2	13
	Weak	9	2	11
Transfection	Strong	3	8	11
	Intermediate	13	5	18
	Weak	8	2	10
Total		47	23	70

5.3.1.3 Biochemical characterization of Ade$^+$ colonies by Aβ-Sup35NR-MC chimeric protein

Three representative Ade$^+$ colonies generated by Aβ-Sup35NR-MC chimeric protein that had different phenotypic stringencies, namely strong, intermediate, and weak, including an Ade- control containing Aβ-Sup35NR-MC, and the Ade$^+$ isolate with an intermediate phenotypic stringency that was cured with 5mM GuHCl, were analyzed using semi-denaturing detergent agarose gel electrophoresis[69] (SDD-AGE) as described in Chapter 2. The weak and intermediate Ade$^+$ isolates containing Aβ-Sup35NR-MC produced detergent-resistant polymers in the yeast cells (Figure 5-4) as is typical of yeast prions and amyloids and promoted the immobilization of endogenous Sup35 protein into an aggregated fraction. The strong Ade$^+$ isolate could not be detected, and interestingly it was proven later by direct plasmid shuffle, discussed further in this chapter, that this isolate is not dependent on Aβ-Sup35NR-MC (data not shown). The cured version of the Ade$^+$ isolate with an intermediate phenotypic stringency migrated as monomers through the gel, confirming the prion-like characteristic of the isolates.

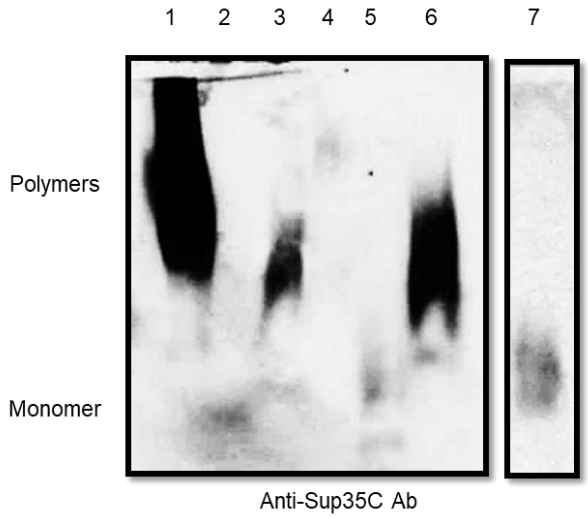

Figure 5-6. Biochemical characterization of Ade$^+$ isolates generated in the presence of Aβ-Sup35NR-MC. The representative Ade$^+$ isolates of different stringencies (weak, strong and intermediate – lanes 3, 4 and 6, respectively), as well as control strains, GT81-1C, [*PSI*$^+$] (lane 1) and GT409, [*psi*$^-$] (lane 2) strains, the original Ade$^-$ ([*aβ*$^-$]) strain (lane 5), and a GuHCl-cured derivative of the intermediate Ade$^+$ isolate (lane 7, from a different gel) were analyzed by semi-denaturing detergent agarose gel electrophoresis (SDD-AGE) followed by the reaction to the Sup35C-specific antibody. Positions of monomers and detergent-resistant polymers are indicated. The strong Ade$^+$ isolate used in this experiment was later identified as a false potential (see below, Fig 5-10 and Table 5-3).

5.3.1.4 Generation of [*Aβ*$^+$] strains in yeast by transfection with *in vitro* produced Aβ amyloids

So far, the phenotypic properties of the Ade$^+$ isolates generated spontaneously by Aβ-NR-MC chimeric protein have been characterized. In the case of prion proteins, phenotypic manifestation of the strain-specific patterns is achieved via interactions between the chimeric protein and the cellular machinery, but the molecular differences underlying these patterns are controlled by the prion protein itself. To provide a strong support for a mechanism of protein-only templating, it was checked if [*Aβ42-NR-MC*] could maintain and propagate a prion pattern if synthetically seeded Aβ42 or Aβ40 aggregates were added to it. To do this, the yeast transfection protocol was performed[107] using the materials

described in materials methods section, 5-2-2 and as illustrated in Fig 5-7A. The yeast cells carrying [*URA3 Aβ-NR-MC*] plasmid was transfected with Aβ42 or Aβ40 aggregates and transfectants were patched on -Ura medium, along with the colonies obtained in the strain that was not transfected with any aggregates, and replica plated to -Ade to check for growth. Only the yeast cells transfected with Aβ42 aggregates grow on -Ade (Figure 5-7B and Table 5-2). Colony purification of the Ade^+ papillae from the original -Ura plate containing the transfectants on YPD media demonstrated the formation of Ade^+ colonies of different phenotypic stringencies and they showed different levels of growth on -Ade media. (Figure 5-7C). The Ade^+ colonies from were divided into three groups designated as “strong”, “intermediate” and “weak” strains based on growth on –Ade medium and color on YPD medium. The vast majority of Ade^+ colonies induced by the Aβ-based chimeric construct were curable by serial passages on medium containing GuHCl, thus confirming that the GuHCl-curable nonsense suppression state was stably maintained by daughter cells (Figure 5-5C, Table 5-2). This result was consistent with what was obtained with spontaneous formed Ade^+ colonies.

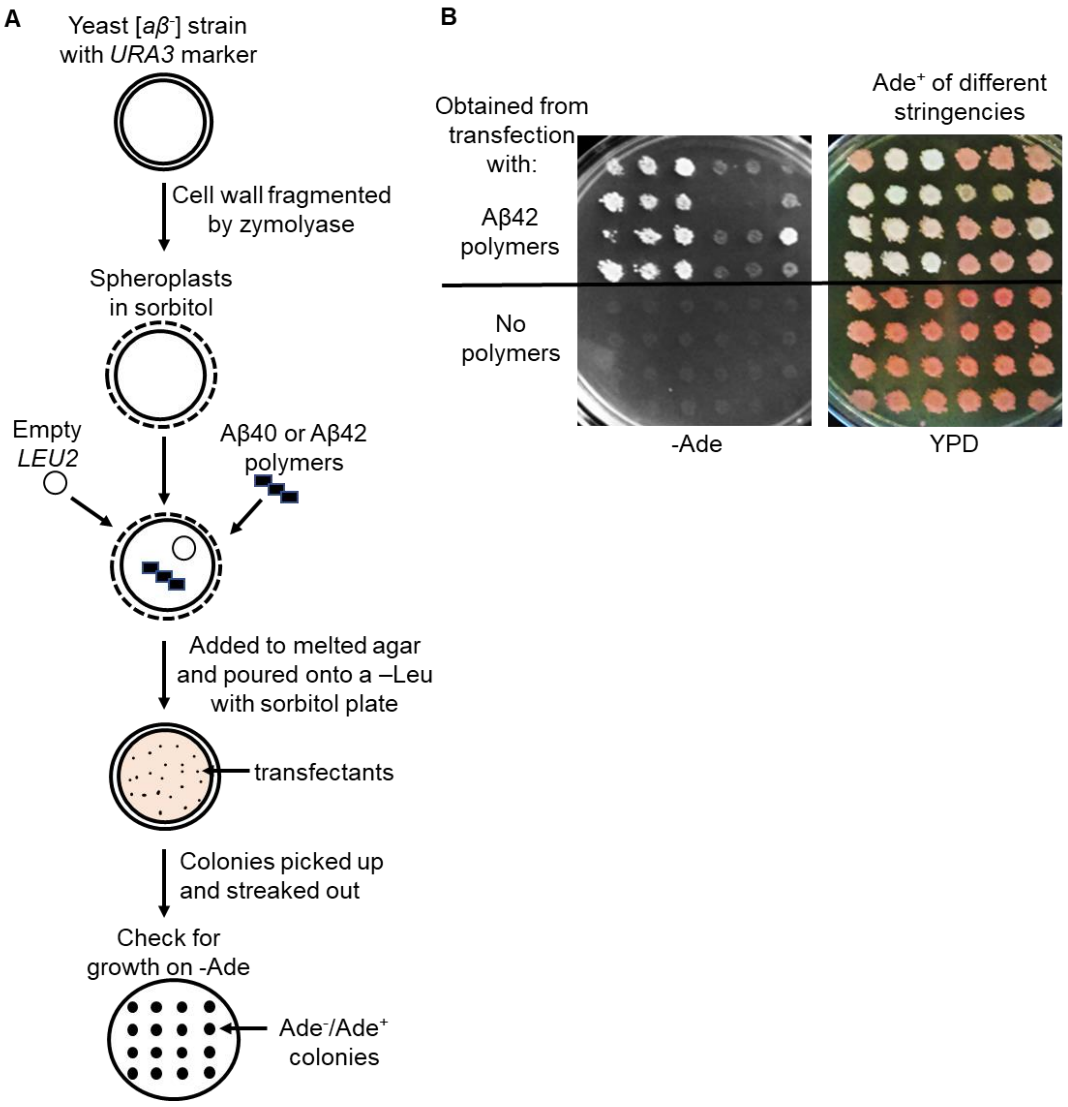

Figure 5-7. Generation of Ade$^+$ colonies after transfection of Aß aggregates into yeast. A- Summary of transfection procedure. B - Representative Ade$^+$ transfectants obtained after Aß42 or Aß42 aggregates were transfected into a [*psi*$^-$] strain carrying [*URA3 Aβ-NR-MC*] plasmid. Yeast cells were grown on –Ade medium (for suppression assay) at 30°C for 8 days. The Ade$^+$ transfectants, after colony purification, exhibited different phenotypic stringencies. These derivatives lost the ability to grow on –Ade medium after 20-40 generations in the presence of GuHCl (refer Table 5-1) . Yeast cells were grown on YPD (for color assay) and on –Ade medium (for suppression assay) at 30°C for 5 days.

Table 5-2. Summary of a proportion of Ade$^+$ colonies generated by Aβ-NR-MC after different transfection experiments

Type of Aβ aggregate used for transfection	Experiment	Total number of colonies tested	Ade$^+$ isolates tested			Total number of Ade$^+$ colonies tested
			Strong	Intermediate	Weak	
Aβ42	I	30	2	2	1	5
	II	21	2	3	3	8
	III	159	14	28	24	66
Total (for Aβ42)		210	18	33	28	79
Aβ40	I	31	4	3	2	9
Control	I	16	0	0	0	0
	II	21	0	0	0	0
	III	105	0	0	0	0
Total (for control)		142	0	0	0	0

5.3.1.5 Phenotypic characterization and identification of [$A\beta^+$] strains in yeast

To eliminate the possibility that the Ade$^+$ colonies generated spontaneously or by transfection is dependent on Sup35MC region which codes for a major portion of the Aβ-NR-MC chimera, or if the Ade$^+$ colonies are maintained with the help of a nuclear element or cellular machinery in yeast, a series of plasmid shuffles were made to replace [*URA3 Aβ-NR-MC*] plasmid with a different plasmid bearing pmSUP35-Aβ-NR-MC, to check if the Ade$^+$ phenotype was not changed with a different plasmid. To do this, a direct plasmid shuffle (Figure 5-6) was performed. The Ade$^+$ isolates generated by [*URA3 Aβ-NR-MC*] plasmid, either spontaneously or via transfection, was either - a) transformed with [*LEU2 Aβ-NR-MC*] or a control [*LEU2 MC*] plasmid or b) mated with a Ade$^-$ strain carrying [*LEU2 Aβ-NR-MC*] or a control [*LEU2 MC*] plasmid and containing an opposite mating type and was isogenic to the strain with the Ade$^+$ isolates carrying [*LEU2 SUP35-Aβ-NR-MC*]. The resulting haploid (in the case of transformation) or diploid (in the case of mating) was selected on -Ura-Leu-Ade. The [*URA3 Aβ-NR-MC*] plasmid was shuffled out by

counterselection on 5-FOA medium. 3 individual Ade$^+$ isolates per plasmid combination was checked on -Ade for nonsense suppression (Fig 5-6). If the nonsense suppression by the Ade$^+$ isolates could be maintained in the presence [*LEU2 Aβ-NR-MC*] before and after the loss of [*LEU2 Aβ-NR-MC*]; and if the nonsense suppression by the Ade$^+$ isolates was eliminated when the Ade$^+$ isolates was introduced with [*LEU2 SUP35-MC*] before and after the loss of [*URA3 Aβ-NR-MC*], then that particular Ade$^+$ isolate was considered a [*Aβ*$^+$] potential and was further characterized by reverse plasmid shuffle. The Ade$^+$ isolates that demonstrated growth in both the presence of [*LEU2 Aβ-NR-MC*] or [*LEU2 SUP35 MC*] was eliminated as a false [*Aβ*$^+$] potential and was confirmed to not be maintained by [*Aβ-NR-MC*].

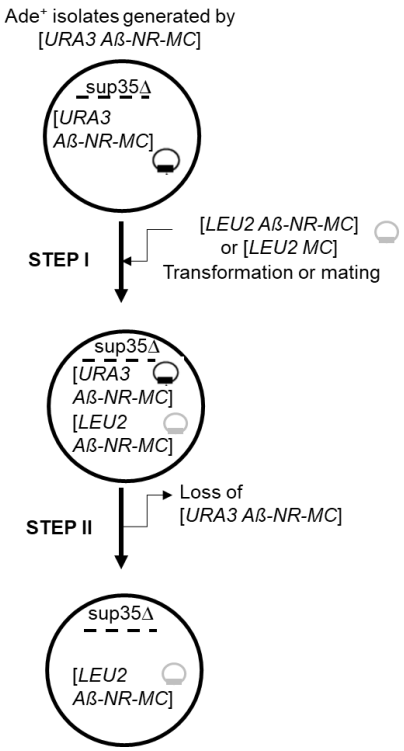

Figure 5-8. Analysis of Ade$^+$ isolates generated by Aß-NR-MC chimera by direct plasmid shuffle.

Direct plasmid shuffle (STEP I)

As per the procedure (Figure 5-6) and outcomes described above, the Ade$^+$ isolates from spontaneous and transfection experiments (Figures 5-3, 5-5, Table 5-4, 5-5), underwent a direct plasmid shuffle to replace [*URA3 Aβ-NR-MC*] with [*LEU2 Aβ-NR-MC*] or [*LEU2 MC*]. Two Ade$^+$ isolates, each representative of a [*Aβ*$^+$] potential and a false [*Aβ*$^+$] potential is shown (Figure 5-8, STEP I). Ade$^-$ isolate carrying [*URA3 Aβ-NR-MC*] was used as a control. In Step I, Ade$^+$ isolates 1 and 2 carrying [*URA3 Aβ-NR-MC*] could co-exist with [*LEU2 Aβ-NR-MC*] as demonstrated by growth on -Ura-Leu-Ade, indicating that the Ade$^+$ phenotype could be maintained. However, Ade$^+$ isolate 1 with [*URA3 Aβ-NR-MC*] and [*LEU2 MC*] also demonstrated growth on -Ura-Leu-Ade, indicating that this isolate is not controlled by [*Aβ-NR-MC*], unlike isolate 2 in which the presence of both [*URA3 Aβ-NR-MC*] and [*LEU2 MC*], could not maintain the Ade$^+$ phenotype. The Ade$^-$ control could not grow in the presence of any plasmid as it did not possess an Ade$^+$ phenotype to begin with.

Direct plasmid shuffle (STEP II)

After the loss of [*URA3 Aβ-NR-MC*] (Figure 5-6), Ade$^+$ isolates 1 could retain nonsense suppression in the presence of both [*LEU2 SUP35- Aβ-NR-MC*] or [*LEU2 MC*], thus indicating that this isolate demonstrated a prion-like phenotype, that is not maintained only by [*Aβ-NR-MC*] and is not characterized further. Ade$^+$ isolates 2 could retain nonsense suppression only in the presence of both [*LEU2 SUP35- Aβ-NR-MC*] and not [*LEU2 MC*], thus indicating that this isolate demonstrated a prion-like phenotype that is maintained only by [*Aβ-NR-MC*] and is further characterized by reverse shuffle.

The dependence or independence of Sup35MC region for [Aβ$^+$] propagation. [*Aβ*$^+$] potentials among the Ade$^+$ isolates generated by Aβ-NR-MC chimera that could be

maintained exclusively by Aβ-NR-MC were successfully obtained. While the isolates generated by Aβ-NR-MC chimera could be maintained by [*Aβ-NR-MC*], an important step was to ensure that the Ade$^+$ phenotype could not be maintained by [*MC*], and thus be restored when the original inducer plasmid, [*LEU2 Aβ-NR-MC*], was reintroduced to the isolates. To confirm this, it had to be demonstrated that [*Aβ*$^+$] potentials from STEP II that were transformed with [*LEU2 Aß-NR-MC*] could maintain the Ade$^+$ phenotype after a reintroduction of the original [*URA3 Aß-NR-MC*]. Also, the [*Aβ*$^+$] potentials from STEP II that were transformed via shuffle with [*LEU2 MC*] should not be able to maintain the Ade$^+$ phenotype after a reintroduction of the original [*URA3 Aß-NR-MC*],

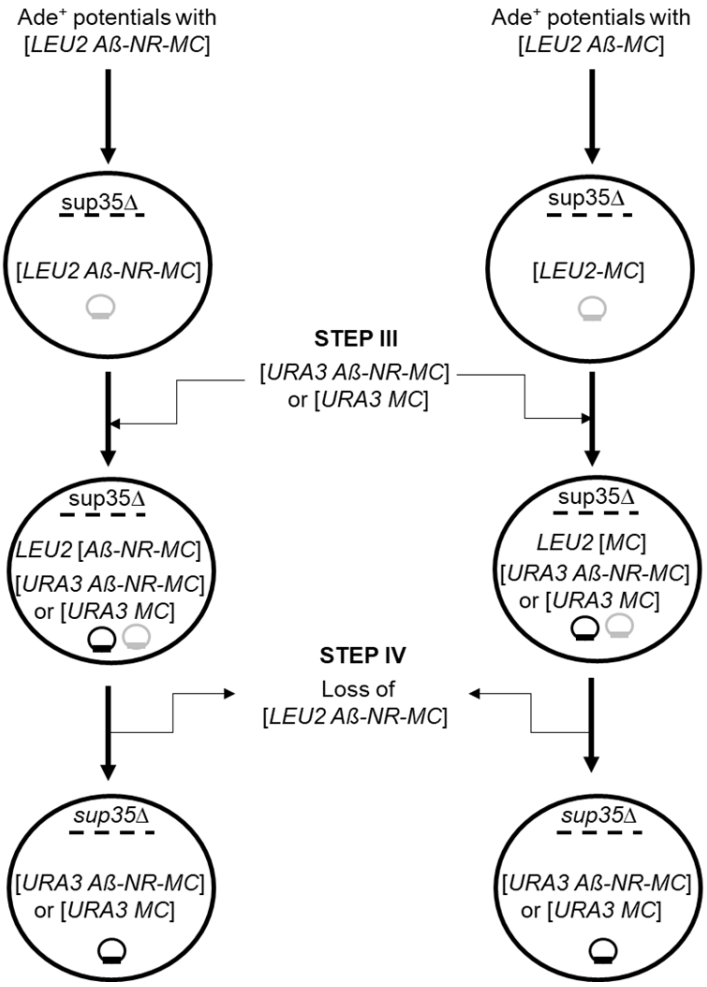

Figure 5-9. Analysis of Ade$^+$ potentials by reverse plasmid shuffle.

Reverse plasmid shuffle (STEP III)

The [*Aβ*$^{+}$] potential (isolate 2 in this case) containing strains from STEP II carrying [*LEU2 Aβ-NR-MC*] plasmid or control [*LEU2 MC*] plasmid, were reintroduced with [*URA3 Aβ-NR-MC*] plasmid or control [*URA3 MC*] plasmid by transformation, and their phenotypes were checked by growth on -Ura-Leu-Ade. The Ade^{+} phenotype could be maintained by the isolate 2 (representative of [*Aβ*$^{+}$]) with [*LEU2 Aβ-NR-MC*] after the reintroduction of [*URA3 Aβ-NR-MC*] as demonstrated by growth on -Ura-Leu-Ade. As expected, the isolate 2 with [*LEU2 MC*] that was transformed with [*LEU2 Aβ-NR-MC*] or control [*LEU2 MC*], could not produce an Ade^{+} phenotype, as demonstrated by a lack of growth on -Ura-Leu-Ade for both combinations. This was a preliminary confirmation that [*MC*] could not maintain the Ade^{+} phenotype generated by [*URA3 Aβ-NR-MC*] and as a result, cannot transmit the amyloid template to [*LEU2 Aβ-NR-MC*].

Reverse plasmid shuffle (STEP IV)

After the loss of [*LEU2 Aβ-NR-MC*] or [*LEU2 MC*] via reverse plasmid shuffle (Figure 5-7), the phenotypes of Ade^{+} isolates with [*URA3 Aβ-NR-MC*] or [*URA3 MC*] was checked on -Ade. Ade^{+} Isolate 2 with [*URA3 Aβ-NR-MC*] demonstrated nonsense suppression, as indicated by growth on -Ade. The Ade^{-} and Ade^{+} versions of Isolate 2 with [*URA3 MC*] could not grow on -Ade. This definitively confirmed that the Ade^{+} phenotype generated by [*URA3 Aβ-NR-MC*] could transmit a prion-like state to [*LEU2 Aβ-NR-MC*] and propagate the same in yeast. This was evidenced by the maintenance of the prion state after the reintroduction of the [*URA3 Aβ-NR-MC*] (originally used for spontaneous formation and transfection experiments), followed by a loss of the intermediate [*LEU2 Aβ-NR-MC*]. Additionally, the Ade^{+} phenotype generated by [*URA3 Aβ-NR-MC*] could not be transferred to [*LEU2 MC*] and thus, could not be propagated in yeast after a reintroduction of the

[*URA3 Aβ-NR-MC*] plasmid. The potentials that were obtained after analysis by direct and reverse shuffles were termed as [*Aβ*$^{+}$], denoting that these isolates are generated and propagated by Aβ-NR-MC chimeric protein. All the Ade^{+} isolates obtained from spontaneous formation and transfection experiments were verified by direct and reverse plasmid shuffles, and the proportion of Ade^{+} isolates/[*Aβ*$^{+}$] potentials that demonstrated different strain stringencies as per their color on YPD were also recorded (Table 5-6, 5-7)

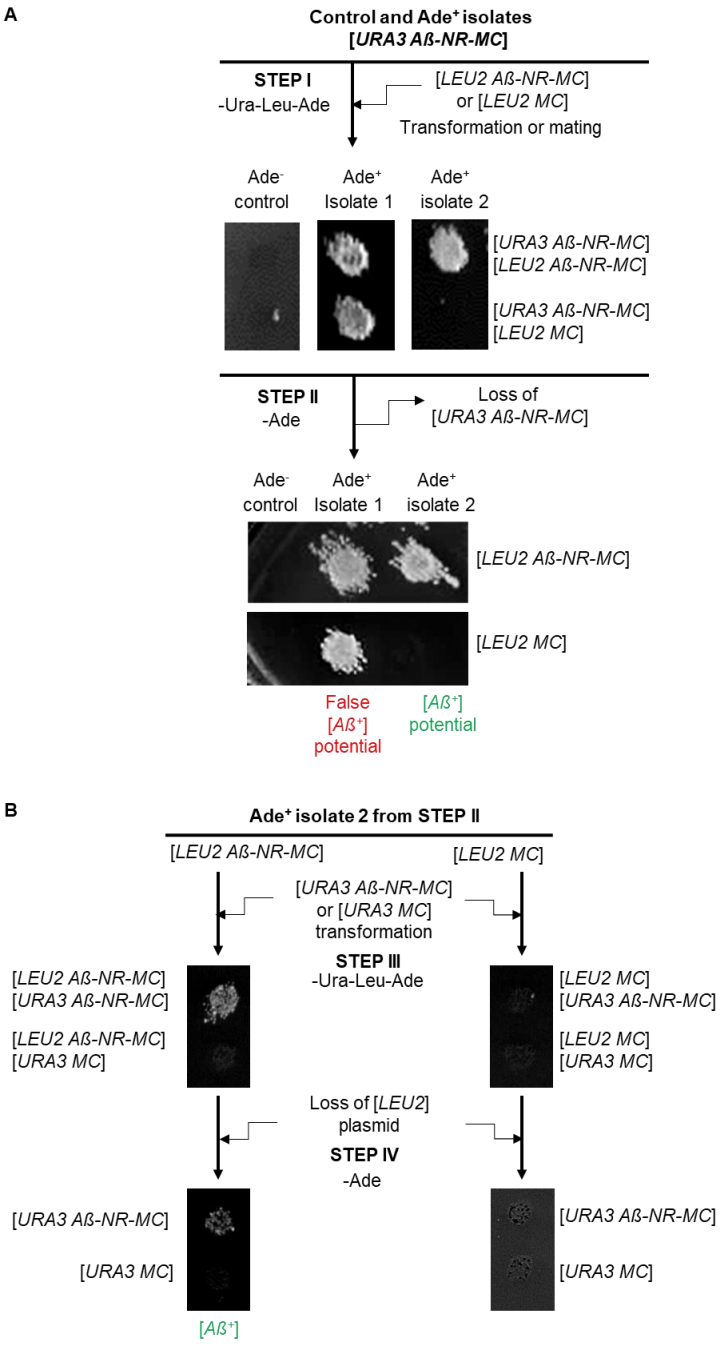

Figure 5-10. Analysis of Ade$^+$ isolate 2 by direct and reverse plasmid shuffle. (Steps I and II) - A representative of an Ade$^+$ isolate, formed spontaneously or via transfection, that produced a false [*Aß*$^+$] potential and a [*Aß*$^+$] potential is shown. The Ade$^+$ isolates including an Ade$^-$ control was introduced with [*LEU2 Aß-NR-MC*] *or* [*LEU2 MC*] and underwent a direct plasmid shuffle to lose [*URA3 Aß-NR-MC*]. The Ade$^+$ phenotype could be maintained by Ade$^+$ isolate 2. (Steps III and IV) Ade$^+$ isolate 2 was reintroduced with [*URA3 Aß-NR-MC*] or [*URA3 MC*] and went through reverse shuffle to lose [*LEU2 Aß-NR-MC*] or [*LEU2 MC*]. The Ade$^+$ phenotype could be maintained by [*URA3 Aß-NR-MC*] but not by [*URA3 MC*].

Table 5-3. Proportion of [*Aβ*$^+$] among Ade$^+$ colonies as determined by direct and reverse plasmid shuffle

Origin of Ade$^+$ colonies	Phenotypic stringency	Number of Ade$^+$ colonies analyzed by direct shuffle			Number of [*Aβ*$^+$] potentials tested and confirmed by reverse shuffle
		False [*Aβ*$^+$] potential	[*Aβ*$^+$] potential	Total Ade$^+$ tested	
Spontaneous	Strong	1	0	1	0
	Intermediate	0	1	1	1
	Weak	0	1	1	1
	Total	**1**	**2**	**3**	**2**
Transfection with Aβ42	Strong	8	9	17	9
	Intermediate	4	27	31	25
	Weak	1	17	18	17
	Total	**13**	**53**	**66**	**51**
Total		**14**	**55**	**69**	**53**

5.3.2 Identification of prion-like phenotype generated by human tau peptide in yeast

The neuronal inclusions of Alzheimer's disease are made of the microtubule-associated protein tau, in a hyperphosphorylated state[50,51]. Abundant filamentous tau inclusions are not limited to Alzheimer's disease. They are the defining neuropathological characteristic of frontotemporal dementias as well. However, to the best of our knowledge, there are no yeast model for amyloid formation and propagation by tau. In section 5-3-1, we confirmed that the replacement of the Sup35 prion domain (Sup35N) by Aβ42 caused a termination defect and results in protein oligomerization. Thus, this model could not be applied for specifically studying Aβ-based strains as Aβ had to be maintained in non-polymerized form and switched to the polymerized form in a controlled manner. However, the repeat domain of tau is not as amyloidogenic as Aβ and thus we used the approach of replacing the Sup35 prion domain (Sup35N) by a wildtype and mutant version of tau

repeat domain (RD) (Figure 5-1) to establish a yeast model for the formation of tau-dependent phenotypically detectable prion.

5.3.2.1 Expression of chimeric constructs containing wild-type or mutant tau fused to Sup35MC in yeast

We have also constructed the chimeric version of the yeast Sup35 protein, tau(WT)-MC, in which the whole Sup35N region was replaced by the repeat domain (RD) of tau encompassing amino acid positions from 244 to 372 (Figure 5-1). Tau mutations in familial frontotemporal dementia and parkinsonism linked to chromosome 17[51] (FTDP-17) are missense mutations that are located in the microtubule-binding RD or close to it. In addition to tau(WT)-MC, we have also constructed a version of tau-MC construct named as tau(Mut)-MC, containing two missense mutations, P301L and V337M, in exon 9 and exon 10 respectively. Both these constructs were placed under the control of the copper-inducible yeast promoter (P_{CUP1}). Initially, a yeast strain expressing only pmCUP1-tau(WT)-MC or pmCUP1-tau(Mut)-MC was constructed using a plasmid shuffle procedure used for constructing pmCUP1-Aβ-MC (Figure 5-3). A *S. cerevisiae* [*psi*$^-$] ***sup35Δ*** strain with the SUP35 gene on a *LEU2* plasmid was transformed by *URA3* plasmids bearing [*tau(WT)-MC*] or [*tau(Mut)-MC*] as well as a control, [*MC*]. Transformants were obtained on medium lacking uracil and leucine (−Ura, Leu) that is selective for both plasmids and checked for suppression of the *ade1-14* reporter on both medium lacking only adenine (−Ade) and medium lacking uracil, leucine, and adenine (−Ura, Leu, Ade). These media were used to determine whether the newly introduced tau-MC chimeric proteins were immediately converted into a non-functional form or if it remained functional. In parallel, transformants were streaked out on −Ura medium and replica plated to −Leu medium, to identify the Ura+ Leu- colonies that lost the original *LEU2* plasmid. Only one Ura+ Leu-

colony was analyzed from each individual transformant, to ensure independence of all colonies from each other.

5.3.2.2 Phenotypic detection of Ade^+ colonies formed by tau-based chimeric proteins in yeast

Replacement of Sup35N by tau(WT) or tau(Mut) slightly decreased functionality of Sup35 in translation termination, leading to growth of cells containing tau(WT)-MC as well as tau (Mut)-MC (without complete Sup35) on –Ura-Leu-Ade medium at background concentrations (3 µm) of $CuSO_4$. However, growth on –Ura-Leu-Ade was eliminated by addition of 10 µm of $CuSO_4$, apparently due to increase in tau(WT)-MC abundance (Figure 5-11A). After the loss of *LEU2 Sup35*, a transient increase in tau(WT)-MC or tau(Mut)-MC levels on the medium with 100 µm $CuSO_4$ lead to formation of Ade^+ papillae capable of growing on –Ade medium with 10 µm $CuSO_4$ (Figure 5-11B). Moreover, the tau(Mut)-MC construct previously shown to promote tau aggregation in the mammalian cell models, produced Ade^+ prion derivatives with higher frequency compared to tau(WT)-MC (Figure 5-11B). This Ade^+ phenotype formed by tau(WT)-MC (data not shown) and tau(Mut)-MC was heritable in mitotic divisions and curable by GuHCl, thus manifesting itself as a prion (Figure 5-11C). Cell lysates from strains with tau(Mut)-MC, before and after transient induction with 100 µm $CuSO_4$, were analyzed using semi-denaturing detergent agarose gel electrophoresis (SDD-AGE) as described in Chapter 2. Tau(Mut)-MC induced with 100 µm $CuSO_4$ produced detergent-resistant polymers in the yeast cells (Figure 5-4D) as is typical of yeast prions and amyloids and promoted the immobilization of endogenous Sup35 protein into an aggregated fraction, confirming the prion-like characteristic of the isolate.

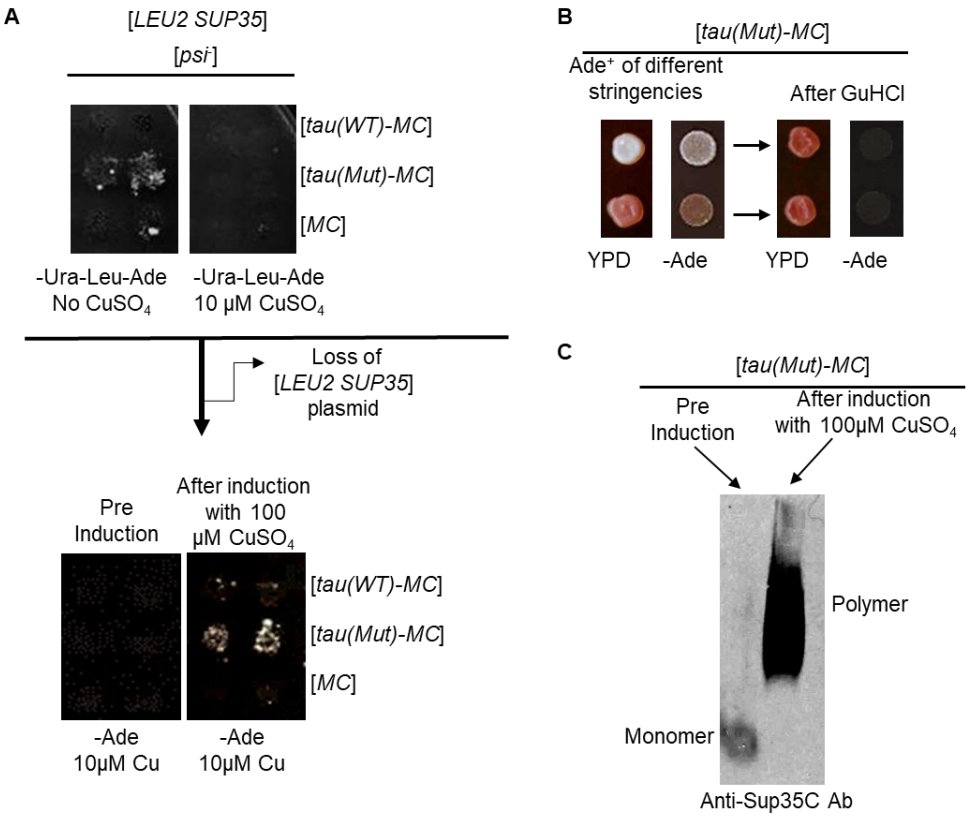

Figure 5-11. Phenotypic detection of Ade$^+$ phenotype formed by tau-MC chimeras. (A) The [*psi$^-$ pin$^-$*] strain expressing both Sup35 protein and tau-MC chimeric proteins were more functional in terminating translation in the presence of 10μM $CuSO_4$. After losing [*LEU2 SUP35*] by plasmid shuffle procedure, a transient increase in tau-MC levels on the medium with 100 μm $CuSO_4$ lead to formation of Ade$^+$ papillae capable of growing on –Ade medium with 10 μm of $CuSO_4$ after 10 days of incubation (B) The colony purified Ade$^+$ papillae from mutated tau(Mut)-MC exhibited different phenotypic stringencies and lost the ability to grow on –Ade medium in the presence of GuHCl. (C) For biochemical characterization, cell lysates from strains expressing tau(Mut)-MC before and after transient induction with 100 μm of $CuSO_4$ was analyzed by SDD-AGE followed by the reaction to the Sup35C-specific antibody.

5.4 Discussion

Prion formation by Aβ and tau in yeast independent of Sup35N or Sup35Q/N-domains in yeast. Previous studies[45] and our data (Figure 5-4), chimeric Aβ-Sup35 constructs containing Aβ42 instead of the whole Sup35N region are partly non-functional in termination of translation, apparently because they instantly form polymers in yeast,

making a switch between the non-amyloid and amyloid states, and controlled formation of Aβ-dependent prion strains, impossible. We found that the repeat domain of tau fused to Sup35MC could be retained in a functional state in the presence of continuous overproduction of the chimeric protein to increase the levels of Sup35MC (Figure 5-11). The non-functionality Aβ-MC can be attributed either to the highly amyloidogenic nature of Aβ42 causing cellular toxicity and resulting in instant aggregation or due to lack of the Sup35N portion including a region of oligopeptide repeats (NRs, Figure 5-2), which is implicated in interactions with the chaperone machinery, composed of the Hsp104, Hsp70 and Hsp40 proteins and is required for the fragmentation of Sup35 prion aggregates. We have shown that the replacement of Aβ with the Q/N rich aggregation prone domain of Sup35 could be maintained in a functional form (Figure 5-5). The resulting chimeric protein was expected to nucleate a prion more efficiently than other models[53,54] as well as fusions to Sup35C, due to the high amyloidogenicity of Aβ and due to the presence of OR region of Sup35 that is essential for prion propagation, thus enabling the study of Aβ- and tau-based prion nucleation and propagation in yeast.

Aβ-NR-MC and tau-MC chimeric (wildtype and mutant) chimeric proteins, while functional, could switch to a prion form and cause nonsense suppression, in the absence of the aggregation-prone Q/N domain of Sup35 in the case of Aβ (Figure 5-5A) or the prion domain of Sup35 in the case of tau (Figure 5-11). The Ade^{+} phenotypes of different stringencies by Aβ-NR-MC and tau-MC chimeric proteins could also be propagated to daughter cells after many generations and cured by the prion-eliminating agent GuHCl, thus following a non-Mendelian pattern of inheritance, like yeast prion proteins[32] (Figure 5-5B, 5-11, and Table 5-1).

Formation of Aβ-dependent strains after transfection with Aβ1-42 or Aβ1-40 aggregates. The “transfection” process[32,107] differs from spontaneous formation of prion isolates by an

introduction of a pre-formed aggregate, reflecting characteristic of unique conditions of its induction environment. Typically, in the same species, the phenotype of a particular prion template or variant is expected to be faithfully perpetuated in a recipient protein of the same or similar sequence. However, transfection of prion material into a new species may cause the transfected prion to exhibit a phenotype unlike spontaneously formed prion in the same cell environment. This may occur even though the recipient strain expresses the same protein. Transfection, thus, becomes a valuable tool, giving us the ability to examine one and the same prion variant in different cellular backgrounds, providing insight into the effects of the cell environment on prion maintenance and propagation of prion strains. Aβ1-42 or Aβ1-40 aggregates following transfection into yeast carrying Aβ-NR-MC chimeric protein could generate different [*Aβ*$^+$] strains, as detected on YPD color assay and -Ade suppression assay (Figure 5-7, 5-12, and Table 5-2).

Role of Sup35MC in [Aβ$^+$] and potentially [TAU$^+$] strain propagation. For Aβ, the plasmid shuffle results (Figure 5-10, Table 5-3) confirmed that a majority of Ade$^+$ potentials formed by Aβ-NR-MC chimeric protein via spontaneous formation or by transfection, later verified to be [*Aβ*$^+$], were maintained and propagated in strains expressing only Aβ-NR-MC and not by Sup35MC (or Sup35C – data not shown), indicating that [*Aβ*$^+$] formation and propagation is primarily driven either by Aβ or Aβ-NR. The small majority that was not dependent on Aβ-NR-MC for the Ade$^+$ phenotype could be due to the formation of [*MCS*$^+$] (data not published, refer Meng Sun Thesis in Georgia Tech repository), a prion-like state caused by Sup35MC in the absence of the prion domain of Sup35. Unlike *[Aβ$^+$],* [*MCS*$^+$] followed a Mendelian pattern of inheritance, indicating the involvement of a nuclear element indicating that the prion-like factor and a nuclear factor can co-exist, and both may contribute to [*MCS*$^+$]. This makes it crucial to analyze all the colonies obtained either spontaneously or by transfection with direct and reverse shuffles to eliminate the

possibility of prion-like states like [*MCS*$^+$]. In a study[108] where a wild-type aggregation-prone protein, human heterogeneous nuclear ribonucleoprotein, hnRNPA2-Sup35 fusion was employed as the sole copy of Sup35, it remains to be understood if the Ade$^+$ phenotype is a result hnRNPA2B1 or due to the formation of another prion/nuclear factor that is contributing towards the prion phenotype, making a detailed characterization of the prion phenotypes crucial.

Impact of Aβ and tau on spectra of induced [Aβ$^+$] and potentially [TAU$^+$] strains. Both yeast and mammalian prion and amyloid proteins are known to form various variants or "strains" that differ from each other by phenotypic and biochemical characteristics and are apparently controlled by distinct protein conformations. In the case of [*PSI*$^+$], strains can differ from each other in the stringency of termination defect, mitotic stability, aggregate size, fragmentation by chaperones etc. We have shown that Aβ-NR-MC and tau-MC chimeric proteins can also induce a spectra of prion variants in yeast. It has also been suggested that the oligopeptide repeats facilitate prion fragmentation by Hsp104[41] either by providing a binding site for Hsp104 or by changing the conformation of the amyloid fiber core to allow Hsp104 to bind to it. Interestingly, a higher proportion of intermediate and weak [*Aβ*$^+$] strains were generated compared to strong [*Aβ*$^+$] strains by spontaneous formation as well as transfection (Table 5-2, 5-3). This is consistent with the fact that stronger prion strains are mitotically less stable than weak and intermediate prion strains and thus, are efficiently fragmentated by the cellular machinery[32] composed of Hsp104 and its partners whereas the other variants are more stable and thus allow a monomer addition to the prion fiber, thus propagating the prion variant in a more controlled and stable fashion. Alternatively, the prion fiber formed by intermediate and weak [*Aβ*$^+$] strains could be compositionally different compared to the stronger [*Aβ*$^+$] strains[92]. A possible explanation for the formation of [*Aβ*$^+$] variants is the formation of distinct initial nuclei by

Aβ as explained in Chapters 3 and 4 for prion nucleation by mammalian proteins, followed by an expansion of the amyloid region to the attached Sup35NR-MC domain. Depending on the amyloid template formed by Aβ-NR-MC chimera, it can be hypothesized that Hsp104 binding to the amyloid core and the resulting fragmentation would vary, thus producing different strains.

5.5 Conclusions

- Chimeric proteins, Aβ-NR-MC or tau-MC, in which the aggregation domain of Sup35 was substituted by either Aβ1-42 or tau244-372 (Wildtype or with mutations P301L, V337M), were functional in translation termination and could spontaneously convert into a partly non-functional prion state.
- Formation of detergent-resistant aggregates by the chimeric Aβ-NR-MC or tau-MC proteins in a prion state were confirmed by a biochemical approach.
- Propagation of prion strains produced by Aβ-NR-MC protein depended entirely on the Aβ-NR region, as these strains are not propagated by Sup35MC (or C)
- Transfection with *in vitro* produced Aβ1-40 or Aβ1-42 amyloids induced a conversion of Aβ-NR-MC protein into a prion state.

OVERALL CONCLUSIONS

- Fusion of mammalian amyloidogenic proteins to the prion domain of a yeast protein Sup35 nucleated a prion in yeast in the absence of pre-existing prions.
- Fusion of multimerization-prone non-amyloidogenic proteins to the prion domain of Sup35 could not nucleate [*PSI*$^{+}$]
- The amyloidogenic patterns of a mammalian protein drove the prion formation and propagation in the yeast model.
- The effects of alterations in human Amyloid beta (Aβ1-42) peptide associated with Alzheimer's disease (AD) fused to Sup35N to promote amyloid nucleation in yeast showed a similar trend to *in vitro* studies and structural models for Aβ1-42
- A small-scale chemical screen identified metal ions that could promote amyloid nucleation by Aβ1-42 fused to Sup35N.
- Human Aβ peptide associated with AD as well as the wild-type and mutated repeat domain (RD) of human tau protein, associated with AD and frontotemporal dementia, generated and propagated a polymeric prion state in yeast, when substituted for the aggregation-prone region of the yeast protein Sup35.
- *In vitro* produced Aβ polymers converted an Aβ-based chimeric protein into a polymeric state after transfection into yeast.
- Aβ- and tau-based chimeric proteins propagated distinct prion strains in the yeast cell.

IMPACT AND FUTURE PERSPECTIVES

The results present in this work highlight the contribution of amyloid/prion properties of mammalian amyloidogenic proteins to drive the initial nucleation and propagation of prion strains in yeast. The significance of this work is the development of sensitive and selective systems that produce a phenotypic output that can be easily detected in yeast. Additionally, non-amyloidogenic multimer forming proteins can eliminated as false positives using the same system.

In Chapters 3 and 4, amyloidogenic proteins that could nucleate a prion in yeast were identified and the prion properties of one such protein, Amyloid beta, was explored in detail. An interesting finding from the same is the promotion of prion by an amyloidogenic portion of myocilin peptide composed of a very short stretch of amino acids that previously produced amyloid polymers *in vitro* in the lab of our collaborator, Dr. Raquel Lieberman. Myocilin is not a well-established amyloid and the only evidence for its amyloid properties are from *in vitro* experiments. Our work is the first line of evidence for prion properties of myocilin in a cell-based model. Recent studies related to Alzheimer's disease (AD), point towards tau, an amyloidogenic protein studied in Chapter 5, as the main culprit in AD pathology and in fact, a new data mining analysis done on 51 independent multiple mice models of AD correlate with phosphorylated tau as the main cause for cognitive decline in AD, potentially exacerbated by Amyloid beta. Prion nucleation experiments using different isoforms of tau that have been shown to have pro- and anti-aggregation properties in animal models or *in vitro* will be performed to identify sequences that influence prion nucleation in yeast. To model phosphorylated tau in yeast, the kinases - Mds1 and Pho85 which are the functional yeast orthologues of mammalian Gsk-3β and Cdk5 whose deletion has been previously shown to cause an increased phosphorylation of tau, will be

used. In addition to known and lesser known amyloidogenic proteins, novel proteins with different levels of amyloidogenicity can also be studied for their amyloid/prion properties in yeast.

In Chapter 5, a system was developed to identify and characterize amyloidogenic proteins that could propagate prion strains on their own in yeast. Amyloid beta and different isoforms of tau faithfully formed and propagated prion strains in yeast. Till date, there are no yeast models that can effectively monitor the propagation of strains by amyloidogenic proteins in yeast, especially via transfection with amyloid polymers. One of the main and an unexplored drawback in treating amyloid diseases is potentially, the existence of different variants and a lack of understanding and detection of the specific variant that is being treated. This is certainly the case for diseases caused by PrP but increasing evidence in the field of amyloid biology does not exclude the possibility of this being the case for certain amyloid diseases caused by proteins with transmissible properties. This opens an array of opportunities to study prion propagation using the model developed in our work. As a follow-up to the collaborative work with research groups at Emory as demonstrated in Chapter 5, the system we have developed will be employed to study the propagation of prion strains in yeast after transfection with seeded Aβ40 or Aβ42 extracts as well as extracts from the brains of AD and non-demented patients with amyloid plaques. This will provide us with an understanding if the prion template in each strain is faithfully propagated or if they undergo some kind of selection to propagate a different spectra of prion strains, taking into consideration the cellular environment of yeast. Another interesting scientific question that can potentially be immediately addressed due to resource availability is to use our system to check for self-seeding of tau using tau-MC chimeric proteins by seeded and unseeded tau amyloid extracts as well as to check for cross-seeding of tau by Aβ amyloid extracts including the ones extracted from the brains

of AD and non-AD patients, to evaluate the propagation of tau-based prions strains and if indeed, there is a cross-talk between the proteins involved in AD. If there is a pattern that shows strain conversion in the presence of different amyloid templates, this would be important and useful to design therapies that can employ these peptides to delay and even prevent disease progression in humans or mammals by converting the prion strain to a conformation that is not propagated at all or at least, propagated less efficiently.

APPENDIX

Table A. Yeast strains used in this study

Strain name	Prion background	Genotype
GT81-1C	[*PSI*$^+$ *PIN*$^+$]	*MAT***a** *ade1-14 his3 leu2-3,112 lys2 trp1 ura3-52*
GT81-1D	[*PSI*$^+$ *PIN*$^+$]	*MAT*α *ade1-14 his3 leu2-3,112 lys2 trp1 ura3-52*
GT409	[*psi*$^-$ *pin*$^-$]	*MAT***a** *ade1-14 his3 leu2-3,112 lys2 trp1 ura3-52*
GT159	[*psi*$^-$ *PIN*$^+$]	*MAT***a** *ade1-14 his3 leu2-3,112 lys2 trp1 ura3-52*
GT564	[*psi*$^-$ *pin*$^-$]	*MAT***a** *ade1-14 his3 leu2-3,112 lys2 trp1 ura3-52 rnq1*Δ*::HIS3Sp*
GT197	[*psi*$^-$ *pin*$^-$]	*MAT*α *ade1-14 his3 leu2-3,112 lys2 trp1 ura3-52*
GT17	[*psi*$^-$ *pin*$^-$]	*MAT***a** *ade1-14 his3 leu2 trp1 ura3-52*
33G-D373	[*psi*$^-$ *pin*$^-$]	*MAT*α *ade2-144 717 his7 lys9 pha2 trp1 ura3-52 leu2-3,112*
OT56 (ψ+1-1-74-D694)	[*PSI*$^+$ *PIN*$^+$]	*MATa ade1-14 his3-*Δ*200 leu2-3,112 trp1-289 ura3-52*
OT55 (ψ+7-74-D694)	[*PSI*$^+$ *PIN*$^+$]	*MAT***a** *ade1-14 his3-*Δ*200 leu2-3,112 trp1-289 ura3-52*
GT671	[*psi*$^-$ *pin*$^-$]	*MAT*α *ade1-14 his3Δ (or 11,15) lys2 ura3-52 leu2-3,112 trp1 sup35::HIS3* [*CEN LEU2 SUP35*]
GT680	[*psi*$^-$ *pin*$^-$]	*MAT*α *ade1-14 his3Δ (or 11,15) lys2 ura3-52 leu2-3,112 trp1 sup35::HIS3* [*CEN URA3 SUP35*]
GT2126	[*psi*$^-$ *pin*$^-$]	*MAT*α *ade1-14 his3Δ (or 11,15) lys2 ura3-52 leu2-3,112 trp1 sup35::HIS3* [*CEN URA3 Aβ1-42-NR-MC*]
GT2132	[*psi*$^-$ *pin*$^-$]	*MAT*α *ade1-14 his3Δ (or 11,15) lys2 ura3-52 leu2-3,112 trp1 sup35::HIS3* [*CEN URA3 tau RD P301L, V337M-MC*]
GT2132	[*psi*$^-$ *pin*$^-$]	*MAT*α *ade1-14 his3Δ (or 11,15) lys2 ura3-52 leu2-3,112 trp1 sup35::HIS3* [*CEN URA3 tau RD-MC*]
GT2180	[*psi*$^-$ *pin*$^-$]	*MAT*α *ade1-14 his3Δ (or 11,15) lys2 ura3-52 leu2-3,112 trp1 sup35::HIS3* [*CEN LEU2 Aβ1-42-NR-MC*]
GT2265	[*psi*$^-$ *pin*$^-$]	*MAT***a** *ade1-14 his3Δ (or 11,15) lys2 ura3-52 leu2-3,112 trp1 sup35::HIS3* [*CEN LEU2 Aβ1-42-NR-MC*]
GT2266	[*psi*$^-$ *pin*$^-$]	*MAT***a** *ade1-14 his3Δ (or 11,15) lys2 ura3-52 leu2-3,112 trp1 sup35::HIS3* [*CEN LEU2 Sup35MC*]

Table B. *Saccharomyces cerevisiae – Escherichia coli* shuttle plasmids used in this study

Plasmid name	Plasmid type	Yeast marker	Promoter	Expression cassette under promoter	Source
pLA1	*CEN*	*HIS3*	P_{GAL}	None	Ref. 109 (Newnam et al., 1999)
pLA1-Sup35	*CEN*	*HIS3*	P_{GAL}	*SUP35*	Ref. 110 (Chernoff et al., 1999); ref. 111 (Chernova et al., 2003)
pLA1-Sup35N	*CEN*	*HIS3*	P_{GAL}	*SUP35N*	Ref. 110 (Chernoff et al., 1999)
pLA1-Sup35N-PrP90-230	*CEN*	*HIS3*	P_{GAL}	*SUP35N-prnp90-230*	This study
pLA1-Sup35N-Aβ1-42	*CEN*	*HIS3*	P_{GAL}	*SUP35N-Aβ1-42*	This study
pLA1-Sup35NM-PrP90-230	*CEN*	*HIS3*	P_{GAL}	*SUPNM-prnp90-230*	This study
pLA1-Sup35NM-Aβ1-42	*CEN*	*HIS3*	P_{GAL}	*SUP35NM-Aβ1-42*	This study
pmCUP1	*CEN*	*URA3*	P_{CUP1}	None	Ref. 75 (Serio et al., 1999)
pmCUP1-nERI	*CEN*	*URA3*	P_{CUP1}	None	This study
pmCUP1-PrP90-231-GFP(URA3)	*CEN*	*URA3*	P_{CUP1}	*prnp90-231-GFP*	Ref. 49 (Rubel et al., 2008)
pmCUP1-Aβ1-42-GFP(URA3)	*CEN*	*URA3*	P_{CUP1}	*Aβ1-42-GFP*	This study
pmCUP1-Sup35N	*CEN*	*URA3*	P_{CUP1}	*SUP35N*	This study
pmCUP1-Sup35N-PrP90-230	*CEN*	*URA3*	P_{CUP1}	*SUP35N-prnp90-230*	This study
pmCUP1-Sup35N-Aβ1-42	*CEN*	*URA3*	P_{CUP1}	*SUP35N-Aβ1-42*	This study
pmCUP1-Sup35N-Aβ3-42	*CEN*	*URA3*	P_{CUP1}	*SUP35N-Aβ3-42*	This study
pmCUP1-nERI-Sup35N-Aβ3-42	*CEN*	*URA3*	P_{CUP1}	*SUP35N-Aβ3-42*	This study
pmCUP1-nERI-Sup35N-Aβm1-42	*CEN*	*URA3*	P_{CUP1}	*SUP35N-Aβm1-42*	This study
pmCUP1-nERI-Sup35N-NAC61-93	*CEN*	*URA3*	P_{CUP1}	*SUP35NAC61-93*	This study

pmCUP1-nERI-Sup35N-IAPP41-69	*CEN*	*URA3*	P_{CUP1}	*SUP35N-IAPP41-69*	This study
pmCUP1-Sup35N-Myocilin426-441	*CEN*	*URA3*	P_{CUP1}	*SUP35N-Myocilin426-441*	This study
pmCUP1-nERI-Sup35N-GFP	*CEN*	*URA3*	P_{CUP1}	*SUP35N-GFP*	This study
pmCUP1-Sup35N-Ade2	*CEN*	*URA3*	P_{CUP1}	*SUP35N-ADE2*	This study
pmCUP1-nERI-Sup35N-lacZ	*CEN*	*URA3*	P_{CUP1}	*SUP35N-lacZ*	This study
pmCUP1-Sup35NM-PrP90-230	*CEN*	*URA3*	P_{CUP1}	*SUP35NM-prnp90-230*	This study
pmCUP1-Sup35NM-Aβ1-42	*CEN*	*URA3*	P_{CUP1}	*SUP35NM-Aβ1-42*	This study
pmCUP1-Sup35NM-NAC61-93	*CEN*	*URA3*	P_{CUP1}	*SUP35NM-NAC61-93*	This study
pmCUP1-Sup35NM-IAPP41-69	*CEN*	*URA3*	P_{CUP1}	*SUP35NM-IAPP41-69*	This study
pmCUP1-Sup35NM-GFP	*CEN*	*URA3*	P_{CUP1}	*SUP35NM-GFP*	Ref. 112 (Patino et al., 1996)
pmCUP1-Sup35NM-Ade2	*CEN*	*URA3*	P_{CUP1}	*SUP35NM-ADE2*	This study
pmCUP1- nERI-Sup35NM-lacZ	*CEN*	*URA3*	P_{CUP1}	*SUP35NM-lacZ*	This study
pmCUP1-Sup35N-PrP90-119	*CEN*	*URA3*	P_{CUP1}	*SUP35N-prnp90-119*	This study
pmCUP1-Sup35N-PrP120-230	*CEN*	*URA3*	P_{CUP1}	*SUP35N-prnp120-230*	This study
pmCUP1-Sup35N-PrP90-144	*CEN*	*URA3*	P_{CUP1}	*SUP35N-prnp90-144*	This study
pmCUP1-Sup35N-PrP90-159	*CEN*	*URA3*	P_{CUP1}	*SUP35N-prnp90-159*	This study
pmCUP1-Sup35N-PrP90-171	*CEN*	*URA3*	P_{CUP1}	*SUP35N-prnp90-171*	This study
pmCUP1-Sup35N-PrP90-119	*CEN*	*URA3*	P_{CUP1}	*SUP35N-prnp90-119*	This study
pmCUP1-Sup35NM-PrP90-159	*CEN*	*URA3*	P_{CUP1}	*SUP35NM-prnp90-159*	This study
pmCUP1-Sup35NM-PrP23-230	*CEN*	*URA3*	P_{CUP1}	*SUP35NM-prnp23-230*	This study

pmCUP1-Sup35N-PrP90-230 P101L	*CEN*	*URA3*	P_{CUP1}	*SUP35NM-prnp90-230 (P101L)*	This study
pmCUP1-Sup35N-PrP90-230 Q167R	*CEN*	*URA3*	P_{CUP1}	*SUP35NM-prnp90-230 (Q167R)*	This study
pLH105	*CEN*	*LEU2*	P_{GPD}	*HSP104*	Gift of S. Lindquist, cited in ref. 110 (Chernoff et al., 1999)
pmCUP1-nERI-Sup35N-Aβ1-40	*CEN*	*URA3*	P_{CUP1}	*SUP35N-Aβ1-40*	This study
pmCUP1-nERI-Sup35NM-Aβ1-40	*CEN*	*URA3*	P_{CUP1}	*SUP35NM-Aβ1-40*	This study
pmCUP1- nERI-Sup35N- Aβm1-42 F19S	*CEN*	*URA3*	P_{CUP1}	*SUP35N-Aβm1-42 (F19S)*	This study
pmCUP1- nERI-Sup35N- Aβm1-42-F20S	*CEN*	*URA3*	P_{CUP1}	*SUP35N-Aβm1-42-F20S*	This study
pmCUP1-nERI-Sup35N-Aβm1-42-I31P	*CEN*	*URA3*	P_{CUP1}	*SUP35N-Aβm1-42-I31P*	This study
pmCUP1-Sup35N-Aβ1-42*** (F19S, F20S, I31P*)*	*CEN*	*URA3*	P_{CUP1}	*SUP35N-Aβ1-42*** (F19S, F20S, I31P)*	This study
pmCUP1- nERI-Sup35N- Aβm1-42-D23N		*URA3*	P_{CUP1}	*SUP35N-Aβm1-42-D23N*	This study
pmCUP1- nERI-Sup35N- Aβm1-42-K28E	*CEN*	*URA3*	P_{CUP1}	*SUP35N-Aβm1-42-K28E*	This study
pmCUP1- nERI-Sup35N- Aβm1-42-D23K	*CEN*	*URA3*	P_{CUP1}	*SUP35N-Aβm1-42-D23K*	This study
pmCUP1- nERI-Sup35N- Aβm1-42-D23K, K28E	*CEN*	*URA3*	P_{CUP1}	*SUP35N-Aβm1-42-D23K, K28E*	This study
pmCUP1- nERI-Sup35N- Aβm1-42-H13L	*CEN*	*URA3*	P_{CUP1}	*SUP35N-Aβm1-42-H13L*	This study
pmCUP1- nERI-Sup35N- Aβm1-42-A21E,D23A	*CEN*	*URA3*	P_{CUP1}	*SUP35N-Aβm1-42-A21E, D23A*	This study
pmCUP1- nERI-Sup35N- Aβm1-42-G23V	*CEN*	*URA3*	P_{CUP1}	*SUP35N-Aβm1-42-G23V*	This study

pmCUP1- nERI-Sup35N- Aβm1-42-F19K	*CEN*	*URA3*	P_{CUP1}	*SUP35N-Aβm1-42-F19K*	This study
pmCUP1-Sup35N-HA	*CEN*	*URA3*	P_{CUP1}	*SUP35N-HA*	This study
pmCUP1-Sup35N-PrP90-230-HA	*CEN*	*URA3*	P_{CUP1}	*SUP35N-prnp90-230-HA*	This study
pmCUP1-MC	*CEN*	*URA3*	P_{CUP1}	*SUP35MC*	Chernoff Lab
pmCUP1-Aβ1-42-MC	*CEN*	*URA3*	P_{CUP1}	*Aβ1-42-SUP35-MC*	Chernoff Lab
pmCUP1-tau RD (WT)-MC	*CEN*	*URA3*	P_{CUP1}	*tau-SUP35-MC*	Chernoff Lab
pmCUP1-tau RD P301L, V337M(mut)-MC	*CEN*	*URA3*	P_{CUP1}	*tau P301L, V337M-SUP35-MC*	Chernoff Lab
pmCUP1	*CEN*	*URA3*	P_{CUP1}	None	Ref. 75 (Serio et al., 1999)
p316-pmSUP35-Sup35	*CEN*	*URA3*	P_{SUP35}	*SUP35*	Chernoff Lab
pmSUP35-Aβ1-42-NR-MC	*CEN*	*URA3*	P_{SUP35}	*Aβ1-42-SUP35-NR-MC*	Chernoff Lab
pRS415	*CEN*	*LEU2*	*None*	*None*	Chernoff Lab
pmSUP35-Aβ1-42-NR-MC	*CEN*	*LEU2*	P_{SUP35}	*Aβ1-42-SUP35-NR-MC*	Chernoff Lab
pmSUP35-MC	*CEN*	*LEU2*	P_{SUP35}	*SUP35MC*	Chernoff Lab
Yep13	*2micron*	*LEU2*	None	None	Chernoff Lab
YRpHO	*2micron*	*URA3*	None	None	Chernoff Lab

Table C. Oligonucleotide primers used in this study

Name	Sequence 5'-3'	Direction
Sup35N BamHI	GCGTGGATCCGTCGCCACCATGTCC	Forward
Sup35N SacI	TTGGAGCTCTTATCAACCTTGAGACTGTGGT TGGAA	Reverse
Sup35N-HA XbaI	AGTCTCTAGATCAAGCGTAATCTGGTACGTC GTATGGGTAACC TTGAGACTGTGGTTGGAA	Reverse
PrP90-230-HA XbaI	AGTCTCTAGATCAAGCGTAATCTGGTACGTC GTATGGGTAGGA TCTTCTCCCGTCGTAATA	Reverse
PrP90-119 XbaI	GC TCT AGA TTA TGC CCC AGC TGC CGC AGC	Reverse
N-PrP90-144 XbaI	TAATTCTAGATCAGTCGTTGCCAAAATGGAT C	Reverse
PrP90-159 Xba1	TAATTCTAGATCATTGGTTAGGGTAGCGGTA CATG	Reverse
PrP90-171 Xba1	TAATTCTAGATCACTGGTTGCTGTACTGATC CACTGG	Reverse
PrP90-119 XbaI	GCTCTAGATTATGCCCCAGCTGCCGCAGC	Reverse
PrP90-230 P101L	CAGTGGAACAAGCTCAGCAAACCAAAAACC	Forward
PrP90-230 P101L	GGTTTTTGGTTTGCTGAGCTTGTTCCACTG	Reverse
PrP90-230 Q167R	CAGGCCAGTGGATCGATACAGCAACCAGAA C	Forward
PrP90-230 Q167R	GTTCTGGTTGCTGTATCGATCCACTGGCCTG	Reverse
Aβ1-42-EcoRI	CAAGAATTCGATGCAGAATTCCGACATGAC	Forward
Aβ1-42 NotI	TTGGCGGCCGCTTACGCTATGACAACACCG CC	Reverse
Aβ1-42 XbaI	TTGTCTAGATTACGCTATGACAACACCGCC	Reverse
EcoRI-NAC	GACTGAATTCGAGCAAGTAACTAATGTAGGT	Forward
NAC-HA NotI	AGTCGCGGCCGCTCAAGCGTAATCTGGTAC GTCGTATGGGTAACCAGTAGCCGCTGCAAT GGA	Reverse
ECORI-Myo Pro 2	AATTCGTCGCCAATGCCTTCATCATCTGTGG CACCTTGTACACCGTCAGCAGCTACTGAT	Forward
Myo-XbaI Pro 2	GTCAGTAGCTGCTGACGGTGTACAAGGTGC CACAGAT GATGAAGGCATTGGCGACAGATC	Reverse
EcoRI 23-230 PrP	TGGGAATTCAAAAAGCGGCCAAAGCCTGG	Forward
EcoRI LacZ	GCGTGAATTCATGGATCCCGTCGTTTTACAA CGTCGTGAC	Forward
LacZ XbaI	GACTTCTAGATTATTTTTGACACCAGACCAA CTGGTAATG	Reverse
Sup35N SacII	GACTCCGCGGACCTTGAGACTGTGGTTGGA AACCAGCTTG	Reverse
NotI IAPP	AGTCGCGGCCGCTCAGTAAGTGTTACTACC AAC	Reverse
Aβ1-42 K28E	CAGAAGATGTGGGTTCAAACGAGGGTGCAA TCATTGGACTCAT	Forward

Aβ1-42 K28E	ATGAGTCCAATGATTGCACCCTCGTTTGAAC CCAATCTTCTG	Reverse
Aβ1-42 D23N	CAAAAATTGGTGTTCTTTGCAGAAAATGTGG GTTCAAACAAAGGTGCAA	Forward
Aβ1-42 D23N	TTGCACCTTTGTTTGAACCCACATTTTCTGC AAAGAACACCAATTTTTG	Reverse
Aβ1-42 D23K	GTGGGTTCAAACAAAGGTGCAATCATTG	Forward
Aβ1-42 D23K	CAATGATTGCACCTTTGTTTGAACCCAC	Reverse
Aβ1-42 F19S	CATCAAAAATTGGTGTCCTTTGCAGAAGATG TGG	Forward
Aβ1-42 F19S	CCACATCTTCTGCAAAGGACACCAATTTTTG ATG	Reverse
Aβ1-42 F20S	CAAAAATTGGTGTTCTCTGCAGAAGATGTGG G	Forward
Aβ1-42 F20S	CCCACATCTTCTGCAGAGAACACCAATTTTT G	Reverse
Aβ1-42 I31P	GTTCAAACAAAGGTGCACCCATTGGACTCAT GGTGG	Forward
Aβ1-42 I31P	CCACCATGAGTCCAATGGGTGCACCTTTGTT TGAAC	Reverse
Aβ1-42 H13L	ACATGACTCAGGATATGAAGTTCTTCATCAA AAATTGGTGTTCTTTG	Forward
Aβ1-42 H13L	CAAAGAACACCAATTTTTGATGAAGAACTTC ATATCCTGAGTCATGT	Reverse
Aβ1-42 A21E, D23A	ATCAAAAATTGGTGTTCTTTGAAGAAGCTGT GGGTTCAAACAAAGGTGC	Forward
Aβ1-42 A21E, D23A	GCACCTTTGTTTGAACCCACAGCTTCTTCAA AGAACACCAATTTTTGAT	Reverse
Aβ1-42 G25V	GTTCTTTGCAGAAGATGTGGTTTCAAACAAA GGTGCAATCA	Forward
Aβ1-42 G25V	TGATTGCACCTTTGTTTGAAACCACATCTTCT GCAAAGAAC	Reverse
Aβ1-42 F19K	TATGAAGTTCATCATCAAAAATTGGTGAAGT TTGCAGAAGATGTGGGTTCAAACAAA	Forward
Aβ1-42 F19K	TTTGTTTGAACCCACATCTTCTGCAAACTTCA CCAATTTTTGATGATGAACTTCATA	Reverse
Aß42 MC BamHI	GCGTGGATCCGTCGCCACCATGGATGCAGA ATTCCG ACATGAC	Forward
Aß42 MC BglII	AGTCAGATCTCGCTATGACAACACCGCCCA C	Reverse
Tau(244-372) MC BamHI	GCGTGGATCCGTCGCCACCATGCAGACAGC CCCC GTG	Forward
Tau (244-372) MC BglII	AGTCAGATCTTTCAATCTTTTTATTTCCTCCG CC	Reverse
Aß42 PstI	ACC TGC AGG CGC TAT GAC AAC ACC GCC CAC	Reverse

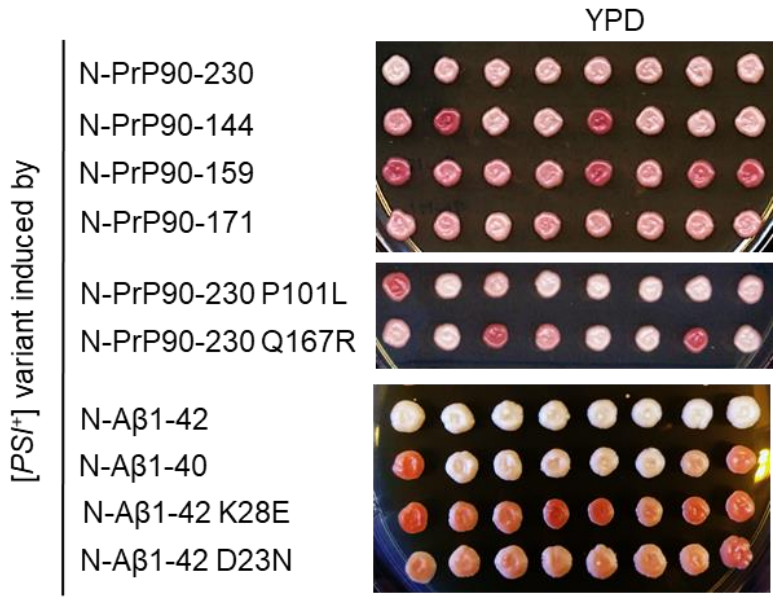

Figure A. Qualitative analysis [*PSI*$^{+}$] variants induced by N-Aβ-based chimeric constructs in yeast. A subset of a spectra of [*PSI*$^{+}$] variants induced by various chimeric constructs in yeast were scored in comparison to control strong and weak strains, OT56 and OT55 respectively. [*PSI*$^{+}$] variants that had a phenotype ranging in between strong and weak [*PSI*$^{+}$] variants were scored as intermediate [*PSI*$^{+}$] variants. Refer Tables 3-3 and 4-2 for a quantitative analysis.

REFERENCES

1. Knowles, T. P., Vendruscolo, M., & Dobson, C. M. (2014) The amyloid state and its association with protein misfolding diseases. Nature Reviews Molecular Cell Biology, 15: 384-396. doi:10.1038/nrm3810

2. Cobb, N.J., Surewicz, W.K. (2009) Prion diseases and their biochemical mechanisms. Biochemistry. 48: 2574-85. doi:10.1021/bi900108v

3. Chakraborti, C., Chaudhury, K. P., & Biswas, R. R. (2014). Primary conjunctival amyloidosis. Oman Journal of Ophthalmology. 7, 16–18. doi: 10.4103/0974-620X.127914

4. Nizhnikov, A.A., Antonets, K.S., Bondarev, S.A., Inge-Vechtomov, S.G., Derkatch, I.L. (2016) Prions, amyloids, and RNA: Pieces of a puzzle. Prion. 10:182-206. doi:10.1080/19336896.2016.1181253

5. Soto C. (2003). Unfolding the role of protein misfolding in neurodegenerative diseases. Nat Rev Neurosci. 4:49–60.

6. Moreno-Gonzalez, I., & Soto, C. (2011). Misfolded protein aggregates: Mechanisms, structures and potential for disease transmission. Seminars in Cell & Developmental Biology, 22(5), 482-487. doi:10.1016/j.semcdb.2011.04.002

7. James, B.D., Leurgans, S., Hebert, L.E., Scherr, P.A., Yaffe, K., Bennett, B.D. (2014). Contribution of Alzheimer disease to mortality in the United States. Neurology. 82:1045–1050. doi:10.1212/01.wn1.0000455099.43083.c6

8. Alzheimer's Association. (2017) Alzheimer's disease facts and figures. Alzheimers Dement. 13:325–73.

9. Jones, R. W., Romeo, R., Trigg, R., Knapp, M., Sato, A., King, D., Niecko, T., Lacey, L.; DADE Investigator Group. (2015) Dependence in Alzheimer's disease and service use costs, quality of life, and caregiver burden: The DADE study. Alzheimer's & Dementia. 11:280-90. doi: 10.1016/j.jalz.2014.03.001

10. Campos-Pea, V., Gmez, R., & Antonio, M. (2014). Genetics of Alzheimer´s Disease. Neurochemistry. 43:622-31. doi: 10.1016/j.arcmed.2012.10.017.

11. Irvine, G. B., El-Agnaf, O. M., Shankar, G. M., and Walsh, D. M. (2008) Protein aggregation in the brain: the molecular basis for Alzheimer's and Parkinson's diseases. Mol.Med.14:451–464.

12. Thomas, B. & Oliver, W. (2010). Intracellular accumulation of amyloid-beta – a predictor for synaptic dysfunction and neuron loss in Alzheimer's disease. Front. Ag. Neurosci. 2:8. doi: 10.3389/fnagi.2010.00008

13. Kassler, K., Horn, A. H., & Sticht, H. (2009). Effect of pathogenic mutations on the structure and dynamics of Alzheimer's Aβ42-amyloid oligomers. Journal of Molecular Modeling, 16:1011-1020. doi:10.1007/s00894-009-0611-1

14. Grabowski, T.J., Cho, H.S., Vonsattel, J.P.G., Rebeck, G.W., Greenberg, S.M. (2001). Novel amyloid precursor protein mutation in an Iowa family with dementia and severe cerebral amyloid angiopathy. Annals of Neurology. 49:697-705. doi:10.1002/ana.1009

15. Mietelska-Porowska, A., Wasik, U., Goras, M., Filipek, A., & Niewiadomska, G. (2014). Tau Protein Modifications and Interactions: Their Role in Function and Dysfunction. International Journal of Molecular Sciences, 15:4671-4713. doi:10.3390/ijms15034671

16. Näslund, J., Schierhorn, A., Hellman, U., Lannfelt, L., Roses, A. D., Tjernberg, L. O., Greengard, P. (1994). Relative abundance of Alzheimer A beta amyloid peptide variants in Alzheimer disease and normal aging. Proceedings of the National Academy of Sciences of the United States of America, 91:8378–8382.

17. Irvine, G.B., El-Agnaf, O.M., Shankar, G.M., Walsh, D.M. (2008) Protein aggregation in the brain: the molecular basis for Alzheimer's and Parkinson's diseases. Molecular Medicine. 14:451-64. doi:10.2119/2007-00100.

18. Prusiner SB. (1993) Genetic and infectious prion diseases. Archives of Neurology. 50:1129-53. doi:10.1001/archneur.1993.00540110011002

19. Prusiner, S.B. (1997) Prion diseases and the BSE crisis. Science. 1997;278:245–51. doi: 10.1126/science.278.5336.245

20. Abdallah, A., Wang, P., Richt, J. A., & Sreevatsan, S. (2012). Y145Stop is sufficient to induce de novo generation prions using protein misfolding cyclic amplification. Prion. 6:81–88. http://doi.org/10.4161/pri.6.1.18493

21. Heske, J., Heller, U., Winklhofer, K. F., & Tatzelt, J. (2003). The C-terminal Globular Domain of the Prion Protein Is Necessary and Sufficient for Import into the Endoplasmic Reticulum. Journal of Biological Chemistry, 279:5435-5443. doi:10.1074/jbc.m309570pathogenic

22. Coleman, B. M., Harrison, C.F. Masters. C.L. Barnham, K.J. Lawson, V.A., Hill, A.F. Pathogenic Mutations within the Hydrophobic Domain of the Prion Protein Lead to the Formation of Protease-Sensitive Prion Species with Increased Lethality.” Journal of Virology. 88(5):2690-703. doi: 10.1128/JVI.02720-13

23. Giráldez-Pérez, R. M., Antolín-Vallespín, M., Muñoz, M. D., & Sánchez-Capelo, A. (2014). Models of α-synuclein aggregation in Parkinson’s disease. Acta Neuropathologica Communications, 2: 176. http://doi.org/10.1186/s40478-014-0176-9

24. Xu, L., & Pu, J. (2016). Alpha-Synuclein in Parkinson’s Disease: From Pathogenetic Dysfunction to Potential Clinical Application. Parkinson’s Disease, 2016: 1720621. http://doi.org/10.1155/2016/1720621

25. Kahn, S.E., Andrikopoulos, S., Verchere, C.B. (1999). Islet amyloid: a long-recognized but underappreciated pathological feature of type 2 Diabetes. Diabetes. 48:241–53. doi:10.2337/diabetes.48.2.241

26. Westermark, P. (1994). Amyloid and polypeptide hormones: what is their interrelationship? Amyloid. 1:47–58. doi:10.3109/13506129409148624

27. Bruttini, M., Longo, I., Frezzotti, P., Ciappetta, R., Randazzo, A., Orzalesi, N., Fumagalli, E., Caporossi, A., Frezzotti, R., Renieri, A. (2003) Mutations in the Myocilin Gene in Families With Primary Open-angle Glaucoma and Juvenile Open-angle Glaucoma. Arch Ophthalmol. 121(7):1034–1038. doi:10.1001/archopht.121.7.1034

28. Clark, A., Kawase, K., English-Wright, S., Lane, D., Steely, H., Yamamoto, T., Kitazawa, Y., Kwon, Y.H., Fingert, J.H., Swiderski, R.E., Mullins, R.F., Hageman, G.S., Alward, W.L., Sheffield, V.C., Stone, E.M. (2001). Expression of the glaucoma gene myocilin (MYOC) in the human optic nerve head. FASEB. 15:1251-3.

29. Orwig, S. D., Perry, C. W., Kim, L. Y., Turnage, K. C., Zhang, R., Vollrath, D., … Lieberman, R. L. (2012). Amyloid fibril formation by the glaucoma-associated olfactomedin domain of myocilin. Journal of Molecular Biology, 421:242–255. http://doi.org/10.1016/j.jmb.2011.12.016

30. Chen, J.-W., Zhao, L., Zhang, F., Li, L., Gu, Y.-H., Zhou, J.-Y. Dong, C.-B. (2015). Clinical Characteristics, Radiological Features and Gene Mutation in 10 Chinese Families with Spinocerebellar Ataxias. Chinese Medical Journal, 128:1714–1723. http://doi.org/10.4103/0366-6999.159340

31. Juenemann, K., Wiemhoefer, A., & Reits, E. A. (2015). Detection of ubiquitinated huntingtin species in intracellular aggregates. Frontiers in Molecular Neuroscience. 8:1-2. http://doi.org/10.3389/fnmol.2015.00001

32. Liebman, S.W., Chernoff, Y.O. (2012). Prions in yeast. Genetics. 191:1041–72. doi:10.1534/genetics.111.137760

33. Chernoff, Y.O., Derkatch, I.L., Inge-Vechtomov, S.G. (1993). Multicopy SUP35 gene induces de novo appearance of psi-like factors in the yeast Saccharomyces cerevisiae. Current Genetics. 24:268-70. doi:10.1007/BF00351802

34. Derkatch, I.L., Chernoff, Y.O., Kushnirov, V.V., Inge-Vechtomov, S.G., Liebman, S.W. (1996). Genesis and variability of [PSI] prion factors in Saccharomyces cerevisiae. Genetics. 144:1375-86. PMCID: PMC1207691

35. Masison, D.C., Wickner, R.B. (1995). Prion-inducing domain of yeast Ure2p and protease resistance of Ure2p in prion-containing cells. Science. 270:93-5. doi:10.1126/science.270.5233.93

36. Wickner, R.B. (1994). [URE3] as an altered URE2 protein: evidence for a prion analog in Saccharomyces cerevisiae. Science. 264: 566–9. doi: 10.1126/science.7909170

37. Derkatch, I.L., Bradley, M.E., Zhou, P., Chernoff, Y.O., Liebman, S.W. (1997). Genetic and environmental factors affecting the de novo appearance of the [PSI+] prion in Saccharomyces cerevisiae. Genetics. 147:507–19. PMCID: PMC1208174

38. Derkatch, I.L., Bradley, M.E., Hong, J.Y., Liebman, S.W. (2001). Prions affect the appearance of other prions: the story of [PIN+]. Cell. 106:171–82. doi:10.1016/S0092-8674(01)00427-5.

39. Osherovich, L.Z., Weissman, J.S. (2001). Multiple Gln/Asn-rich prion domains confer susceptibility to induction of the yeast [PSI+] prion. Cell. 106:183–94. doi:10.1016/S0092-8674(01)00440-8

40. Chernova, T. A., Kiktev, D. A., Romanyuk, A. V., Shanks, J. R., Laur, O., Ali, M., Wilkinson, K. D. (2017). Yeast Short-lived Actin Associated Protein Forms a Metastable Prion in Response to Thermal Stress. Cell Reports, 18(3), 751–761. http://doi.org/10.1016/j.celrep.2016.12.082

41. Romanova, N. V., & Chernoff, Y. O. (2009). Hsp104 and Prion Propagation. Protein and Peptide Letters, 16(6), 598–605.

42. Gitler, A. D. (2009). Disease models and mechanisms in the classroom. Disease Models & Mechanisms, 2(3-4), 103–106. http://doi.org/10.1242/dmm.002600

43. Smith, M. G., & Snyder, M. (2006). Yeast as a Model for Human Disease. Current Protocols in Human Genetics. 48: 15.6.1-15.6.8 doi:10.1002/0471142905.hg1506s48

44. Caine, J., Sankovich, S., Antony, H., Waddington, L., Macreadie, P., Varghese, J., & Macreadie, I. (2007). Alzheimers AÎ² fused to green fluorescent protein induces growth stress and a heat shock response. FEMS Yeast Research, 7(8), 1230-1236. doi:10.1111/j.1567-1364.2007.00285.x

45. Park, S.-K., Pegan, S. D., Mesecar, A. D., Jungbauer, L. M., LaDu, M. J., & Liebman, S. W. (2011). Development and validation of a yeast high-throughput screen for inhibitors of Aβ42 oligomerization. Disease Models & Mechanisms, 4(6), 822–831. http://doi.org/10.1242/dmm.007963

46. Caine, J & Volitakis, Irene & Cherny, R & Varghese, Jose & Macreadie, Ian. (2007). Abeta produced as a fusion to maltose binding protein can be readily purified and stably associates with copper and zinc. Protein and peptide letters. 14. 83-6. 10.2174/092986607779117263.

47. Treusch, S., Hamamichi, S., Goodman, J.L. et al. (2011). Functional links between abeta toxicity, endocytic trafficking, and Alzheimer's disease risk factors in yeast. Science. 334:1241–1245.

48. Xiao, Q., Gil, S.-C., Yan, P., Wang, Y., Han, S., Gonzales, E., Lee, J.-M. (2012). Role of Phosphatidylinositol Clathrin Assembly Lymphoid-Myeloid Leukemia (PICALM) in Intracellular Amyloid Precursor Protein (APP) Processing and Amyloid Plaque Pathogenesis. The Journal of Biological Chemistry, 287(25), 21279–21289. http://doi.org/10.1074/jbc.M111.338376

49. Rubel, A.A., Ryzhova, T.A., Antonets, K.S., Chernoff, Y.O., Galkin, A.P. (2013). Identification of PrP sequences essential for the interaction between the PrP polymers and Aβ peptide in a yeast-based assay. Prion.;7:469–76. doi: 10.4161/pri.26867

50. Vandebroek, T., Terwel, D., Vanhelmont, T., Gysemans, M., Haesendonck, C. V., Engelborghs, Y., Leuven, F. V. (2006). Microtubule Binding and Clustering of Human Tau-4R and Tau-P301L Proteins Isolated from Yeast Deficient in Orthologues of Glycogen Synthase Kinase-3β or cdk5. Journal of Biological Chemistry, 281(35), 25388-25397. doi:10.1074/jbc.m602792200

51. Badiola, N., de Oliveira, R. M., Herrera, F., Guardia-Laguarta, C., Gonçalves, S. A., Pera, M., Lleó, A. (2011). Tau Enhances α-Synuclein Aggregation and Toxicity in Cellular Models of Synucleinopathy. PLoS ONE, 6(10), e26609. http://doi.org/10.1371/journal.pone.0026609

52. Combs, B., & Gamblin, T. C. (2012). FTDP-17 Tau Mutations Induce Distinct Effects on Aggregation and Microtubule Interactions. Biochemistry, 51(43), 8597-8607. doi:10.1021/bi3010818

53. Alberti, S., Halfmann, R., King, O., Kapila, A., Lindquist, S. (2009). A systematic survey identifies prions and illuminates sequence features of prionogenic proteins. Cell. 137:146–58. doi: 10.1016/j.cell.2009.02.044.

54. Sondheimer, N., Lindquist, S.L. (2000). Rnq1: an epigenetic modifier of protein function in yeast. Mol Cell. 5:163–72. doi: 10.1016/S1097-2765(00)80412-8.

55. Jossé, L., Marchante, R., Zenthon, J., von der Haar, T., & Tuite, M. F. (2012). Probing the role of structural features of mouse PrP in yeast by expression as Sup35-PrP fusions. Prion, 6(3), 201–210. http://doi.org/10.4161/pri.19214

56. Outeiro, T. F. (2003). Yeast Cells Provide Insight into Alpha-Synuclein Biology and Pathobiology. Science, 302(5651), 1772-1775. doi:10.1126/science.1090439

57. Shrestha, A., & Megeney, L. A. (2015). Yeast proteinopathy models: a robust tool for deciphering the basis of neurodegeneration. Microbial Cell, 2(12), 458–465. http://doi.org/10.15698/mic2015.12.243

58. Büttner S, Delay C, Franssens V, Bammens T, Ruli D, Zaunschirm S, et al. (2010) Synphilin-1 Enhances α-Synuclein Aggregation in Yeast and Contributes to Cellular Stress and Cell Death in a Sir2-Dependent Manner. PLoS ONE. 5(10): e13700. https://doi.org/10.1371/journal.pone.0013700

59. Kijanska, M., Dohnal, I., Reiter, W., Kaspar, S., Stoffel, I., Ammerer, G., Peter, M. (2010). Activation of Atg1 kinase in autophagy by regulated phosphorylation. Autophagy, 6(8), 1168-1178. doi:10.4161/auto.6.8.13849

60. Liang, J., Clark-Dixon, C., Wang, S., Flower, T. R., Williams-Hart, T., Zweig, R., Witt, S. N. (2008). Novel suppressors of α-synuclein toxicity identified using yeast. Human Molecular Genetics, 17(23), 3784–3795. http://doi.org/10.1093/hmg/ddn276

61. Tenreiro, S., & Outeiro, T. F. (2010). Simple is good: yeast models of neurodegeneration. FEMS Yeast Research, 10(8), 970-979. doi:10.1111/j.1567-1364.2010.00649.x

62. Goehler, H., Dröge, A., Lurz, R., Schnoegl, S., Chernoff, Y.O., Wanker, E.E. (2010) Pathogenic Polyglutamine Tracts Are Potent Inducers of Spontaneous Sup35 and Rnq1 Amyloidogenesis. PLoS ONE 5: e9642. https://doi.org/10.1371/journal.pone.0009642

63. Kantcheva, R. B., Mason, R., & Giorgini, F. (2014). Aggregation-Prone Proteins Modulate Huntingtin Inclusion Body Formation in Yeast. PLoS Currents, 6, ecurrents.hd.501008f3051342c9a5c0cd0f3a5bf3a4.

64. Gong H, Romanova NV, Allen KD, Chandramowlishwaran, P., Gokhale, K., Newnam, G. P., Mieczkowski, P. Sherman., M.Y. Chernoff, Y. O (2012) Polyglutamine Toxicity Is Controlled by Prion Composition and Gene Dosage in Yeast. PLoS Genet 8: e1002634. https://doi.org/10.1371/journal.pgen.1002634

65. Figley, M. D., & Gitler, A. D. (2013). Yeast genetic screen reveals novel therapeutic strategy for ALS. Rare Diseases, 1, e24420. http://doi.org/10.4161/rdis.24420

66. Johnson, B. S., Mccaffery, J. M., Lindquist, S., & Gitler, A. D. (2008). A yeast TDP-43 proteinopathy model: Exploring the molecular determinants of TDP-43 aggregation and cellular toxicity. Proceedings of the National Academy of Sciences, 105(17), 6439-6444. doi:10.1073/pnas.0802082105

67. Kaiser, C., Michaelis, S., Mitchell, A. Methods in Yeast Genetics: A Cold Spring Harbor Laboratory Course Manual. Cold Spring Harbor, NY: Cold Spring Harbor Laboratory Press. 1994. ISBN- 0879694513

68. Ghahramani, S. Fundamentals of Probability. 2nd edn. New Jersey: Pearson Prentice Hall. 2000. ISBN 0-13-145340-8

69. Halfmann, R., Lindquist, S.L. (2008). Screening for amyloid aggregation by semi-denaturing detergent-agarose gel electrophoresis. Journal of Visualized Experiments. 17:e838. doi:10.3791/838

70. Krammer, C., Suhre, M.H., Kremmer, E., Diemer, C., Hess, S., Schätzl, H.M., et al. (2008) Prion protein/protein interactions: fusion with yeast Sup35p-NM modulates cytosolic PrP aggregation in mammalian cells. The FASEB Journal. 22:762-73. doi:10.1096/fj.07-8733com

71. Fischer, M., Rülicke, T., Raeber, A., Sailer, A., Moser, M., Oesch, B. (!996) Prion protein (PrP) with amino-proximal deletions restoring susceptibility of PrP knockout mice to scrapie. The EMBO Journal. 15:1255–64. doi:10.5167/uzh-1867

72. Van Nostrand, W.E., Melchor, J.P., Cho, H.S., Greenberg, S.M., Rebeck, G.W. (2001) Pathogenic effects of D23N Iowa mutant amyloid beta protein. The Journal of Biological Chemistry. 276:32860–6. doi: 10.1074/jbc.M104135200

73. Chernova, T.A., Romanyuk, A.V., Karpova, T.S., Shanks, J.R., Ali, M., Howie, R.L., O'Dell, A., McNally, J.G., Liebman. S.W. Chernoff. Y.O., Wilkinson, K.D. (2011) Prion induction by the short-lived, stress-induced protein Lsb2 is regulated by ubiquitination and association with the actin cytoskeleton. Molecular Cell. 43:242–52. doi:10.1016/j.molcel.2011.07.001

74. Li, S.X., Tong, Y.P., Xie, X.C., Wang, Q.H., Zhou, H.N., Han, Y. (2007) Octameric structure of the human bifunctional enzyme PAICS in purine biosynthesis. Journal of Molecular Biology. 366:1603-14. doi:10.1016/j.jmb.2006.12.027

75. Serio, T.R., Lindquist, S.L. (1999). [PSI+]: an epigenetic modulator of translation termination efficiency. Annual Review of Cell and Developmental Biology. 15:661–703. doi: 10.1146/annurev.cellbio.15.1.661

76. Chernoff, Y.O., Lindquist, S.L., Ono, B., Inge-Vechtomov, S.G., Liebman, S.W. (1995) Role of the chaperone protein Hsp104 in propagation of the yeast prion-like factor [psi+]. Science. 268: 880–4. doi:10.1016/0168-9525(95)90533-2

77. Chernova, T.A., Wilkinson, K.D., Chernoff, Y.O. (2017) Prions, chaperones and proteostasis in yeast. Cold Spring Harbor Perspectives in Biology. 9: pii:a023663. doi:10.1101/CSHPERSPECT.a023663

78. Perrier, V., Kaneko, K., Safar, J., Vergara, J., Tremblay, P., DeArmond, S.J. (2002) Dominant-negative inhibition of prion replication in transgenic mice. Proceedings of the National Academy of Sciences of USA. 99:13079-84. doi:10.1073/pnas.182425299

79. Ghetti, B., Piccardo, P., Frangione, B., Bugiani, O., Giaccone, G., Young, K. (1996) Prion protein amyloidosis. Brain Pathology. 6:127–45. doi:10.1111/j.1750-3639.1996.tb00796.x

80. Kitamoto, T., Iizuka, R., Tateishi, J. (1993) An amber mutation of prion protein in Gerstmann- Sträussler syndrome with mutant PrP plaques. Biochemical and Biophysical Research Communications. 192:532–7. doi:10.1006/bbrc.1993.1447

81. Lorenz, H., Windl, O., Kretzschmar, H.A. (2002) Cellular phenotyping of secretory and nuclear prion proteins associated with inherited prion diseases. The Journal of Biological Chemistry. 277:8508–8516. doi:10.1074/jbc.M110197200

82. Kochneva-Pervukhova, N.V., Poznyakovski, A.I., Smirnov, V.N., Ter-Avanesyan, M.D. (1998) C-terminal truncation of the Sup35 protein increases the frequency of de novo generation of a prion-based [PSI+] determinant in Saccharomyces cerevisiae. Current Genetics. 34:146-51. PMID: 9724418

83. Zhou, P., Derkatch, I.L., Liebman, S.W. (2001) The relationship between visible intracellular aggregates that appear after overexpression of Sup35 and the yeast prion-like elements [PSI+] and [PIN+]. Molecular Microbiology. 39: 37-46. doi: 10.1046/j.1365-2958.2001.02224.x

84. Tanaka, M., Collins, S.R., Toyama, B.H., Weissman, J.S. (2006) The physical basis of how prion conformations determine strain phenotypes. Nature. 442:585–9. doi: 10.1038/nature04922

85. Newby, G.A., Kiriakov, S., Hallacli, E., Kayatekin, C., Tsvetkov, P., Mancuso , C.P., Bonner, J. M., Hesse, W.R., Chakrabortee, S., Manogaran, A.L., Liebman, S.W., Lindquist, S.L., Khalil, A.S. (2017) Genetic tool to track protein aggregates and control protein inheritance. Cell. 171: 966-979. doi: 10.1016/j.cell.2017.09.041

86. Choe, Y.J., Ryu, Y., Kim, H.J., Seok, Y.J. (2009) Increased [PSI+] appearance by fusion of Rnq1 with the prion domain of Sup35 in Saccharomyces cerevisiae. Eukaryotic Cell. 8:968–76. doi:10.1128/EC.00353-08

87. Cobb, N.J., Sönnichsen, F.D., McHaourab, H., Surewicz, W.K. (2007) Molecular architecture of human prion protein amyloid: a parallel, in-register β-structure. Proceedings of the National Academy of Sciences of USA. 104:18946–51. doi:10.1073/pnas.0706522104

88. Saijo, E., Hughson, A.G., Raymond, G.J., Suzuki, A., Horiuchi, M., Caughey, B.. (2016) PrPSc-specific antibody reveals C-terminal conformational differences between prion strains. Journal of Virology. 90:4905-13. doi: 10.1128/JVI.00088-16.

89. Bartz, J.C. (2016) Prion strain diversity. Cold Spring Harbor Perspectives in Medicine. 6:pii:a024349. doi:0.1101/cshperspect.a024349

90. Ghaemmaghami, S. (2016) Biology and genetics of PrP prion strains. Cold Spring Harbor Perspectives in Medicine. 6:pii:a026922. doi:10.1101/cshperspect.a026922

91. Cohen, M., Appleby, B., Safar, J.G. (2016) Distinct prion-like strains of amyloid beta implicated in phenotypic diversity of Alzheimer's disease. Prion. 10:9-17. doi:10.1080/19336896.2015.1123371

92. Makarava, N., & Baskakov, I.V. (2013) The evolution of transmissible prions: the role of deformed templating. PLOS Pathogens. 9:e1003759. doi:10.1371/journal.ppat.1003759

93. Kajava, A. V., Baxa, U., & Steven, A. C. (2010). β arcades: recurring motifs in naturally occurring and disease-related amyloid fibrils. The FASEB Journal, 24:1311-1319. doi:10.1096/fj.09-145979

94. Colvin, M.T., Silvers, R., Ni, Q.Z., Can, T.V., Sergeyev, I., Rosay, M., et al. (2016) Atomic resolution structure of monomorphic Aβ42 amyloid fibrils. Journal of the American Chemical Society. 138:9663-74. doi:10.1021/jacs.6b05129

95. Walti, M.A., Ravotti, F., Arai, H., Glabe, C.G., Wall, J.S., Böckmann, A. et al. (2016). Atomic-resolution structure of a disease-relevant Aβ (1-42) amyloid fibril. Proceedings of the National Academy of Sciences of USA. 113:4976–84. doi: 10.1073/pnas.1600749113

96. Mori, H., Takio, K., Ogawara, M., Selkoe, D.J. (1992) Mass spectrometry of purified amyloid beta protein in Alzheimer's disease. The Journal of Biological Chemistry. 267:17082–86. PMID: 1512246

97. Jarrett, J.T., Berger, E.P., Lansbury, P.T. (1993) The carboxy terminus of the β-amyloid protein is critical for the seeding of amyloid formation - implications for the pathogenesis of Alzheimer's disease. Biochemistry. 32:4693–7. doi:10.1021/bi00069a001

98. Hilbich, C., Kisters-Woike, B., Reed, J., Masters, C.L., Beyreuther, K. (1992) Substitutions of hydrophobic amino acids reduce the amyloidogenicity of Alzheimer's disease beta A4 peptides. Journal of Molecular Biology. 228:460–73. doi:10.1016/0022-2836(92)90835-8

99. Morimoto, A., Irie, K., Murakamim K., Masuda, Y., Ohigashi, H., Nagaom M., et al. (2004) Analysis of the secondary structure of beta-amyloid (Abeta42) fibrils by systematic proline replacement. The Journal of Biological Chemistry. 279:52781–8. doi:10.1074/jbc.M406262200

100. Williams, A.D., Portelius, E., Kheterpal, I., Guo, J.T., Cook, K.D., Xu,Y., et al. Mapping abeta amyloid fibril secondary structure using scanning proline mutagenesis. (2004) Journal of Molecular Biology. 335:833–42. doi: 10.1016/j.jmb.2003.11.008

101. Tycko, R. (2006) Molecular structure of amyloid fibrils: insights from solid-state NMR. Quarterly Review of Biophysics. 39:1-55. doi: 10.1017/S0033583506004173

102. Xiao, Y., Ma, B., McElheny, D., Parthasarathy, S., Long, F., Hoshi, M., et al. (2015) Aβ(1-42) fibril structure illuminates self-recognition and replication of amyloid in Alzheimer's disease. Nature Structural and Molecular Biology. 22:499-505. doi: 10.1038/nsmb.2991

103. Rezaei-Ghaleh, N., Giller, K., Becker, S., & Zweckstetter, M. (2011). Effect of Zinc Binding on β-Amyloid Structure and Dynamics: Implications for AβAggregation. Biophysical Journal, 101: 1202–1211. http://doi.org/10.1016/j.bpj.2011.06.062

104. Duce, J. A., & Bush, A. I. (2010). Biological metals and Alzheimers disease: Implications for therapeutics and diagnostics. Progress in Neurobiology, 92:1-18. doi:10.1016/j.pneurobio.2010.04.003

105. Gu, H., Robison, G., Hong, L., Barrea, R., Wei, X., Farlow, M. R., Zheng, W. (2012). Increased β-amyloid deposition in Tg-SWDI transgenic mouse brain following in vivo lead exposure. Toxicology Letters, 213:211-219. doi:10.1016/j.toxlet.2012.07.002

106. Haber, J. E. (2012). Mating-Type Genes and MAT Switching in Saccharomyces cerevisiae. Genetics, 191:33–64. http://doi.org/10.1534/genetics.111.134577

107. Tanaka, M., Chien, P., Naber, N.C., Roger, S., Weissman, J. (2004). Conformational variations in an infectious protein determine prion strain differences. Nature. 428: 323-8. 10.1038/nature02392.

108. Paul, K. R., Molliex, A., Cascarina, S., Boncella, A. E., Taylor, J. P., & Ross, E. D. (2017). Effects of Mutations on the Aggregation Propensity of the Human Prion-Like Protein hnRNPA2B1. Molecular and Cellular Biology, 37:e00652-16. doi:10.1128/mcb.00652-16

109. Newnam, GP, Wegrzyn RD, Lindquist SL, Chernoff YO. (1999) Antagonistic

interactions between yeast chaperones Hsp104 and Hsp70 in prion curing. Molecular and Cellular Biology. 19:1325–33. doi:10.1128/MCB.19.2.1325

110. Chernoff YO, Newnam GP, Kumar J, Allen K, Zink AD. (1999) Evidence for a protein mutator in yeast: Role of the Hsp70-related chaperone Ssb in formation, stability, and toxicity of the [PSI] prion. Molecular and Cellular Biology. 19:8103–12. doi:10.1128/MCB.19.12.8103

111. Chernova TA, Allen KD, Wesoloski LM, Shanks JR, Chernoff YO, Wilkinson KD. (2003) Pleiotropic effects of Ubp6 loss on drug sensitivities and yeast prion are due to depletion of free ubiquitin pool. The Journal of Biological Chemistry. 278:52102-15. doi:10.1074/jbc.M310283200

112. Patino MM, Liu JJ, Glover JR, Lindquist SL. (1996) Support for the prion hypothesis for inheritance of a phenotypic trait in yeast. Science. 273:622-6. doi:10.1126/science.273.5275.622.